Diplomaterv

Garamvölgyi Zsolt

Nyilatkozat

Alulírott Garamvölgyi Zsolt, a Budapesti Műszaki és Gazdaságtudományi Egyetem hallgatója kijelentem, hogy ezt a diplomatervet meg nem engedett segítség nélkül, saját magam készítettem, és a diplomatervben csak a megadott forrásokat használtam fel. Minden olyan részt, amelyet szó szerint, vagy azonos értelemben, de átfogalmazva más forrásból átvettem, egyértelműen, a forrás megadásával megjelöltem.

Garamvölgyi Zsolt
hallgató

Physics-based Modeling of Membranes
for Sound Synthesis Applications

M.Sc. thesis

Zsolt Garamvölgyi

Supervisor:

Balázs Bank
Ph.D.

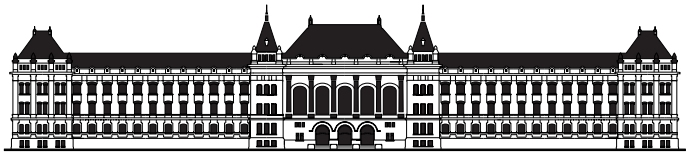

Budapest University of Technology and Economics
Department of Measurement and Information Systems
2008

Kivonat

A dolgozat membránrezgés fizikai alapú modellezésével foglalkozik. A membrán modellezésének célja olyan fizikai alapú dobmodellek létrehozása, amelyek alkalmasak valódi hangszerek hangjának reprodukálására. A fizikai alapú hangszermodellezés mint hangszintézis technika, számos előnnyel rendelkezik a hangszintézis egyéb módszereivel szemben. Ezek közül a legfontosabb, hogy egyetlen jól felépített modell segítségével számos eltérő hang hozható létre, valamint hogy az emberi beavatkozás viszonylag élethűen modellezhető.

A dolgozat három fő részre osztható. A második fejezet összefoglalja az egy- és kétdimenziós elosztott rezgő rendszerek modellezésének matematikai alapjait. A parciális differenciálegyenletek általános tulajdonságainak rövid áttekintése után az ideális húr valamint a membrán leírására alkalmas egyenletek kerülnek bemutatásra. Különös hangsúlyt kap a kör alakú membrán peremfeltételeinek vizsgálata különböző koordinátarendszerekben.

A harmadik fejezetben a választott fizikai alapú eljárás, a véges differencia módszer kerül bemutatásra. A véges differencia sémák legfontosabb tulajdonságai, a konvergencia, konzisztencia, numerikus stabilitás és diszperzió definiálása és részletes ismertetése szilárd alapot szolgáltat a numerikus modellek további vizsgálatához. A sémák numerikus stabilitásának vizsgálatára a térbeli Fourier-transzformáción alapuló von Neumann analízis módszere kerül ismertetésre.

Az előző fejezetek eredményeire támaszkodva a negyedik fejezetben számos különböző membránmodell vizsgálatára kerül sor. Nagy hangsúlyt kap a kétdimenziós rendszerekben fellépő iránymenti numerikus diszperzió vizsgálata, valamint a különböző diszkretizációs módszerek, úgy mint a Descartes- ill. trianguláris koordinátarendszerben történő, a negyedrendű és az interpolált diszkretizáció összehasonlítása.

Kulcsszavak: fizikai alapú modellezés, hangszintézis, véges differencia módszer, kétdimenziós hullámegyenlet, digitális jelfeldolgozás

Abstract

In this thesis, physics-based models of the elastic membrane will be presented. These numerical models of the membrane can be used as a component of a drum model, which can be applied for recreating the sound of the actual instrument in a way unique to this sound synthesis technique. Compared to other synthesis methods, physics-based modeling has several advantages. The most important benefits are the variety of sounds that can be produced by a single instrument model and the natural response to human interaction.

The thesis is divided into three parts. In Chapter 2, the partial differential equations of the string and the membrane are presented. The mathematical foundations of instrument modeling discussed in this chapter are used as a starting point in the subsequent chapters.

In Chapter 3, the fundamentals of the finite difference method are overviewed. The concepts of convergence, consistency, stability and numerical dispersion are defined and examined in great detail for the one-dimensional case. For stability- and dispersion analysis of finite difference schemes, the technique of von Neumann analysis is presented.

In Chapter 4, the concepts introduced in the previous chapter are extended to the two-dimensional case, and several types of membrane models are overviewed and analyzed. These include the models discretized in the Cartesian and the triangular coordinate systems, finite difference schemes of increased accuracy and interpolated schemes. The properties of these models are compared with respect to stability, dispersion error and computational complexity. Lossy and nonlinear models of the membrane are also discussed. Particular emphasis is laid on implementation issues, including the realization of circular boundary conditions in different coordinate systems.

Keywords: physics-based modeling, sound synthesis, finite difference method, two-dimensional wave equation, digital signal processing

Contents

Chapter 1

Introduction

Physics-based modeling has been used to analyze a wide range of real-world phenomena in many fields of science and engineering. Modeling the processes in nature is beneficial both from theoretical and practical points of view. Besides the better understanding of the surrounding physical world, which has always been the ultimate goal of science, the results can be effectively used in design and verification of electronic and mechanical devices or in weather prediction, to mention a few applications.

Modeling usually starts by obtaining the mathematical representation, i.e., a set of partial differential equations (PDEs) of the physical system of interest. In order to obtain a model that can be implemented on a digital computer, algorithms for numerically solving the PDEs have to be constructed. In practice, this means that the physical problem described by the differential equations has to be reformulated as a set of algebraic equations that can be implemented in software. This step, namely, the reformulation of the PDEs is referred to as *discretization*. The high computational complexity of numerically solving these equations usually prevents real-time implementations from being realized, however, in most fields of science and engineering real-time realization is not a requirement.

This is not the case in the field of sound synthesis. When a musician strikes a note on his keyboard, he will not tolerate a delay even as long as a hundred of milliseconds. The fact that real-time implementation is of prime importance in sound synthesis has prohibited physics-based instrument modeling from becoming a viable approach until the last few decades. The evolution of digital signal processing hardware and algorithms, however, enabled physics-based modeling to become one of the most promising synthesis methods at the present time.

Traditional, signal-based sound synthesis methods model the sound of the instrument without making any assumptions about the physical structure of the instrument. These techniques include abstract methods, spectral modeling techniques and models based on the processing of pre-recorded samples [Smith 1991; Tolonen et al. 1998]. Physics-based synthesis has several advantages over these methods. The most important benefits are the meaningful model parameters and the way the model takes human interaction into account. In the case of signal-based synthesis techniques, the adjustable parameters usually cannot be easily related to the physical properties of the instrument, which makes finding the

desirable sound difficult. On the other hand, in the case of a physics-based instrument model, the adjustable parameters are directly associated with physical specifics of the modeled instrument. For example, if the sound of a piano is to be recreated, in a model based on pre-recorded samples, the sound of each note has to be stored in order to yield natural sounding results. In the physics-based model, only a few physical parameters, e.g., the length and thickness of the string have to be adjusted for each note, and the changes in sound are taken into account automatically.

The importance of human interaction can be easily illustrated in the case of a drum. The drum can be struck at any point of the membrane, in a variety of ways. These differences in the excitation create audible effects in the sound of the instrument. In a sample-based model, this means that all the different sounds that can be produced by the instrument have to be recorded and stored. However, in this model, there is no way to describe the effect of several consecutive strokes to each other, which would be desirable to make the sound lively and natural. In a properly constructed physics-based model, these features are readily included.

The main parts of the physical instrument model have to correspond to the parts of the instrument itself. These are the sound source, which is a vibrating elastic structure (e.g., a string or a membrane), and the resonant body. The vibrations created by the sound source are amplified and the timbre is modified to some extent by the body. In practice, modeling the resonant body is often implemented by filtering the sound of the source. Two additional factors have significant influence on the sound of the instrument, namely, excitation and sound propagation in the air. In some cases, excitation can be regarded as a part of the instrument (e.g., the hammer in the piano), in others, they are somewhat separated (like the drum and the drumstick). However, in both cases, an excitation model has to be included in the physical model of the instrument to yield realistic results. Sound propagation has to be modeled in order to describe the relation between the vibrations of the instrument and the sound perceived by the human ear. Actually, the displacement-time or velocity-time functions of several points of the instrument model have to be summed in some way to yield a function of sound pressure with respect to time.

Instruments based on sound sources that can be modeled by one-dimensional structures (stringed and wind instruments) have been objects of research in the last few decades. In 1994, the first physics-based synthesizer, which can recreate the sound of several wind instruments in a quite natural way, the Yamaha VL-1 was introduced. However, instruments based on two-dimensional vibrating structures, like membranes and plates, have become objects of scientific research only in the last decade, so this can be considered a relatively new field of research.

The subject of this thesis is physics-based modeling of acoustic membranes, that is, constructing and examining physical membrane models that can be used in a real-time drum model. From the number of physics-based modeling techniques developed so far the author has choosen the *finite difference method* (FDM, in the literature also referred to as the finite difference time domain method, FDTD). Besides the finite element method (FEM), the FDM is the most widespread technique in physics-based modeling, whose foundations

were laid down in the first half of the twentieth century[1]. According to [Välimäki 2004], one of the earliest examples of applying this method to modeling musical instruments can be found in [Hiller and Ruiz 1971a] and [Hiller and Ruiz 1971b].

The most important advantages of the finite difference method are the relative ease of deriving and implementing discretized physical models it provides and its potential real-time applicability. This last statement does not mean that, in general, the FDM is the most suitable method for real-time applications. There are other techniques, most importantly, the *digital waveguide method*, that, in many cases, have better properties with respect to computational complexity. However, as the FDM is closely related to these methods, and consequently many of the achievements made while examining its properties directly apply to other techniques, according to the opinion of the author, studying the finite difference method is a good starting point for anyone who is interested in physics-based modeling of musical instruments.

Besides the examination of some of the most recent developments in the field of membrane modeling, one of the main objects of writing this thesis was to review and summarize the very basics of the FDM in a thorough yet relatively easily understandable way. For this purpose, most of the mathematical relations that have turned up during the research were derived and reviewed by the author. While this has helped the author himself to comprehend the details of finite difference modeling, it also made it possible to unify the different types of notation used in the literature into a uniform notational framework. Many of the derivations are included in this thesis in order to help the reader in the interpretation of the results. The author is hopeful that in consequence, the reader unfamiliar yet interested in physical modeling of musical instruments can use this thesis as an introductory textbook that can be profitably consulted. A comprehensive review and comparison of various physics-based sound synthesis methods can be found in [Välimäki et al. 2006].

The thesis is divided into three main parts. In Chapter 2, the mathematical models, i.e., the PDEs of some basic vibrating physical structures will be presented. As the thesis is manly devoted to the discretization and numerical analysis of these mathematical models, only the essentials of this field will be reviewed. These include general remarks on partial differential equations, the wave equation in one and two dimensions and the concept of normal modes and spatial frequency. Emphasis will be laid on the formulation of the two-dimensional wave equation in different coordinate systems and on the boundary conditions that correspond to a circular membrane. At the and of the chapter, more accurate models of the acoustic membrane will be presented, which take some perceptually important physical phenomena into account.

In Chapter 3, the fundamentals of the finite difference method will be presented in great detail. As an illustrative example, the model of an ideal string will be used. The concepts of convergence, consistency and stability introduced in this chapter form the framework for the analysis of the discretized models throughout the thesis. It will be shown that one of the most important properties of a finite difference model is numerical stability. For

[1] According to [Trefethen 1996, p. 147], the finite difference method was first used by L. F. Richardson in his book *Weather Prediction by Numerical Processes*, first published in 1922.

the analysis of discretized models from this point of view, the method of von Neumann analysis will be presented. This technique will prove to be useful also at examining the dispersion properties of a model.

In Chapter 4, the results of the previous chapter will be extended and used for deriving and examining several types of finite difference membrane models. The basic model introduced at the beginning of the chapter will be improved in two distinct ways, which correspond to the results of Chapter 2: on one hand, different types of discretization based on the Cartesian and the triangular coordinate systems will be presented and analyzed, on the other hand, the membrane model will be extended with damping and nonlinear behavior. Special emphasis will be laid on the discussion of numerical dispersion in two dimensions. A comparison of several types of membrane models will be presented in Section 4.5.

Chapter 2

Partial Differential Equations for Oscillating Mechanical Systems

In this chapter, we will present the mathematical models for the two basic structures that will be discussed in the subsequent chapters: the string and the membrane. In Section 2.1, we will briefly summarize the basic properties of partial differential equations. In Section 2.2, the one-dimensional wave equation will be presented. By examining the solutions of the boundary-value problem, the concept of normal modes will be introduced. In Section 2.3, several forms of the two-dimensional wave equation will be examined: the wave equation in the Cartesian, cylindrical and triangular coordinate systems. It will be shown how the boundary conditions corresponding to a circular membrane can be transformed to each of these coordinate systems. The cylindrical form of the wave equation will not be discretized in the subsequent chapters, however, its analytical solution yields the frequencies of the normal modes, which can be used for comparison with the modal frequencies of the discretized membrane models. For the Cartesian form of the PDE, it will be shown how to include some physical phenomena, namely, damping and nonlinear behavior, that are essential for a natural sounding membrane model.

2.1 General Remarks on Partial Differential Equations

A partial differential equation (PDE) is an equation that contains partial derivatives of the unknown function. PDEs can be written in the general form of

$$P\{u\} = f. \tag{2.1}$$

P is a differential operator, u is a function of several variables. For example, the equation of an ideal string is

$$\frac{\partial^2 u}{\partial t^2} - c^2 \frac{\partial^2 u}{\partial x^2} = 0 \tag{2.2}$$

or, in a shorter notation,

$$u_{tt} - c^2 u_{xx} = 0. \tag{2.3}$$

The two types of notation are equivalent. In this equation the differential operator is defined by

$$P\{u\} = \frac{\partial^2 u}{\partial t^2} - c^2 \frac{\partial^2 u}{\partial x^2} \tag{2.4}$$

and f is identically zero.

The *order* of the PDE is the greatest number of derivatives in any term of P. If P is a linear operator, that is,

$$P\{a_1 u_1 + a_2 u_2\} = a_1 P\{u_1\} + a_2 P\{u_2\} \tag{2.5}$$

where a_1 and a_2 are arbitrary constants, u_1 and u_2 are functions, then the PDE is *linear*. If f is identically zero, then the equation is called *homogeneous*, otherwise it is *inhomogeneous*. Hereafter, we will only deal with *homogeneous linear* equations. In this thesis, the function u denotes the displacement of a string or a membrane, and depends on the time and one or two space variables.

Differential equations have in general infinite number of solutions. In order to specify a particular one, *initial conditions* have to be provided. For a PDE of second order with respect to time, u and u_t has to be given at the initial time $t = 0$.

While investigating a phenomenon, we are generally interested in the behavior of the physical system over a finite, bounded domain of space. This domain can be specified by *boundary conditions*. For example, boundary conditions can be used to describe how a string of finite length is terminated at its ends. In this thesis, we will only use boundary conditions that specify identically zero displacement outside a bounded domain of space, however, in general, time-dependent boundary conditions can also be specified. A partial differential equation with its initial and boundary conditions is called an *initial-boundary value problem*.

In order to be suited for numerical analysis, a PDE has to be *well posed* as an initial value problem. A well posed problem satisfies the following conditions:

- The solution exists
- The solution is unique
- The solution is stable

Uniqueness means that at most one function satisfies the PDE with the given initial and boundary conditions. Stability, in this sense, means that with arbitrary small difference in the initial and boundary conditions, the difference of the solutions cannot be arbitrary large, that is, the solution depends continuously on the initial and boundary conditions. Although they are closely related, the stability of initial value problems should not be confused with the stability of finite difference schemes that will be defined in Chapter 3.

In [Bensa et al. 2003], a general class of wave-equations with one spatial dimension is shown to be well posed using a method based on the spatial Fourier-transform. The method described can also be applied to problems with more spatial dimensions, thus the

well posedness of the initial-value problems reviewed in this thesis can be easily verified. As detailed analysis of PDEs is outside the scope of this thesis, knowing that the problems under review are well posed, no further attention to this topic will be paid. More information on well posedness can be found, e.g., in [Zwillinger 1997, Section 24].

2.2 The Wave Equation in One Dimension: Modeling a String

First, let us consider the one dimensional wave equation, as follows (see [Kinsler et al. 1999, p. 39]):

$$\frac{\partial^2 u}{\partial t^2} = c^2 \frac{\partial^2 u}{\partial x^2}. \tag{2.6}$$

Eq. (2.6) may be regarded as the mathematical model of an ideal string (a string with no dissipation due to internal or external effects) of infinite length. The function $u = u(x,t)$ denotes the transversal displacement that depends on the position along the string, x, and the time t. The parameter c is called the *phase speed* or *phase velocity* and it is determined by the tension and the mass of the string as follows:

$$c = \sqrt{\frac{T}{\rho_L}} \tag{2.7}$$

where T is the tension in N, and ρ_L is the linear mass density in kg/m. The general solution can be written in the following form[1]:

$$u(x,t) = u_1(ct - x) + u_2(ct + x). \tag{2.8}$$

That is, the solution consists of two waves travelling in opposite directions without loss or distortion. The functions $u_1(x)$ and $u_2(x)$ are determined by the initial and boundary conditions. As initial conditions, the initial displacement $u(x,0)$ and initial velocity $u_t(x,0)$ have to be given. Boundary conditions are determined by the way the string is terminated at its ends. For a string of length L with fixed ends the following boundary conditions will be used:

$$u(x,t) = 0 \qquad \text{if} \qquad |x - x_0| \geq \frac{L}{2} \tag{2.9}$$

where x_0 denotes the midpoint of the string. Without loss of generality, we will use $x_0 = L/2$, which implies that the two ends of the string correspond to the points with $x = 0$ and $x = L$, respectively. As in this case

$$u(0,t) = u_1(ct - 0) + u_2(ct + 0) = 0 \tag{2.10}$$

it is clear that $u_1(x) = -u_2(x)$ which means that the incoming waves at fixed ends are reflected with inverted phase. It can also be shown that $u_1(x)$ equals to the half of the initial displacement. These results are illustrated in Fig. 2.1 and 2.2.

[1] This solution of the wave equation was found by d'Alembert in 1747.

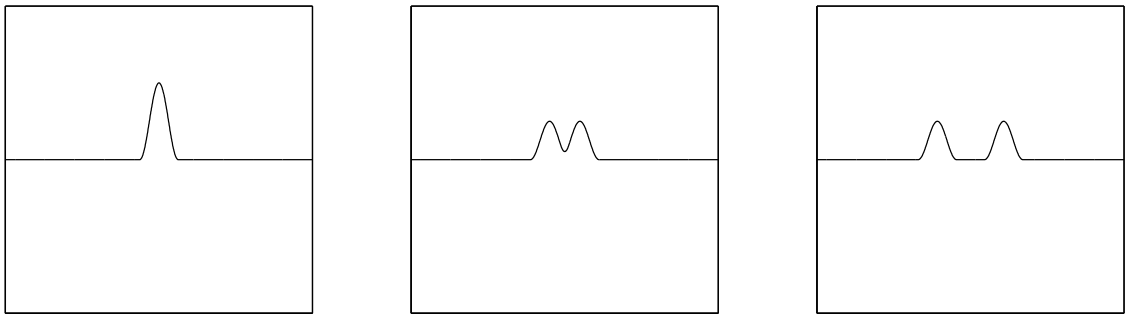

Figure 2.1: Solution of the one-dimensional wave equation at consequtive time steps with the initial displacement specified.

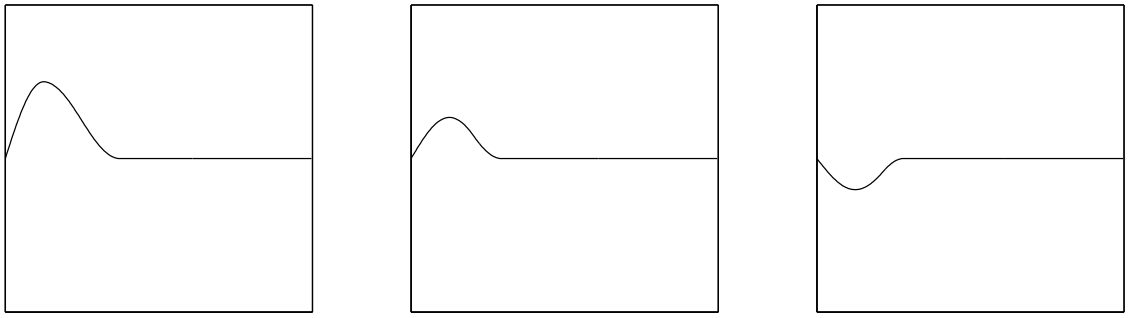

Figure 2.2: Reflection of the waves at the left-hand side boundary in the case of a string with fixed ends. The figures display the displacement of the string at consequtive time steps.

The solution can also be written in the following form (see, e.g., [Kinsler et al. 1999, p. 53]):

$$u(x,t) \quad = \quad \sum_n C_n \cos\left(\omega_n t + \phi_n\right) \sin \beta_n x \tag{2.11}$$

where

$$\beta_n = \frac{\pi n}{L} = \frac{\omega_n}{c} = 2\pi \frac{f_n}{c} \tag{2.12}$$

is the *wave number* or spatial frequency. From the definition, it is apparent that the unit of β is rad/m. The frequency ω_1 is called the fundamental frequency and $\omega_n = n\omega_1$ are the overtones (for $n \geq 2$). The space-dependent $\sin \beta_n x$ functions are the *normal modes*. It can be seen in Eq. (2.12) that only discrete values of ω_n and β_n are allowed, and these values are determined by the boundary conditions. The constants C_n and ϕ_n depend on the initial conditions and can be obtained by means of Fourier analysis (see [Kinsler et al. 1999, p. 54]).

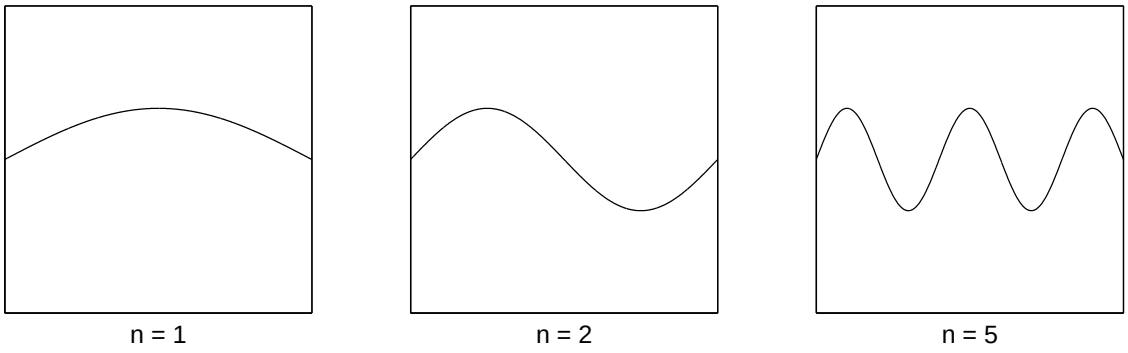

Figure 2.3: Normal modes of a string

2.3 The Wave Equation in Two Dimensions: Modeling a Membrane

2.3.1 The Wave Equation in Cartesian Coordinate System

The two-dimensional wave equation in Cartesian coordinate system is

$$\frac{\partial^2 u}{\partial t^2} = c^2 \left(\frac{\partial^2 u}{\partial x^2} + \frac{\partial^2 u}{\partial y^2} \right). \tag{2.13}$$

Beside time, the displacement u depends on the position along both the x and y axes. Thus, the initial displacement and the initial velocity is given as $u(x, y, 0) = u_0(x, y)$ and $u_t(x, y, 0) = u_{t,0}(x, y)$, respectively. The phase velocity c is now defined as

$$c \;=\; \sqrt{\frac{\mathscr{T}}{\rho_S}} \tag{2.14}$$

The parameter $\mathscr{T}$ is the membrane tension in N/m, and ρ_S is the surface mass density in kg/m^2. It is assumed that the membrane is stretched uniformly in all directions, and a line segment of length dl is pulled apart with a force $\mathscr{T} dl$. This assumption is only valid if the displacement of the membrane is small because the tension in a real membrane is not independent on the displacement. A more realistic model, which takes this phenomenon into account will be introduced in Section 2.3.5.

The shape of the membrane is determined by the boundary conditions. A square membrane of the size $L \times L$ with fixed rim can be modeled using the boundary conditions

$$u(x, y, t) = 0 \qquad \text{if} \qquad |x - x_0| \geq \frac{L}{2} \qquad \text{or} \qquad |y - y_0| \geq \frac{L}{2} \tag{2.15}$$

where x_0 and y_0 denote the coordinates of the center of the membrane. Similarly to the one-dimensional case, the solution can be written as a superposition of normal modes:

$$u(x, y, t) \;=\; \sum_n \sum_m C_{n,m} \cos\left(\omega_{n,m} t + \phi_{n,m}\right) \sin \beta_n x \sin \beta_m y. \tag{2.16}$$

The normal modes are defined by the wave numbers $\beta_n = \frac{n\pi}{L}$ and $\beta_m = \frac{m\pi}{L}$. Frequencies of

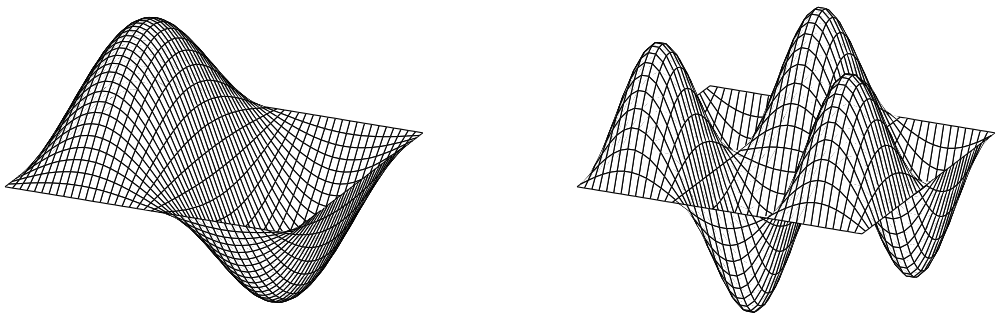

Figure 2.4: Normal modes of a square membrane for $(n, m) = (2, 1)$ and $(3, 2)$

the normal modes can be calculated by the following formula [Fletcher and Rossing 1998]:

$$\omega_{n,m} = 2\pi f_{n,m} = c\sqrt{\beta_n^2 + \beta_m^2}. \tag{2.17}$$

Values of the mode frequencies will be used to verify if the discretized model is a good approximation of the physical phenomenon.

Boundary conditions for a circular membrane in Cartesian coordinate system are

$$u(x, y, t) = 0 \qquad \text{if} \qquad (x - x_0)^2 + (y - y_0)^2 \geq R^2 \tag{2.18}$$

that is, the displacement is zero in every point whose distance from the center (x_0, y_0) is greater than or equal to the radius of the membrane. This form of circular boundary conditions will be useful while discretizing the model in Cartesian coordinate system. For analytical solution, however, it is more convenient to use a different form of the differential equation.

2.3.2 The Wave Equation in Cylindrical Coordinate System

The wave equation in cylindrical coordinates is

$$\frac{\partial^2 u}{\partial t^2} = c^2 \left(\frac{\partial^2 u}{\partial r^2} + \frac{1}{r}\frac{\partial u}{\partial r} + \frac{1}{r^2}\frac{\partial^2 u}{\partial \Theta^2} \right). \tag{2.19}$$

If the center of the membrane is the point for which $r = 0$ then the boundary conditions for a circular membrane can be written in a simpler form:

$$u(r, \Theta, t) = 0 \qquad \text{if} \qquad r \geq R. \tag{2.20}$$

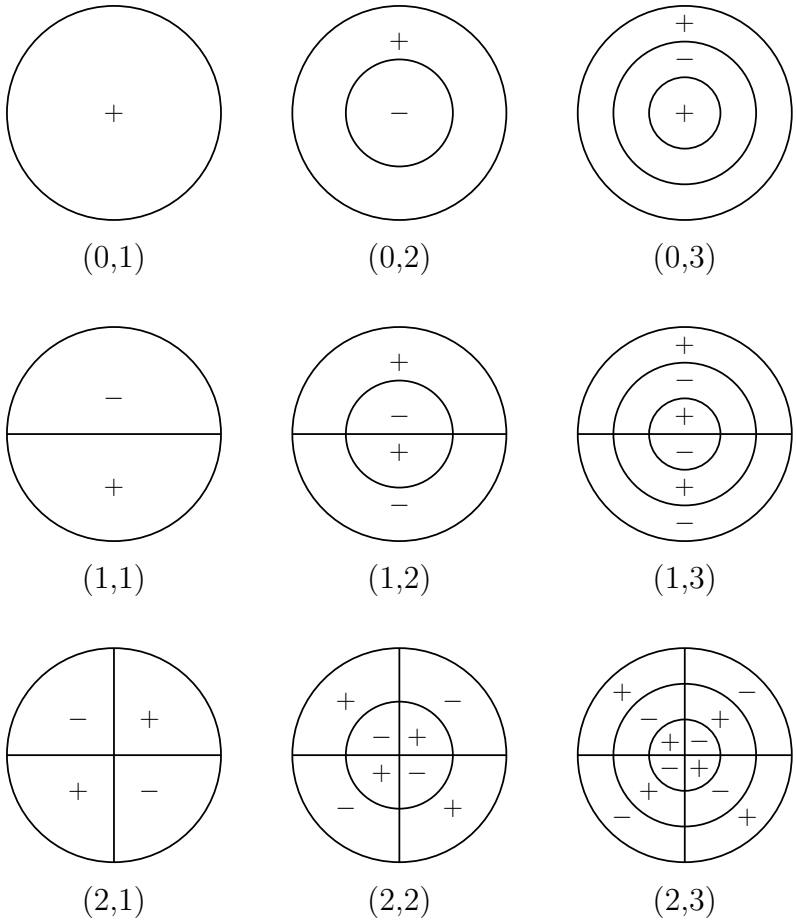

Figure 2.5: Normal modes of the circular membrane. At any time, the values of displacement of the membrane sections denoted by '+´ and '−´, respectively, are of opposite sign.

The solution for Eq. (2.19) can also be written as a superposition of normal modes (see Fig. 2.5). The modes of the circular membrane can be analitically expressed using Bessel functions, however, for the purpose of model verification, knowing the mode frequencies is sufficient. According to [Fletcher and Rossing 1998], the fundamental frequency can be calculated using the formula

$$f_{0,1} = \frac{2.405}{2\pi R} c. \tag{2.21}$$

Mode frequencies for other modes can be calculated by multiplying $f_{0,1}$ by the relative frequency of the mode of interest. Some of the relative frequencies are listed in Table 2.1.

The relation between the temporal and spatial frequency of a normal mode can be written in the following form (see [Kinsler et al. 1999, p. 97]):

$$f_{m,n} = \beta_{m,n} \frac{c}{2\pi}. \tag{2.22}$$

$f_{0,1} = 1.000 f_{0,1}$	$f_{2,2} = 3.501 f_{0,1}$
$f_{1,1} = 1.594 f_{0,1}$	$f_{0,3} = 3.600 f_{0,1}$
$f_{2,1} = 2.136 f_{0,1}$	$f_{5,1} = 3.652 f_{0,1}$
$f_{0,2} = 2.296 f_{0,1}$	$f_{3,2} = 4.060 f_{0,1}$
$f_{3,1} = 2.653 f_{0,1}$	$f_{6,1} = 4.154 f_{0,1}$
$f_{1,2} = 2.918 f_{0,1}$	$f_{1,3} = 4.230 f_{0,1}$
$f_{4,1} = 3.156 f_{0,1}$	$f_{2,3} = 4.832 f_{0,1}$

Table 2.1: Relative mode frequencies of the circular membrane ([Fletcher and Rossing 1998], [Kinsler et al. 1999]).

2.3.3 The Wave Equation in Triangular Coordinate System

There is another form of the wave equation that proves itself to be useful during spatial discretization, namely, the equation in triangular coordinates. The triangular coordinate system is defined by the x and w axes, whose relative angle is 60° (see Fig. 2.6). The reason for using a third axis, z, is that it leads to a simpler form of the equation. Eq. (2.13) in triangular coordinates is

$$\frac{\partial^2 u}{\partial t^2} = c^2 \frac{2}{3} \left(\frac{\partial^2 u}{\partial x^2} + \frac{\partial^2 u}{\partial w^2} + \frac{\partial^2 u}{\partial z^2} \right). \tag{2.23}$$

The derivation of this equation can be found in Appendix A. We will not attempt to solve this equation analytically, as it has no advantages over the above-mentioned forms regarding the boundary conditions. However, as it will be shown, Eq. (2.23) does have some attractive properties with respect to spatial discretization.

Let us express the circular boundary conditions in triangular coordinates. The unit vector along the w axis ($\mathbf{e_w}$) is defined as

$$\mathbf{e_w} = \frac{1}{2}\mathbf{e_x} + \frac{\sqrt{3}}{2}\mathbf{e_y}. \tag{2.24}$$

where $\mathbf{e_x}$ and $\mathbf{e_y}$ form the basis of the Cartesian coordinate system. For any $\mathbf{a}$ vector in the triangular coordinate system it is true that

$$\mathbf{a} = x'\mathbf{e_x} + w\mathbf{e_w} = \tag{2.25}$$

$$= x'\mathbf{e_x} + w\left(\frac{1}{2}\mathbf{e_x} + \frac{\sqrt{3}}{2}\mathbf{e_y}\right) = \tag{2.26}$$

$$= \left(x' + \frac{w}{2}\right)\mathbf{e_x} + \left(\frac{\sqrt{3}}{2}w\right)\mathbf{e_y}. \tag{2.27}$$

According to Eq. (2.27), the Cartesian coordinates of any vector, provided its triangular coordinates are known, can be obtained by the following linear transform:

$$\begin{bmatrix} x \\ y \end{bmatrix} = \begin{bmatrix} 1 & 1/2 \\ 0 & \sqrt{3}/2 \end{bmatrix} \begin{bmatrix} x' \\ w \end{bmatrix} \tag{2.28}$$

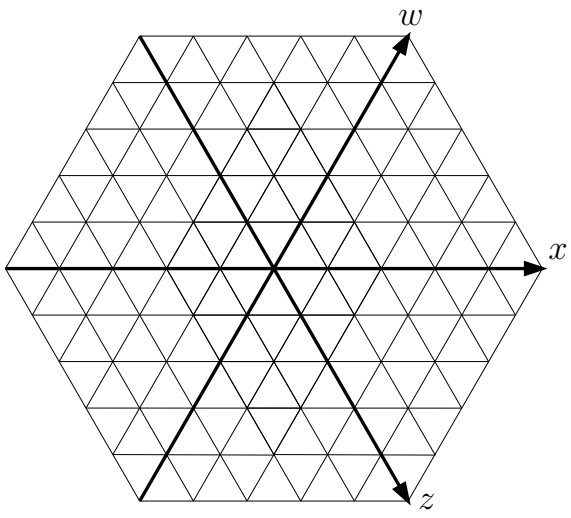

Figure 2.6: The triangular coordinate system

or by using vector notation

$$\mathbf{x} \;=\; \mathbf{S}^{-1}\mathbf{x}' \tag{2.29}$$

where $\mathbf{x} = [\ x \quad y\ ]^{\mathrm{T}}$ and $\mathbf{x}' = [\ x' \quad w\ ]^{\mathrm{T}}$, $^{\mathrm{T}}$ denotes transposition. Eq. (2.28) can be inverted, thus

$$\mathbf{x}' \;=\; \mathbf{S}\mathbf{x} \tag{2.30}$$

where

$$\mathbf{S} = \begin{bmatrix} 1 & 1/2 \\ 0 & \sqrt{3}/2 \end{bmatrix}^{-1} = \begin{bmatrix} 1 & -\sqrt{3}/3 \\ 0 & 2\sqrt{3}/3 \end{bmatrix}. \tag{2.31}$$

The boundary condition

$$u(x, y, t) = 0 \qquad \text{if} \qquad (x - x_0)^2 + (y - y_0)^2 \geq R^2 \tag{2.32}$$

thus can be written as

$$u(x', w, t) = 0 \qquad \text{if} \qquad \left(x' + \frac{w}{2} - x_0\right)^2 + \left(\frac{\sqrt{3}}{2}w - y_0\right)^2 \geq R^2 \tag{2.33}$$

or after expressing x_0 and y_0 by their triangular coordinates x_0' and w_0:

$$u(x', w, t) = 0 \qquad \text{if} \qquad \left(x' + \frac{w}{2} - x_0' - \frac{w_0}{2}\right)^2 + \left(\frac{\sqrt{3}}{2}w - \frac{\sqrt{3}}{2}w_0\right)^2 \geq R^2. \tag{2.34}$$

2.3.4 Equations for the Damped Membrane

The PDEs discussed so far are models of vibrating systems whose total energy is constant over time (see [Fletcher and Rossing 1998]), that is, the waves do not decay. In order to obtain a more realistic model, damping has to be introduced. Damping forces arise from internal friction and air resistance, and cause the amplitude of each mode decrease over time.

The following equation takes account of these effects in the simplest way:

$$\frac{\partial^2 u}{\partial t^2} = c^2 \left(\frac{\partial^2 u}{\partial x^2} + \frac{\partial^2 u}{\partial y^2} \right) - d \frac{\partial u}{\partial t}. \tag{2.35}$$

The last term on the right-hand side of the equation represents a force whose magnitude is proportional to the transversal velocity of the string but acts in the opposite direction. In general, the damping coefficient d is frequency-dependent, that is, the modes associated with higher frequencies decay faster. However, a general $d(\omega)$ term cannot be implemented directly by finite difference schemes. According to [Bensa et al. 2003], frequency-dependent damping can be taken into account in the simplest way by replacing $d(\omega)u_t$ by

$$d_1 \frac{\partial u}{\partial t} - d_2 \frac{\partial}{\partial t} \left(\frac{\partial^2 u}{\partial x^2} + \frac{\partial^2 u}{\partial y^2} \right). \tag{2.36}$$

so Eq. (2.35) takes the following form:

$$\frac{\partial^2 u}{\partial t^2} = c^2 \left(\frac{\partial^2 u}{\partial x^2} + \frac{\partial^2 u}{\partial y^2} \right) - d_1 \frac{\partial u}{\partial t} + d_2 \frac{\partial}{\partial t} \left(\frac{\partial^2 u}{\partial x^2} + \frac{\partial^2 u}{\partial y^2} \right). \tag{2.37}$$

2.3.5 Modeling Nonlinear Behaviour

So far, only the linear model of a membrane has been presented. Linearity, in the case of modeling a membrane of a drum, means that if only the amplitude of the excitation is changed then the displacement-time function for any point of the membrane is unchanged in shape, only scaled by a constant factor. However, in the case of many types of drums (e.g., tom-tom, tabla), one of the main features of the sound is that the playing strength, that is, the dynamic level of the excitation affects the sound in a nonlinear[2] way: the pitch of the sound is lowered over time and this effect is more audible if the drum is struck harder (more information on this topic including measurements of several drums can be found in [Dahl 1997]).

This phenomenon is due to the fact that the membrane tension is actually not constant, it depends on the displacement of the membrane, which changes continuously. According to Eq. (2.14), the phase speed, c, is dependent on the tension, and according to Eq. (2.17) and (2.21), the modal frequencies of the membrane depend on the phase speed, which explains why the pitch of the sound is changing over time. The method for obtaining a nonlinear membrane model presented below is referred to as *tension modulation*.

[2]This type of nonlinearity is due to the geometry of the problem, the material of the membrane is assumed to be linear.

The geometric nonlinearity can be taken into account by the following form of the wave equation:

$$\frac{\partial^2 u}{\partial t^2} = \left(\frac{\mathscr{T}(u)}{\rho_S}\right)\left(\frac{\partial^2 u}{\partial x^2} + \frac{\partial^2 u}{\partial y^2}\right). \tag{2.38}$$

As the displacement depends on the variables x, y and t, the tension $\mathscr{T}$ is actually dependent on these variables. Let us assume that the longitudinal waves propagate much faster than the transversal ones. In this case, the tension can be regarded uniform throughout the entire area of the membrane at any time t, and it only depends on the surface of the membrane. As the surface depends only on time, the tension is also dependent only on time. According to [Petrausch and Rabenstein 2005], the following relation can be derived for $\mathscr{T}(t)$:

$$\mathscr{T}(t) \quad = \quad \mathscr{T}_0 + \mathscr{T}_1(t) \tag{2.39}$$

where $\mathscr{T}_0$ is the tension of the membrane with zero displacement, and $\mathscr{T}_1(t)$ is defined as

$$\mathscr{T}_1(t) \quad = \quad \frac{1}{4}\frac{E}{1-p}\frac{1}{L^2}\int_0^L\int_0^L \left(u_x^2 + u_y^2 + \frac{1}{2}u_x^2 u_y^2\right) dxdy. \tag{2.40}$$

The parameters E and p are material constants, the Young-modulus and the Poisson-ratio, respectively, and L is the length along side of the membrane. It will prove to be useful to introduce the scaling factor a_S in the following way:

$$\mathscr{T}(t) \quad = \quad \mathscr{T}_0 + a_S\mathscr{T}_1(t). \tag{2.41}$$

The scaling factor can be used to adjust the properties of the discretized model. Consequently, Eq. (2.38) can be written in the following form:

$$\frac{\partial^2 u}{\partial t^2} = \left(\frac{\mathscr{T}_0 + a_S\mathscr{T}_1(t)}{\rho_S}\right)\left(\frac{\partial^2 u}{\partial x^2} + \frac{\partial^2 u}{\partial y^2}\right). \tag{2.42}$$

It is easy to see that the nonlinear form of the rest of the PDEs can be obtained by making the substitution

$$c^2 \quad = \quad \frac{\mathscr{T}_0 + a_S\mathscr{T}_1(t)}{\rho_S}. \tag{2.43}$$

Accordingly, the nonlinear equation for the damped membrane can be written as

$$\frac{\partial^2 u}{\partial t^2} = \left(\frac{\mathscr{T}_0 + a_S\mathscr{T}_1(t)}{\rho_S}\right)\left(\frac{\partial^2 u}{\partial x^2} + \frac{\partial^2 u}{\partial y^2}\right) - d_1\frac{\partial u}{\partial t} + d_2\frac{\partial}{\partial t}\left(\frac{\partial^2 u}{\partial x^2} + \frac{\partial^2 u}{\partial y^2}\right). \tag{2.44}$$

We will not attempt to solve these equations analytically, however, it will be shown in Chapter 4 that the finite difference method can be easily applied to obtain a discretized model that takes geometrical nonlinearity into account.

Chapter 3

Introduction to the Finite Difference Method

In this chapter, we will introduce the fundamental concepts of finite difference modeling. For this purpose, the ideal string will be used as an demonstrative example. In Section 3.1, a simple *finite difference scheme* (FDS) for the ideal string will be derived and implemented. The *difference operator* notation will be introduced, which will be used also in the subsequent chapters. In Section 3.2, after introducing the *shift operator* notation, the concepts of *convergence*, *consistency*, *stability*, *accuracy* and *numerical dispersion* will be defined and explained. Many of the definitions and theorems presented in this chapter are based on [Strikwerda 1989], however, they are interpreted from the point of view of instrument modeling.

3.1 Modeling a String with Finite Difference Schemes

As an example, let us attempt to solve numerically the following initial-boundary value problem:

$$\begin{aligned} u_{tt} &= c^2 u_{xx} && \text{(PDE)} \\ u_0(x) &= f(x) && \text{(initial conditions)} \\ u_{t,0}(x) &= 0 && \\ u(0,t) = u(L,t) &= 0 && \text{(boundary conditions).} \end{aligned} \tag{3.1}$$

Equation (3.1) corresponds to an ideal string fixed at its ends with zero initial velocity and nonzero initial displacement. The initial velocity is set to zero for simplicity, however, nonzero initial velocity would not cause much difficulty. The solution will be approximated only in discrete points, so let us introduce the grid function v that is defined over the grid $(x_m, t_n) = (mh, nk)$. This function, which is actually a two-dimensional sequence, is used to approximate the values of the continuous function u in the points of the grid. The parameters h and k are the grid spacings, i.e., the distance of two grid points in space and time, respectively, m and n are arbitrary integers. Consequently, $k = 1/f_s$ where f_s is the sampling frequency. The value of v in the grid point (mh, nk) is denoted as v_m^n. The same notation is used for the values of continuous functions in the grid points, e.g., $(u_t)_m^n$

denotes $u_t(mh, nk)$. The points of the grid at $t = nk$ will be referred to as *grid level* n. According to the definition of derivation for continuously differentiable functions,

$$(u_t)_m^n = \lim_{k\to 0} \frac{u_m^{n+1} - u_m^n}{k} = \lim_{k\to 0} \frac{u_m^n - u_m^{n-1}}{k} = \lim_{k\to 0} \frac{u_m^{n+1} - u_m^{n-1}}{2k} \tag{3.2}$$

and

$$(u_x)_m^n = \lim_{h\to 0} \frac{u_{m+1}^n - u_m^n}{h} = \lim_{h\to 0} \frac{u_m^n - u_{m-1}^n}{h} = \lim_{h\to 0} \frac{u_{m+1}^n - u_{m-1}^n}{2h}. \tag{3.3}$$

The first order derivatives of u may be approximated by the terms

$$(u_t)_m^n \approx \frac{v_m^{n+1} - v_m^n}{k} = \delta_{t+}\{v_m^n\} \tag{3.4}$$

$$(u_t)_m^n \approx \frac{v_m^n - v_m^{n-1}}{k} = \delta_{t-}\{v_m^n\} \tag{3.5}$$

$$(u_t)_m^n \approx \frac{v_m^{n+1} - v_m^{n-1}}{2k} = \delta_{t0}\{v_m^n\} \tag{3.6}$$

$$(u_x)_m^n \approx \frac{v_{m+1}^n - v_m^n}{h} = \delta_{x+}\{v_m^n\} \tag{3.7}$$

$$(u_x)_m^n \approx \frac{v_m^n - v_{m-1}^n}{h} = \delta_{x-}\{v_m^n\} \tag{3.8}$$

$$(u_x)_m^n \approx \frac{v_{m+1}^n - v_{m-1}^n}{2h} = \delta_{x0}\{v_m^n\} \tag{3.9}$$

where δ_{t+}, δ_{t-} and δ_{t0} are the forward, backward and central time difference operators, respectively. Similarly, δ_{x+}, δ_{x-} and δ_{x0} are the forward, backward and central space difference operators. Accordingly, Eq. (3.4) and (3.7) are called forward-time and forward-space approximations of the first order derivatives, etc. By applying these operators repeatedly, the following approximations for the second order derivatives can be obtained[1]:

$$(u_{tt})_m^n \approx \delta_{t+}\delta_{t-}\{v_m^n\} = \frac{v_m^{n+1} - 2v_m^n + v_m^{n-1}}{k^2} \tag{3.10}$$

$$(u_{xx})_m^n \approx \delta_{x+}\delta_{x-}\{v_m^n\} = \frac{v_{m+1}^n - 2v_m^n + v_{m-1}^n}{h^2} \tag{3.11}$$

The second order operators $\delta_{t+}\delta_{t+}$ and $\delta_{x+}\delta_{x-}$ will also be denoted as δ_t^2 and δ_x^2, respectively. Now let us replace the derivatives the PDE in Eq. (3.1) by the expressions on the right-hand side of Eq. (3.6) and (3.9), so we obtain

$$\frac{v_m^{n+1} - 2v_m^n + v_m^{n-1}}{k^2} = c^2 \frac{v_{m+1}^n - 2v_m^n + v_{m-1}^n}{h^2}. \tag{3.12}$$

Eq. (3.12) is a *finite difference scheme* for the one-dimensional wave equation. It can be seen that in Eq. (3.12) only one term, namely v_m^{n+1} is on grid level $n + 1$. Expressing this term, we obtain

$$v_m^{n+1} = c^2\lambda^2 \left(v_{m+1}^n + v_{m-1}^n\right) + 2\left(1 - c^2\lambda^2\right) v_m^n - v_m^{n-1} \tag{3.13}$$

[1]For clarity, we will use the notational shortcut $P_1\{P_2\{u\}\} = P_1P_2\{u\}$ if an operator (P_1) is applied to another operator (P_2).

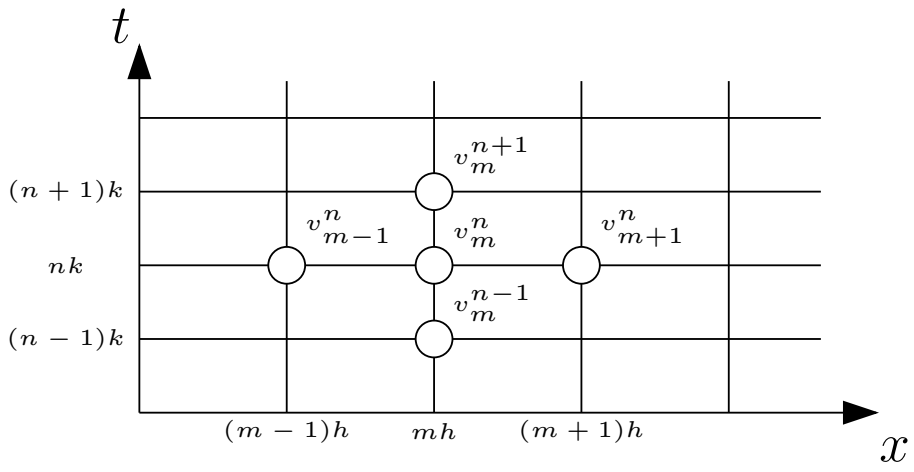

Figure 3.1: Grid points involved in calculating v at the next time step.

The parameter $\lambda = k/h$ is called the *mesh ratio*. Fig. 3.1 can be regarded as a graphical representation of this equation.

If the values of v on grid level $n+1$ can be explicitly expressed like in Eq. (3.13), then the scheme is called *explicit*, otherwise it is *implicit*. The main advantage of using explicit schemes is the inherent ease of implementation. Calculating implicit schemes can be performed by solving a set of linear algebraic equations in every time step. As this is more computationally demanding than calculating explicit schemes, implicit schemes are, in general, less suitable for real-time implementation. For this reason, only explicit schemes are discussed in this thesis.

Eq. (3.13) is called a *two-step scheme* as two time levels, namely, n and $n-1$ are involved in calculating the new values of v_m^n. Both from practical and theoretical point of view, it is advantageous to use two-step and not three- or other multistep schemes for second order PDEs with respect to time since the computational complexity is lower and the relations derived are easier to interpret and evaluate.

From Eq. (3.13), it is clear that if v_m^n is known for all values of m and for any two consecutive values of n, then v can be calculated for any values of m and n by repeatedly applying the difference equation. The value of v_m^0 can be obtained by sampling the initial conditions of Eq. (3.1) as follows:

$$v_m^0 = u_m^0 = u_0(mh). \tag{3.14}$$

The value of v_m^1 can be obtained by using the Taylor-series expansion of u_m^1:

$$u_m^1 \approx u_m^0 + k(u_t)_m^0. \tag{3.15}$$

As in our case the initial velocity $u_{t,0}$ is identically zero, the above expression is simplified to

$$u_m^1 \approx u_m^0 \tag{3.16}$$

```
vold = init_displacement;
vmiddle = init_displacement;
vnew = zeros(1,M);

for ii = 1 : N,
    vmiddle_right = vmiddle(3:M);
    vmiddle_left = vmiddle(1:M-2);

    vnew(2:M-1) = a1*(vmiddle_left + vmiddle_right) ...
                + a2*vmiddle(2:M-1) - vold(2:M-1);
    vnew(1) = 0;
    vnew(M) = 0;

    vold = vmiddle;
    vmiddle = vnew;
end
```

Figure 3.2: MATLAB code extract for modeling the ideal string. *vold*, *vmiddle* and *vnew* denote the arrays of v_m^{n-1}, v_m^n and v_m^{n+1}, respectively. The parameter M corresponds to Γ, which is defined by the equation $(\Gamma - 1)h = L$.

that is, the displacement of the string at time step one can be written as

$$v_m^1 = v_m^0 = u_0(mh). \tag{3.17}$$

Due to the boundary conditions, the displacement at the endpoints of the string has to be set to zero for all time steps, that is,

$$v_0^n = v_{\Gamma-1}^n = 0 \tag{3.18}$$

where Γ is defined by $(\Gamma - 1)h = L$, that is, the string model consists of Γ points. Now we have the discretized form of the initial-boundary value problem:

$$v_m^{n+1} = a_1\left(v_{m+1}^n + v_{m-1}^n\right) + a_2 v_m^n - v_m^{n-1} \tag{3.19}$$

$$v_m^0 = v_m^1 = u_0(mh) \tag{3.20}$$

$$v_0^n = v_{\Gamma-1}^n = 0 \tag{3.21}$$

where $a_1 = c^2\lambda^2$, $a_2 = 2(1 - a_1)$ and $m \in [1, \Gamma - 2]$.

The values of v_m^{n-1}, v_m^n and v_m^{n+1} can be directly mapped to three arrays of length Γ. The MATLAB code extract in Fig. 3.2 is an example of implementing the finite difference string model derived so far.

3.2 Characterization of Finite Difference Schemes

The main idea behind the string model derived in the previous section was to approximate the derivatives of the differential equation by finite differences. The smaller the values of k and h are, the better the approximation is. Nevertheless, the grid spacings cannot be chosen to be arbitrary small for several reasons.

If h is small, then the unknown function in the PDE is approximated in more points. Eq. (3.13) has to be evaluated for every point, that is, smaller values of h cause increased computational load. The same is true for k, that is, if k is decreased then v_m^n has to be calculated for more values of n during a unit of time. In some applications there are other restrictions for the grid spacings. In the case of CD-quality audio, the sampling frequency f_s is 44.1 kHz. Since $k = 1/f_s$ the value of k is also determined.

Our ultimate goal is to find the finite difference scheme and the parameter values that are, in some sense, most suitable for numerically solving a given initial-boundary problem. In this section, we will introduce the mathematical concepts and methods that will form the basis of our further investigation.

3.2.1 Shift Operator Notation

We have seen in the previous section that applying the finite difference method can lead to equations that lack clarity. This is mainly due to the indices that are used to identify a particular point of the grid. In order to make the equations clearer we introduce the shift operator notation. This type of notation will prove to be useful especially in the course of analyzing schemes in higher dimensions.

Let us define the time and space shift operators as follows:

$$\begin{array}{rclcrcl} M\{v_m^n\} & = & v_{m+1}^n & & M^{-1}\{v_m^n\} & = & v_{m-1}^n \\ Z\{v_m^n\} & = & v_m^{n+1} & & Z^{-1}\{v_m^n\} & = & v_m^{n-1}. \end{array} \tag{3.22}$$

The identity operator is defined as

$$I\{v_m^n\} = v_m^n. \tag{3.23}$$

By using shift operators, the difference operators introduced in the previous section can be written as

$$\delta_{t+} = \frac{1}{k}(Z - I) \qquad \delta_{x+} = \frac{1}{h}(M - I) \tag{3.24}$$

$$\delta_{t-} = \frac{1}{k}(I - Z^{-1}) \qquad \delta_{x-} = \frac{1}{h}(I - M^{-1}) \tag{3.25}$$

$$\delta_t^2 = \frac{1}{k^2}(Z - 2I + Z^{-1}) \qquad \delta_x^2 = \frac{1}{h^2}(M - 2I + M^{-1}). \tag{3.26}$$

Every FDS in one spatial dimension can be rewritten in the following form:

$$P_{k,h}\{v_m^n\} = f_m^n \tag{3.27}$$

where $P_{k,h}$ is a finite difference operator that can be constructed as a linear combination of shift and identity operators. Eq. (3.27) can be considered as the discretized form of

the general partial differential equation $P\{u\} = f$. In this thesis we will only attempt to construct finite difference schemes for homogeneous PDEs, so the right-hand side of Eq. (3.27) will always be identically zero. However, the schemes and concepts discussed here can be easily extended for the inhomogeneous case.

As an example, let us derive the shift operator representation of the one-dimensional wave equation. Eq. (3.13) can be rewritten as

$$Z\{v_m^n\} = \left(a_1(M + M^{-1}) + a_2 I - Z^{-1}\right)\{v_m^n\}. \tag{3.28}$$

By rearranging this equation to the form of Eq. (3.27), we obtain

$$P_{k,h} = (Z + Z^{-1}) - a_1(M + M^{-1}) - a_2 I. \tag{3.29}$$

We will use the difference and shift operators for continuous functions too. For instance,

$$M\{u(x,t)\} = u(x + h, t) \tag{3.30}$$

and

$$\delta_{t+}\{u(x,t)\} = \frac{u(x,t+k) - u(x,t)}{k}. \tag{3.31}$$

All of the presented notations (index-, shift operator- and difference operator notation, sometimes mixed) will be used in this thesis because the particular equation under examination determines which one is the most favorable, so the reader should be familiar with all of them.

3.2.2 Convergence, Consistency, Stability

The most basic property a finite difference scheme is expected to have in order to be suitable for modeling purposes is that its solutions are approximating the solutions of the corresponding differential equation. In other words, the approximate solutions of the scheme converge to the exact solutions of the PDE in some sense as the grid spacings tend to zero. This property, namely, *convergence*, is a property of the solutions of the scheme, and it should not be confused with *consistency* defined later, which can be regarded as the convergence of the scheme itself.

Convergence can be defined as follows (see [Strikwerda 1989, p. 19] for an equivalent definition).

Definition 3.1: (Convergence) If any solution, v_m^n, of a finite difference scheme converges[2]to the solution of the approximated partial differential equation, $u(x,t)$, while the grid spacings k and h tend to zero, and v_m^0 converges to $u_0(x)$, then the scheme is convergent.

[2]This is not a mathematically precise definition as it is stated that a grid function converges to a continuous function, and this type of convergence has to be clearly defined. The mathematical details can be found in [Strikwerda 1989].

In general, it can be quite involved to check the convergence of a scheme directly. However, convergence can be traced back to other concepts that are easier to deal with: *consistency* and *stability*.

Definition 3.2: (Consistency of a finite difference operator) The finite difference operator $P_{k,h}$ is consistent with the differential operator P if for any smooth[3]function ϕ

$$\lim_{k,h\to 0}(P\{\phi\} - P_{k,h}\{\phi\}) \quad = \quad 0 \tag{3.32}$$

in each grid point.

Definition 3.3: (Consistency of a finite difference scheme) The FDS according to $P_{k,h}\{v\} = 0$ is consistent with the partial differential equation $P\{u\} = 0$ if $P_{k,h}$ is consistent with P.

Actually, consistency of a scheme means that the expression of the FDS itself converges to the partial differential equation as the grid spacings tend to zero.

As an example, let us show that the second order difference operator δ_t^2 is consistent with the differential operator $\frac{\partial^2}{\partial t^2}$. By using Taylor-series expansion, ϕ_m^{n+1} and ϕ_m^{n-1} can be written in the following form:

$$\phi_m^{n+1} \quad = \quad \phi_m^n + k(\phi_t)_m^n + \frac{k^2}{2}(\phi_{tt})_m^n + \frac{k^3}{6}(\phi_{ttt})_m^n + O(k^4) \tag{3.33}$$

$$\phi_m^{n-1} \quad = \quad \phi_m^n - k(\phi_t)_m^n + \frac{k^2}{2}(\phi_{tt})_m^n - \frac{k^3}{6}(\phi_{ttt})_m^n + O(k^4). \tag{3.34}$$

The big-O symbol is defined as follows:

$$f(x) \quad = \quad O(g(x)) \tag{3.35}$$

means that there exist constants C and x_0 such that

$$|f(x)| \quad \leq \quad Cg(x) \tag{3.36}$$

for all $x \geq x_0$. By using these formulae,

$$\delta_t^2\{\phi\} = \frac{\phi_m^{n+1} - 2\phi_m^n + \phi_m^{n-1}}{k^2} \quad = \quad (\phi_{tt})_m^n + O(k^2). \tag{3.37}$$

This means that

$$\lim_{k\to 0}\left(\phi_{tt} - \delta_t^2\{\phi\}\right) \quad = \quad 0 \tag{3.38}$$

for any values of n and m, that is δ_t^2 is consistent with $\frac{\partial^2}{\partial t^2}$. It is apparent that if every derivative in a PDE is approximated by consistent finite difference operators then the finite difference scheme will also be consistent with the PDE (e.g. Eq. (3.12)).

Consistency is not a sufficient condition for convergence, that is, if a finite difference scheme converges to a PDE, it does not necessarily follow that the solutions of the scheme

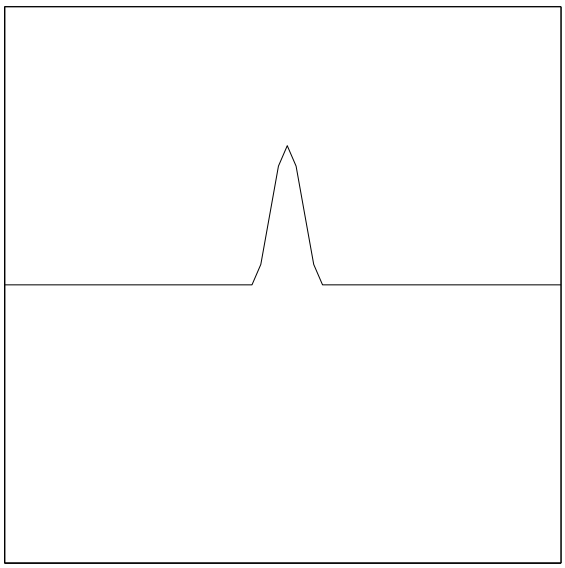

Figure 3.3: Initial displacement of the 64-point string model.

are also convergent. As an example, let us consider a 64-point string model with the initial displacement shown in Fig. 3.3. The finite difference scheme for the string was derived by using the second order difference operators, δ_x^2 and δ_t^2. These operators were shown to be consistent with the differential operators in the one-dimensional wave equation, which means that the scheme is also consistent with the PDE. According to the results of Chapter 2, we expect two waves of the shape in Fig. 3.3 travel to the left and to the right, respectively, and be reflected at the ends of the string with inverted amplitude.

This is the case in Fig. 3.4 which shows the waterfall plot of the string model with parameters $c = 1/\lambda$. The 'slices' of the waterfall plot correspond to the displacement along the string at successive time steps. It can be seen as the initial waveform breaks up into two waves travelling in opposite directions, and they are reflected at the ends of the string with inverted phase. Accordingly, the finite difference scheme with these parameters seems to be a good approximation of the one-dimensional wave equation.

On the other hand, it can be seen in Fig. 3.5, that with slightly different parameter values, the same scheme yields unacceptable results. As we will see, the solution of the scheme in this case is unbounded. Fig. 3.6 shows the same phenomenon from a different point of view: the displacement of the midpoint of the string is plotted against time.

The concept that is needed to describe this phenomenon is stability. Stability can be defined in two different ways. A finite difference scheme is said to be stable if

1. for a fixed value of k, v_m^n is bounded in some sense as $n \to \infty$.

2. for a fixed value of n, v_m^n is bounded in some sense as $k \to 0$.

Following [Strikwerda 1989], we will use the second interpretation of stability since the

[3]Smooth, in this case, means that ϕ is sufficiently differentiable so that $P\{\phi\}$ exists.

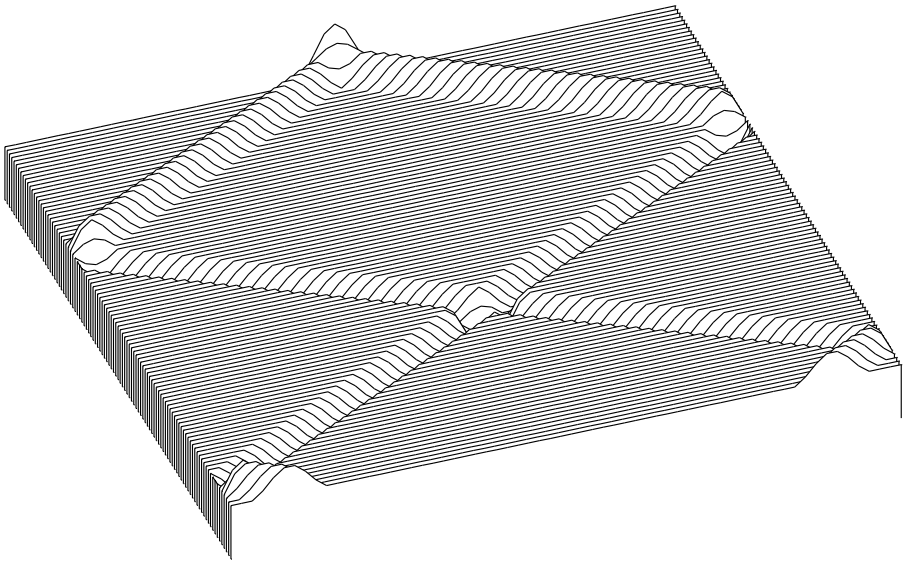

Figure 3.4: Waterfall plot of the stable string model ($c = \frac{1}{\lambda}$).

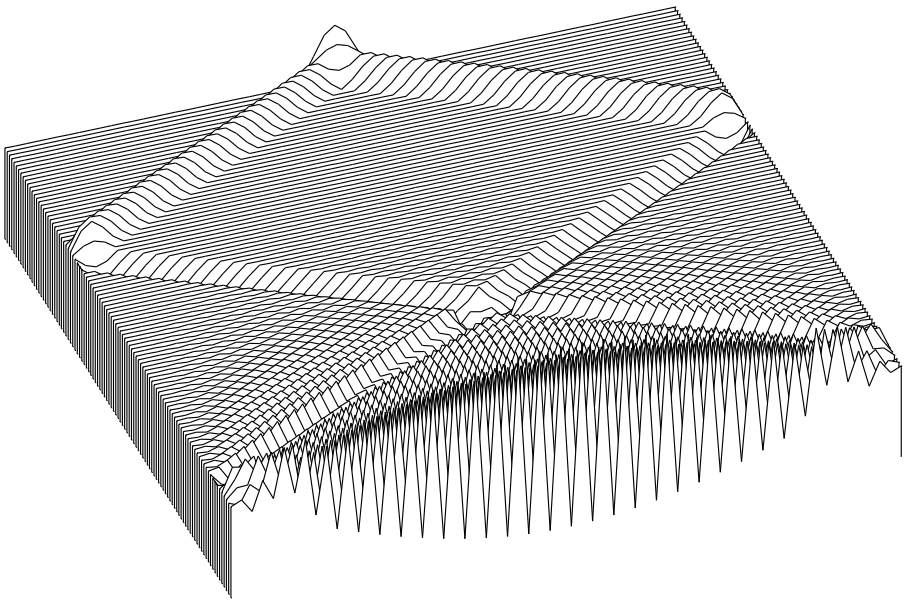

Figure 3.5: Waterfall plot of the unstable string model ($c = \frac{1.0014}{\lambda}$).

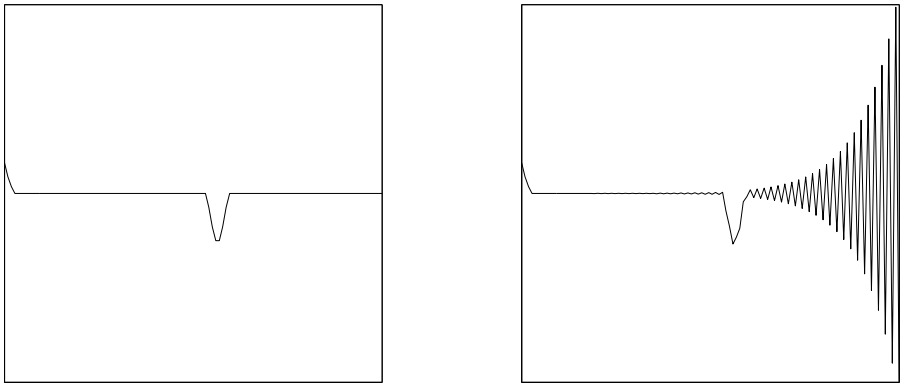

Figure 3.6: The displacement of the midpoint of the string as a function of time. The left and right-hand side figures show the numerically stable and unstable string models, respectively.

subsequent theorems and stability conditions use this definition as a starting-point. First, let us define the L^2 norm of a grid function.

Definition 3.4: (L^2 Norm of a Grid Function)

$$\| w \|_h = \sqrt{h \sum_{m=-\infty}^{\infty} |w_m|^2}. \tag{3.39}$$

Stability may be defined as follows (see [Strikwerda 1989, p. 158]):

Definition 3.5: (Stability of schemes for second-order PDEs) The finite difference scheme $P_{k,h}\{v_m^n\} = 0$ that approximates an equation that is second-order in t is stable if there is an integer I and positive numbers h_0 and k_0 such that for any positive time T, there is a constant C_T such that

$$\| v^n \|_h^2 \leq (1 + n^2)\, C_T \sum_{i=0}^{I} \| v^i \|_h^2 \tag{3.40}$$

for $0 \leq nk \leq T$, $0 < h \leq h_0$, $0 < k \leq k_0$.

Without the term $(1 + n^2)$, this definition expresses the fact that the square L^2 norm of the grid function at any time step n is bounded by the sum of the L^2 norm at the first few time steps multiplied by a constant which is not dependent on the grid spacings k and h. That is, the norm of the grid function does not blow up as k tends to zero. However, second-order PDEs without lower order derivatives allow linear growth in the solution with respect to t, that is why the term $(1 + n^2)$ has to be added. Without this modification, the definition would not allow any consistent scheme for second-order PDEs to be stable.

This definition is not very easy to apply for checking the stability of a scheme directly. However, as it will be shown in the subsequent sections, there exist simple stability conditions based on the definition above.

Now let us introduce the theorem that connects convergence to consistency and stability (see [Strikwerda 1989, p. 26]).

Theorem 3.1: (The Lax-Richtmyer Equivalence Theorem) A finite difference scheme for a partial differential equation for which the initial value problem is well posed is convergent if and only if it is consistent and stable.

The Lax-Richtmyer Equivalence Theorem is regarded as the fundamental theorem of finite difference schemes for partial differential equations. By using this theorem, convergence of a scheme can be verified without using Def. 3.1 directly. As consistency and stability can be examined with a relative ease, checking convergence becomes quite simple.

The Lax-Richtmyer Theorem has been proven using the rigorous definition of stability according to Def. 3.5. This stability definition was constructed, so that a general class of mathematical problems can be examined by the equivalence theorem. However, from the signal processing point of view, Def. 3.5 is not the most suitable formulation of stability.

As an example, let us consider the following equation of the damped string:

$$u_{tt} = c^2 u_{xx} - d_1 u_t. \tag{3.41}$$

If d_1 is positive Eq. (3.41) has solutions that decay over time. However, if d_1 is negative, then the solutions of the equation will grow arbitrary large in absolute value, unless the initial conditions are identically zero. Although this problem cannot be used for modeling real physical systems, it may be a subject to finite difference analysis. The solutions of a convergent scheme have to converge to the solutions of the PDE, that is, they also have to blow up.

According to the Equivalence Theorem, a convergent scheme is stable, that is, a scheme that is convergent to Eq. (3.41) with $d_1 < 0$ is stable in spite of the fact that it has unbounded solutions. As we are only interested in schemes whose solutions do not grow, we will treat Def. 3.5 loosely, and consider a scheme to be stable if its solutions does not blow up over time. This type of stability corresponds to the one used in linear system theory. Neither of this interpretation and the one according to Def. 3.5 implies the other, however, the schemes discussed in this thesis are either stable or unstable in both senses for the great majority of parameter values. The few exceptional cases are of rather theoretical interest, and will not be discussed here.

3.2.3 Von Neumann Stability Analysis

Von Neumann analysis is a powerful method based on the spatial Fourier-transform, which can be used effectively to examine important properties of finite difference schemes. First let us define the spatial Fourier transform for continuous and grid functions FT[Strikwerda 1989, p. 32].

Definition 3.6: (Spatial Fourier-transform) The spatial Fourier-transform of the space-dependent function $u(x)$ and the inverse formula is defined as

$$\mathscr{F}\{u(x)\} = U(\beta) = \frac{1}{\sqrt{2\pi}} \int_{-\infty}^{\infty} u(x) e^{-j\beta x} dx \tag{3.42}$$

$$\mathscr{F}^{-1}\{U(\beta)\} = u(x) = \frac{1}{\sqrt{2\pi}} \int_{-\infty}^{\infty} U(\beta) e^{j\beta x} d\beta \tag{3.43}$$

where β is the spatial frequency. The spatial Fourier-transform of the grid function v_m (discrete-space Fourier-transform) and the inverse formula is defined as

$$\mathscr{F}\{v_m\} = V(\beta) = \frac{1}{\sqrt{2\pi}}\, h \sum_{m=-\infty}^{\infty} v_m e^{-jmh\beta} \tag{3.44}$$

$$\mathscr{F}^{-1}\{V(\beta)\} = v_m = \frac{1}{\sqrt{2\pi}} \int_{-\frac{\pi}{h}}^{\frac{\pi}{h}} V(\beta) e^{jmh\beta} d\beta \tag{3.45}$$

By comparing these formulae with the well-known definition of temporal Fourier-transform, it can be seen that β is the spatial equivalent of the analog angular frequency, ω, and π/h can be regarded as the spatial (angular) Nyquist-frequency. Parseval's relation, which connects the L^2 norm of the grid function and its Fourier-transform, can be written in the following form.

Theorem 3.2: (Parseval's Relation)

$$\| V \|_h^2 = \int_{-\frac{\pi}{h}}^{\frac{\pi}{h}} |V(\beta)|^2 d\beta = h \sum_{m=-\infty}^{\infty} |v_m|^2 = \| v \|_h^2 \tag{3.46}$$

Now let us derive the shift theorem of the discrete-space Fourier-transform which will be used extensively during the analysis of finite difference schemes.

$$\mathscr{F}\{v_{m+K}\} = \frac{1}{\sqrt{2\pi}}\, h \sum_{m=-\infty}^{\infty} v_{m+K} e^{-jmh\beta} \tag{3.47}$$

By using the index variable $l = m + K$, we obtain

$$\mathscr{F}\{v_{m+K}\} = \frac{1}{\sqrt{2\pi}}\, h \sum_{l=-\infty}^{\infty} v_l e^{-j(l-K)h\beta} = \tag{3.48}$$

$$= e^{jKh\beta} \left(\frac{1}{\sqrt{2\pi}}\, h \sum_{l=-\infty}^{\infty} v_l e^{-jlh\beta} \right) = \tag{3.49}$$

$$= e^{jKh\beta} \mathscr{F}\{v_m\} \tag{3.50}$$

that is, we have obtained the following formula:

Theorem 3.3: (Shift Theorem of the Discrete-space Fourier-transform)

$$\mathscr{F}\{v_{m+K}\} = e^{jKh\beta} \mathscr{F}\{v_m\} \tag{3.51}$$

for any integer K.

The shift theorem for continuous functions can be derived in a similar fashion.

Theorem 3.4: (Shift Theorem of the Continuous-space Fourier-transform)

$$\mathscr{F}\{u(x+x_0)\} = e^{j\beta x_0}\mathscr{F}\{u(x)\} \tag{3.52}$$

Let us consider the discrete-space Fourier-transform of the FDS for the one-dimensional wave equation (Eq. (3.13))

$$v_m^{n+1} = c^2\lambda^2\left(v_{m+1}^n + v_{m-1}^n\right) + 2\left(1-c^2\lambda^2\right)v_m^n - v_m^{n-1}. \tag{3.53}$$

The Fourier-transform of the equation can be easily obtained by using the shift theorem:

$$V^{n+1}(\beta) = \left[c^2\lambda^2\left(e^{jh\beta}+e^{-jh\beta}\right) + 2\left(1-c^2\lambda^2\right)\right]V^n(\beta) - V^{n-1}(\beta) = \tag{3.54}$$

$$= 2\left[c^2\lambda^2\left(\cos h\beta - 1\right) + 1\right]V^n(\beta) - V^{n-1}(\beta) \tag{3.55}$$

where $V^n(\beta) = \mathscr{F}\{v_m^n\}$. By rearranging this equation, we obtain

$$V^{n+1}(\beta) - 2DV^n(\beta) + V^{n-1}(\beta) = 0 \tag{3.56}$$

where

$$D = c^2\lambda^2\left(\cos h\beta - 1\right) + 1. \tag{3.57}$$

Eq. (3.56) is a homogeneous linear second-order difference equation for $V^n(\beta)$ whose solution is a series of functions. Let us look for the solution of the form

$$V^n(\beta) = g(\beta)^n. \tag{3.58}$$

Note that on the left hand side of the equation, n denotes the index of the time step, however, on the right hand side it stands for raising to a power. In the following discussion, we will not always emphasize the β-dependence of g, and will write g instead of $g(\beta)$. By substituting Eq. (3.58) into Eq. (3.56), we obtain

$$g^{n+1} - 2Dg^n + g^{n-1} = 0 \tag{3.59}$$

that is,

$$\Phi(g) = g^2 - 2Dg + 1 = 0. \tag{3.60}$$

$\Phi(g)$ is called the *amplification polynomial*, whose roots, in this case, are

$$g_\pm = \frac{2D \pm \sqrt{4D^2-4}}{2} = D \pm \sqrt{D^2-1}. \tag{3.61}$$

The solution of the difference equation is

$$V^n(\beta) = A_+(\beta)g_+(\beta)^n + A_-(\beta)g_-(\beta)^n \qquad (g_+ \neq g_-) \tag{3.62}$$

$$V^n(\beta) = A_+(\beta)g_+(\beta)^n + nB(\beta)g_-(\beta)^{n-1} \qquad (g_+ = g_-) \tag{3.63}$$

where A_+, A_- and B are determined by the initial conditions. The two distinct amplification factors correspond to the two waves propagating in opposite directions along the string. It can be seen that if $g_+ \neq g_-$ and $|g_\pm| \leq 1$, then the L^2 norm of $V^n(\beta)$ will not grow over time for all values of β. According to Parseval's relation, this means that the L^2 norm of the grid function v_m^n will not grow over time either, that is, the scheme is stable. If $g_+ = g_-$ and $|g_\pm| \leq 1$ then the norm of the solution will grow at most linearly with respect to n which, according to Def. 3.5, also results in a stable scheme. According to the above, we can phrase the following stability condition:

Theorem 3.5: (Stability Condition for schemes for second-order PDEs) The necessary and sufficient condition for a finite difference scheme for a second-order PDE to be stable is that the roots g_i of its amplification polynomial $\Phi(g)$ satisfy the inequality

$$|g_i| \leq 1. \tag{3.64}$$

Let us examine what parameter values satisfy this condition. According to Eq. (3.61), there are three cases to consider:

- $D^2 < 1$

  In this case, the two roots form a conjugate complex pair whose absolute value is

  $$|g_\pm| = \sqrt{D^2 + \left(\sqrt{1 - D^2}\right)^2} = 1 \tag{3.65}$$

  that is, the scheme is stable.

- $D^2 = 1$

  In this case there is one multiple root whose absolute value is 1, so the scheme is stable.

- $D^2 > 1$, that is, $D > 1$ or $D < -1$

  If we consider Eq. (3.57) it is apparent that D cannot be greater than 1, so only the case of $D < -1$ has to be examined. In this case

  $$|g_\pm| = \left|D \pm \sqrt{D^2 - 1}\right| = -D \pm \sqrt{D^2 - 1} \tag{3.66}$$

  It can be seen that in this case $|g_-| > 1$, that is, the scheme is unstable if $D < -1$.

Our results are summarized in the following theorem.

Theorem 3.6: (Stability condition) If the amplification polynomial of a finite difference scheme is of the form

$$\Phi(g) = g^2 - 2Dg + 1 = 0 \tag{3.67}$$

where $D \leq 1$ then the necessary and sufficient condition of stability is

$$D \geq -1. \tag{3.68}$$

In the particular case of the ideal string, D is defined by Eq. (3.57), so applying the stability condition yields

$$c^2\lambda^2\left(\cos h\beta - 1\right) + 1 \quad \geq \quad -1 \tag{3.69}$$

$$c^2\lambda^2\left(\cos h\beta - 1\right) \quad \geq \quad -2. \tag{3.70}$$

For all values of β, this is satisfied if $c^2\lambda^2 \leq 1$. Since both c and λ can only take positive values, the stability condition for the finite difference scheme of the ideal string is[4]

$$\lambda \quad \leq \quad \frac{1}{c}. \tag{3.71}$$

This stability condition corresponds to our former results (plotted in Fig. 3.4 and (3.5)), namely, that the scheme with parameters $\lambda = 1/c$ is stable but with $\lambda = 1.0014/c$ (only slightly out of the stability region) it is unstable. Another remark can be made: the roots of the amplification polynomial of a stable string model are either equal (at the stability margin) or form a conjugate complex pair, i.e., their magnitudes are identical.

As, by definition, $\lambda = k/h$, the stability condition can be interpreted in several ways:

- If the grid spacings k and h are given there is a maximum value of c that yields a stable model, i.e., only problems with limited value of the phase speed can be approximated by this scheme. In the case of a string, this means an upper bound for the pitch of the sound generated by the model.

- If the parameters c and k are given, then the minimum value of h is determined, which also defines the maximum number of grid points ($\Gamma_{\max}$).

- If c and h are given, then the maximum value of k and consequently the minimum value of the sampling frequency f_s is determined.

In general, the sampling frequency is already determined by the environment (e.g., the soundcard or the D/A-converter), unless real-time sample rate conversion is used. Usually, the phase speed c is also defined by the physical parameters of the instrument, so only h can be used to adjust the model properties. As it will be shown in the subsequent chapters, using the scheme near the stability margin is generally advantageous. However, the higher number of grid points that corresponds to this case increases the computational load, which may prevent the scheme from being real-time realizable. On the other hand, the smaller the value of Γ is, the fewer normal modes are taken into account by the model, which lowers the quality of the generated sound. According to the above, for the best results, usually the highest possible number of grid points has to be chosen with respect to the stability margin and the available computational resources.

In summary, to determine the stability of a scheme, the following steps have to be performed:

[4]To be mathematically precise, the ratio $k/h = \lambda$ has to be constant. However, from practical point of view, the values of c, k and h can be chosen arbitrarily, and Eq. (3.71) will determine if the resulted scheme for the string is numerically stable or not.

1. Calculate the Fourier-transform the difference equation of the scheme.
2. Derive the amplification polynomial $\Phi(g)$ by making the substitution $V^n(\beta) = g^n$.
3. Obtain the amplification factors g_i by finding the roots of the amplification polynomial.
4. Find the parameter values under which the magnitude of the amplification factors is less than or equal to one.

The ease of this method inheres in the shift theorem, which makes Fourier-transformation of a difference equation equivalent to substitution of complex exponentials.

3.2.4 Accuracy

Accuracy can be regarded as the refined form of the concept of consistency. While the latter only tells us if a finite difference scheme is an approximation of a partial differential equation, accuracy provides more detailed information about this relationship. As with consistency, we first introduce accuracy for finite difference operators and then for finite difference schemes.

Definition 3.7: (Accuracy of a Finite Difference Operator) If the differential operator P contains only derivatives with respect to t then the finite difference operator P_k is said to be a p-order accurate approximation of P if for any smooth function ϕ

$$P\{\phi\} - P_k\{\phi\} = O(k^p). \tag{3.72}$$

Similarly, if the differential operator P contains only derivatives with respect to x then the finite difference operator P_h is said to be a q-order accurate approximation of P if for any smooth function ϕ

$$P\{\phi\} - P_h\{\phi\} = O(h^q). \tag{3.73}$$

If the differential operator P contains derivatives with respect to both t and x then the finite difference operator $P_{k,h}$ is said to be a (p, q) accurate approximation of P if for any smooth function ϕ

$$P\{\phi\} - P_{k,h}\{\phi\} = O(k^p) + O(h^q). \tag{3.74}$$

Definition 3.8: (Accuracy of a Finite Difference Scheme) The finite difference scheme $P_{k,h}\{v\} = 0$ consistent with the partial differential equation $P\{u\} = 0$ is accurate[5]of order (p, q) if $P_{k,h}$ is a (p, q) accurate approximation of P .

[5]The definitions of accuracy presented here do not apply to all finite difference operators and schemes, but they are simple and valid for the schemes examined in this thesis. For a more rigorous treatment of this topic, we refer to [Strikwerda 1989] and [Trefethen 1996].

In words, accuracy gives information about the rate of the convergence of a scheme as the grid spacings tend to zero. This definition inheres the ambiguity that, e.g., if the accuracy of an operator is 2 then it is also accurate of order 1, because

$$P_k\{\phi\} = P\{\phi\} + O(k^2) \qquad \Rightarrow \qquad |P_k\{\phi\} - P\{\phi\}| \leq Ck^2 \tag{3.75}$$

implies that

$$|P_k\{\phi\} - P\{\phi\}| \leq Ck \qquad \Rightarrow \qquad P_k\{\phi\} = P\{\phi\} + O(k) \tag{3.76}$$

if k is not greater than one and C is a positive constant. However, this should not cause any confusion as in the following we will only claim that a scheme or an operator is accurate of order p if it is not accurate of order $p+1$ according to Def. 3.7 and 3.8.

Accuracy, similarly to consistency, can be determined by Taylor-series expansion. It was already shown in Section 3.2.2 that

$$\delta_t^2\{\phi\} = \frac{\phi_m^{n+1} - 2\phi_m^n + \phi_m^{n-1}}{k^2} \quad = \quad (\phi_{tt})_m^n + O(k^2) \tag{3.77}$$

that is, the operator δ_t^2 is a second order accurate approximation of $\partial^2/\partial t^2$. The order of accuracy of the other commonly used difference operators listed in Table 3.1 can be derived in a similar fashion (see Eq. (3.33)).

differential operator approximated	difference operator	order of accuracy
$\partial/\partial t$	δ_{t+}	1
$\partial/\partial t$	δ_{t-}	1
$\partial/\partial t$	δ_{t0}	2
$\partial^2/\partial t^2$	δ_t^2	2

Table 3.1: Order of accuracy of common difference operators.

The scheme for the ideal string was constructed by approximating the differential operator of the one-dimensional wave equation as

$$\phi_{tt} - c^2\phi_{xx} \quad = \quad \delta_t^2\{\phi\} - c^2\delta_x^2\{\phi\} + O(k^2) + O(h^2) \tag{3.78}$$

which means that this finite difference scheme is accurate of order (2,2). It should be clear that if a scheme is constructed by using terms of different orders of accuracy then the accuracy of the scheme is determined by the term which is accurate of the lowest order. For example, the difference operator

$$\delta_t^2 - \delta_{t-} \tag{3.79}$$

is a first-order accurate approximation of the differential operator

$$\frac{\partial^2}{\partial t^2} - \frac{\partial}{\partial t} \tag{3.80}$$

because δ_{t-} is only a first-order accurate approximation of $\partial/\partial t$, although the accuracy of the other term, δ_t^2, is two.

In order not to degrade accuracy of the overall method, the calculation of the grid function at the first time step has to be accurate of at least the same order as the scheme itself. E.g., for the ideal string, the approximation that was used in Section 3.1,

$$u_m^1 \approx u_m^0 + k(u_t)_m^0 + O(k^2) \tag{3.81}$$

is second-order accurate with respect to time. As the finite difference scheme used for modeling the string is accurate of order (2,2), the initialization of the scheme at the first time step is satisfactory.

According to [Strikwerda 1989, p. 63], the accuracy of a scheme is directly related to the error of the solution defined as

$$E(t) = \| u(x_m, t) - v_m^n \|_h \tag{3.82}$$

that is, higher order of accuracy results in decreased error of the solution. This means that using a more accurate scheme, in theory, allows us to use a coarser grid which results in an implementation with fewer instructions per time unit. However, stability means another constraint for the grid spacings so they cannot be chosen arbitrary large. Besides, increased accuracy generally requires more instructions per grid point, which compensates the advantages of the coarser grid.

The error function defined above is an important characteristic in certain applications. However, in the field of instrument modeling, where the main point is to recreate the sound of an instrument, it is not very meaningful since there is no direct relationship between the error of the displacement v_m^n and the fidelity of the sound created. A more important property of an instrument model, with respect to its realistic behavior, is how it preserves the modal frequencies of the actual instrument.

3.2.5 Numerical Dispersion

From the analytical solution of the wave equation, we expect the string model to yield solutions that consist of waves propagating without distortion. However, as it is shown in Fig. 3.7, this is true only at the stability margin. For other parameter values, the components of the solution corresponding to different spatial frequencies travel with different phase velocities. As shown in Fig. 3.8, this causes the modal frequencies to differ from the their theoretical values. This effect is referred to as *numerical dispersion*, which is a consequence of discretization of the PDE, and should not be confused with the dispersion that is inherent in some physical systems.

In order to interpret this behaviour of the scheme, let us first examine the wave equation in the spatial frequency domain. By applying the continuous spatial Fourier-transform to the wave equation

$$\frac{\partial^2 u}{\partial t^2}(x,t) = c^2 \frac{\partial^2 u}{\partial x^2}(x,t) \tag{3.83}$$

we obtain

$$\frac{\partial^2 U}{\partial t^2}(\beta,t) = c^2 (j\beta)^2 U(\beta,t) \tag{3.84}$$

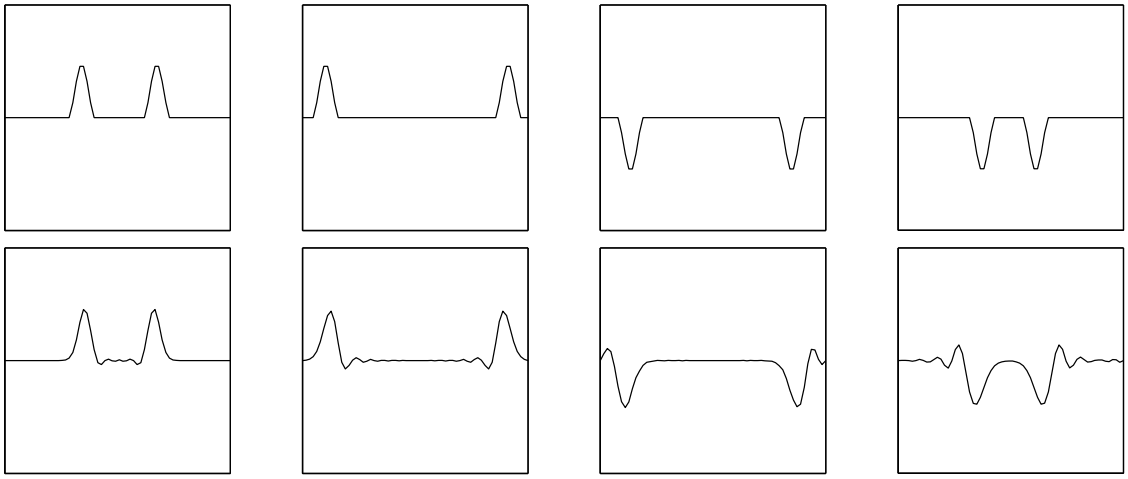

Figure 3.7: The effect of numerical dispersion to the displacement of the string. On the upper figure ($c = 1/\lambda$), the waves propagate without distortion. On the lower figure ($c < 1/\lambda$), due to dispersion, the high-frequency components of the wave propagate slower which causes the shape of the wave distort over time.

which is an ordinary linear differential equation. Let us look for the solution in the form of

$$U(\beta, t) = A(\beta)e^{st}. \tag{3.85}$$

By substituting this expression into the differential equation we obtain

$$s^2 A(\beta)e^{st} = c^2(j\beta)^2 A(\beta)e^{st} \tag{3.86}$$

$$s^2 = c^2(j\beta)^2 \tag{3.87}$$

$$s_\pm = \pm j\beta c \tag{3.88}$$

and the general solution can be written as

$$U(\beta, t) = A_+(\beta)e^{j\beta ct} + A_-(\beta)e^{-j\beta ct}. \tag{3.89}$$

By applying the shift theorem, for the inverse transform we obtain

$$u(x, t) = a_+(x + ct) + a_-(x - ct) \tag{3.90}$$

which corresponds to the results of Chapter 2. Let us sample the expression for $U(\beta, t)$ with respect to time so that we get

$$U(\beta, nk) = U^n(\beta) = A_+(\beta)\left(e^{j\beta ck}\right)^n + A_-(\beta)\left(e^{-j\beta ck}\right)^n = \tag{3.91}$$

$$\tag{3.92}$$

$$= A_+(\beta)\left(e^{j\varphi(\beta)}\right)^n + A_-(\beta)\left(e^{-j\varphi(\beta)}\right)^n. \tag{3.93}$$

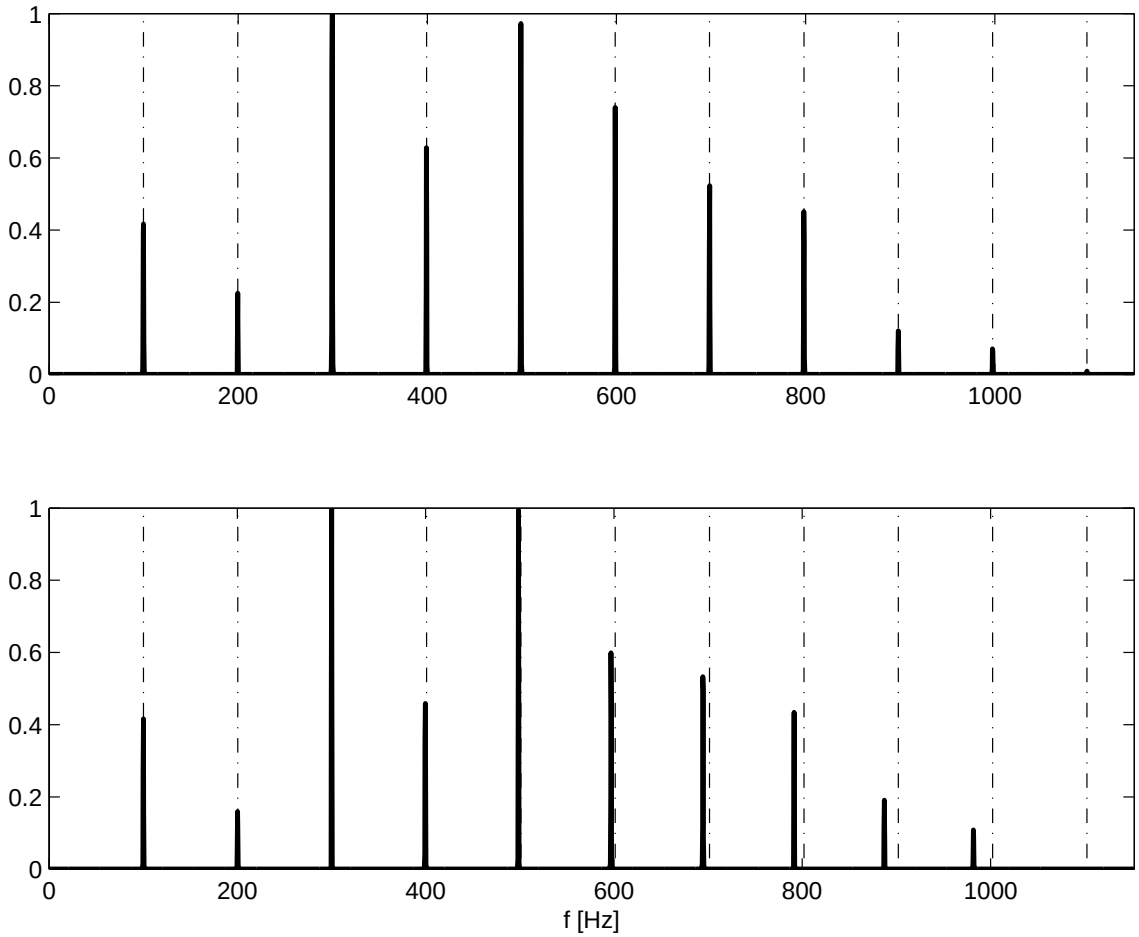

Figure 3.8: The effect of numerical dispersion to the spectrum. The figures show the FFT of the displacement-time function of the string element at 1/10 of the string length with and without numerical dispersion. The parameters c and k are the same, only the number of points, and therefore h, is changed. The upper and lower figures were generated with parameter values $h = ck$ (stability margin) and $h = 5ck$, respectively. The dashed lines show the mode frequencies obtained by analytical solution of wave equation.

By considering the exponential terms, the phase speed may be defined as

$$c(\beta) = \frac{\varphi(\beta)}{k\beta}. \tag{3.94}$$

It is clear that in this case c is independent of β, that is, waves corresponding to each spatial frequency travel with the same speed, there is no dispersion inherent in the ideal string. This property is due to the linearity of $\varphi(\beta)$ with respect to β. By comparing Eq. (3.92) with

$$V^n(\beta) \quad = \quad A_+(\beta)g_+^n + A_-(\beta)g_-^n \tag{3.95}$$

derived in Section 3.2.3, it is clear that $g_\pm$ is an approximation of $e^{\pm j\varphi(\beta)}$. For a stable scheme, $g_\pm$ can be written as

$$g_\pm = G(\beta)e^{\pm j\varphi(\beta)} \tag{3.96}$$

where $G(\beta)$ and $\pm\varphi(\beta)$ are the magnitude and phase of $g_\pm$, respectively. Accordingly, the phase speed of the finite difference scheme, denoted by γ, may be defined as

$$\gamma(\beta) = \frac{\varphi(\beta)}{k\beta} = \frac{arc(g_+)}{k\beta} = \frac{-arc(g_-)}{k\beta}$$

In general, it is difficult to see the meaning behind the lengthy expressions that can be derived for the phase speed, however, numerical evaluation for different parameter values proves to be quite useful. It can be seen in Fig. 3.9 that with parameter values $c = 1/\lambda$, there is no dispersion, the phase velocity is constant for all spatial frequencies. For different parameter values, however, numerical dispersion is present, which causes the waves with higher spatial frequencies propagate slower. It can be seen that by decreasing the value of c, with the other parameters fixed, the phase velocity not only decreases but becomes dependent on the wave number.

3.3 Summary

In this chapter, the fundamentals of finite difference schemes have been introduced. The most important result presented in this chapter is the Lax-Richtmyer Equivalence Theorem, which enables us to verify whether a scheme is an appropriate model for a partial differential equation in a relatively simple way. According to the Equivalence Theorem, the necessary and sufficient condition for a scheme to be convergent is consistency *and* stability. The former property can be easily verified by Taylor-series expansion, and the latter one can be examined by the means of von Neumann analysis presented in Section 3.2.3. The stability conditions stated in this chapter will be used in the subsequent parts of the thesis. Von Neumann analysis was shown to be suitable also for describing the numerical dispersion of finite difference schemes.

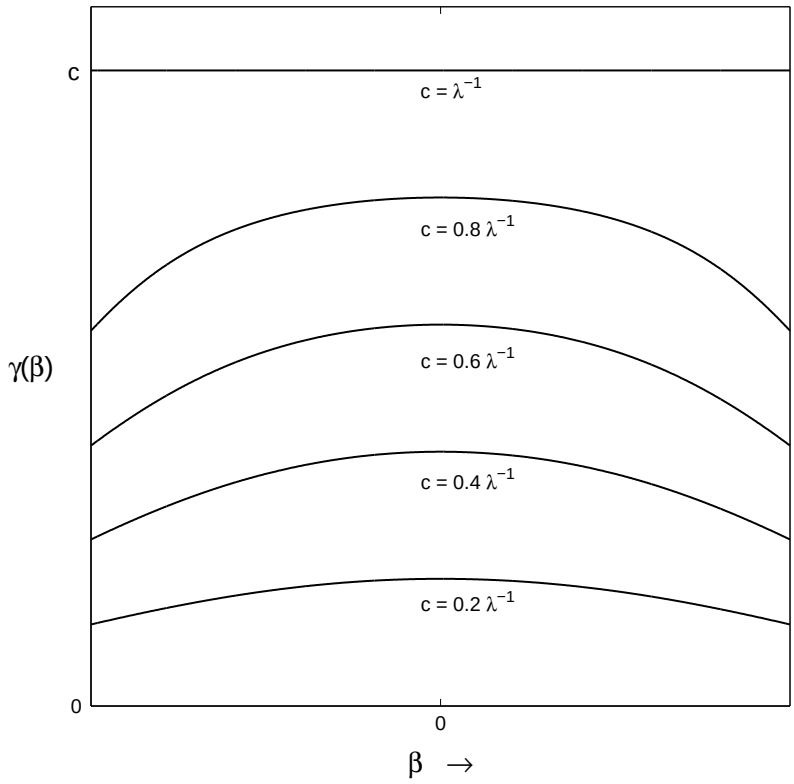

Figure 3.9: Phase velocity of the finite difference scheme of the ideal string for different parameter values.

Chapter 4

Modeling an Acoustic Membrane

In this chapter, several types of finite difference membrane models will be reviewed. Most of the concepts introduced in the previous chapter directly apply to the two-dimensional schemes discussed in the following. However, numerical dispersion is an exception as the direction-dependence of the phase velocity is unique to schemes with two or more spatial dimensions. For this reason, emphasis will be laid on examining the dispersion properties of each derived model.

Two different types of grids with two spatial dimensions will be shown, namely, the ones that correspond to the Cartesian and triangular coordinate systems. Implementation of the boundary conditions corresponding to a circular membrane will be discussed in great detail. In the Cartesian case, it will be shown how to extend the model by taking additional physical phenomena (damping and nonlinearity) into account.

In Section 4.5, four different models for the ideal membrane will be compared from several points of view.

4.1 Discretization in Cartesian Coordinate System

Discretization of the PDE Let us proceed from the two-dimensional wave equation in Cartesian coordinate system:

$$\frac{\partial^2 u}{\partial t^2} = c^2 \left(\frac{\partial^2 u}{\partial x^2} + \frac{\partial^2 u}{\partial y^2} \right). \tag{4.1}$$

The displacement $u(x, y, t)$ now depends on time and two space variables. Similarly to the case of the string, we will attempt to solve initial-boundary value problems. For the square membrane the problem can be formulated as

$$\begin{aligned} u_{tt} &= c^2 \left(u_{xx} + u_{yy} \right) && \text{(PDE)} \\ u_0(x, y) &= f(x, y) && \text{(initial conditions)} \\ u_{t,0}(x, y) &= g(x, y) && \\ u(0, y, t) = u(L, y, t) &= 0 && \text{(boundary conditions)} \\ u(x, 0, t) = u(x, L, t) &= 0. && \end{aligned} \tag{4.2}$$

For the circular membrane, only the boundary conditions are different. According to Chapter 2, the boundary conditions are

$$u(x,y,t) = 0 \qquad \text{if} \qquad (x-x_0)^2 + (y-y_0)^2 \geq R^2 \tag{4.3}$$

For the membrane of the size $L \times L$ we will use $R = x_0 = y_0 = L/2$.

The time and space-shift operators may be defined as follows:

$$\begin{array}{rclcrcl} M\{v^n_{m,l}\} & = & v^n_{m+1,l} & & M^{-1}\{v^n_{m,l}\} & = & v^n_{m-1,l} \\ L\{v^n_{m,l}\} & = & v^n_{m,l+1} & & L^{-1}\{v^n_{m,l}\} & = & v^n_{m,l-1} \\ Z\{v^n_{m,l}\} & = & v^{n+1}_{m,l} & & Z^{-1}\{v^n_{m,l}\} & = & v^{n-1}_{m,l} \end{array} \tag{4.4}$$

The fact that the letter L denotes both the spatial shift operator along the y axis and the length along side of the square membrane should not cause confusion since the context will always clarify what L denotes in the particular expression. As it was shown in Chapter 3, the derivatives in the PDE can be approximated by finite differences[1]:

$$(u_{tt})^n_{m,l} \approx \frac{1}{k^2}\left(Z - 2I + Z^{-1}\right)\{v^n_{m,l}\} = \delta_t^2\{v^n_{m,l}\} \tag{4.5}$$

$$(u_{xx})^n_{m,l} \approx \frac{1}{h^2}\left(M - 2I + M^{-1}\right)\{v^n_{m,l}\} = \delta_x^2\{v^n_{m,l}\} \tag{4.6}$$

$$(u_{yy})^n_{m,l} \approx \frac{1}{h^2}\left(L - 2I + L^{-1}\right)\{v^n_{m,l}\} = \delta_y^2\{v^n_{m,l}\} \tag{4.7}$$

As a shortcut for the spatial operators, we also define the δ_+^2 operator as

$$\delta_+^2 = \delta_x^2 + \delta_y^2 \tag{4.8}$$

(see Fig. 4.1). By substituting these expressions into the wave equation according to Eq. (4.1), we obtain

$$\left(Z - 2I + Z^{-1}\right)\{v^n_{m,l}\} = c^2\lambda^2\left(M - 2I + M^{-1} + L - 2I + L^{-1}\right)\{v^n_{m,l}\} \tag{4.9}$$

that is,

$$v^{n+1}_{m,l} = \left[c^2\lambda^2\left(M + M^{-1} + L + L^{-1}\right) + 2\left(1 - 2c^2\lambda^2\right)I - Z^{-1}\right]\{v^n_{m,l}\} \tag{4.10}$$

The mesh ratio, λ, is again defined as $\lambda = k/h$. As each derivative in the PDE is approximated by a second-order accurate operator the overall scheme will be accurate of the order $(2,2)$. This scheme can be implemented by evaluating the difference equation

$$v^{n+1}_{m,l} = c^2\lambda^2\left(v^n_{m+1,l} + v^n_{m-1,l} + v^n_{m,l+1} + v^n_{m,l-1}\right) + 2\left(1 - 2c^2\lambda^2\right)v^n_{m,l} - v^{n-1}_{m,l} \tag{4.11}$$

for a set of values of m and l determined by the boundary conditions and for each time step n of interest.

[1]The same grid spacings will be used along the x and y axes because the mathematical model under review does not imply otherwise. It is possible that in a more realistic model, which takes the anisotropy of the material into account using different values for the spatial grid spacings along the two coordinate axis has some advantages.

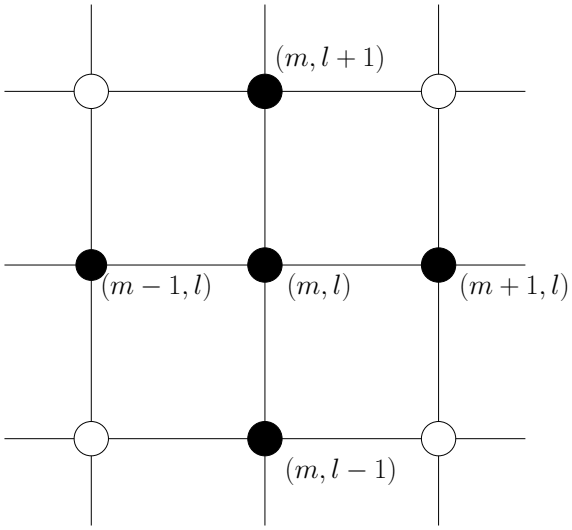

Figure 4.1: Illustration of the δ_+^2 operator. The points involved in the approximation of the spatial derivatives are filled with black.

Discretization of Initial and Boundary Conditions According to the boundary conditions, the displacement in the points with indices $m = 0$, $m = \Gamma - 1$, $l = 0$ and $l = \Gamma - 1$, where Γ is again defined by $L = (\Gamma - 1)h$, is zero for all time steps, so the above expression has to be evaluated for only the $(\Gamma - 2)^2$ inner points (see Fig. 4.2). The displacement is also identically zero in the rest of the grid points outside the boundary (see Eq. (2.15)), so they have not to be stored and calculated. Discretization of the initial displacement $u_0(x, y)$ is evident, however, the consideration of the initial velocity needs some explanation. The Taylor-series expansion for $u(x, y, (n+1)k)$ yields

$$u_{m,l}^{n+1} \approx u_{m,l}^n + k\,(u_t)_{m,l}^n \tag{4.12}$$

that is, the initial velocity can be taken into account by setting the values of v for time step 1 according to the equation

$$v_{m,l}^1 = v_{m,l}^0 + k u_{t,0}(mh, lh) = v_{m,l}^0 + k g(mh, lh). \tag{4.13}$$

According to the results of Section 3.2.4, this initialization procedure does not degrade the overall accuracy of the scheme. So far we have obtained the following discretized form of the initial-boundary value problem for the square membrane:

$$\begin{aligned} v_{m,l}^{n+1} &= a_1 \left(v_{m+1,l}^n + v_{m-1,l}^n + v_{m,l+1}^n + v_{m,l-1}^n \right) + a_2 v_{m,l}^n - v_{m,l}^{n-1} \\ v_{m,l}^0 &= f(mh, lh) \\ v_{m,l}^1 &= v_{m,l}^0 + k g(mh, lh) \\ v_{0,l}^n = v_{\Gamma-1,l}^n &= 0 \\ v_{m,0}^n = v_{m,\Gamma-1}^n &= 0 \end{aligned} \tag{4.14}$$

where $a_1 = c^2\lambda^2$, $a_2 = 2\,(1 - 2a_1)$ and $m, l \in [1, \Gamma - 2]$.

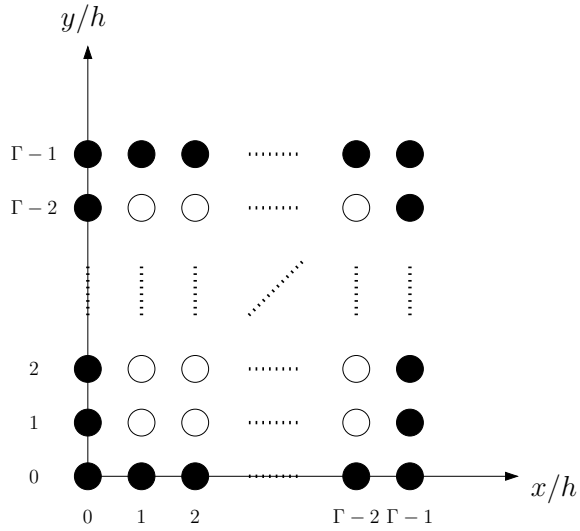

Figure 4.2: Illustration of the boundary conditions for the square membrane. The circles filled with black denote the points of the boundary. The displacement in these points and also outside the boundary is identically zero for all time steps, the difference equation of the scheme has to be evaluated only for the inner points denoted by empty circles.

Implementation of Circular Boundary Conditions The circular boundary conditions can be discretized in the following way. The solution $u(x, y, t)$ is zero for all time steps if the x and y coordinates satisfy the inequality

$$\left(x - \frac{L}{2}\right)^2 + \left(y - \frac{L}{2}\right)^2 \geq \left(\frac{L}{2}\right)^2. \tag{4.15}$$

To be suitable for implementation, the continuous variables in this expression have to be replaced by indices. This can be achieved by using the substitutions

$$x = mh \tag{4.16}$$

$$y = lh \tag{4.17}$$

$$L = (\Gamma - 1)h \tag{4.18}$$

so we obtain

$$\left(mh - \frac{\Gamma - 1}{2}h\right)^2 + \left(lh - \frac{\Gamma - 1}{2}h\right)^2 \geq \left(\frac{\Gamma - 1}{2}h\right)^2. \tag{4.19}$$

The parameter h is present in each term, so the inequality simplifies to

$$\left(m - \frac{\Gamma - 1}{2}\right)^2 + \left(l - \frac{\Gamma - 1}{2}\right)^2 \geq \left(\frac{\Gamma - 1}{2}\right)^2 \tag{4.20}$$

hence we obtain the following discretized form of the boundary conditions:

$$v^n_{m,l} = 0 \qquad \text{if} \qquad \left(m - \frac{\Gamma - 1}{2}\right)^2 + \left(l - \frac{\Gamma - 1}{2}\right)^2 \geq \left(\frac{\Gamma - 1}{2}\right)^2. \tag{4.21}$$

This form of the circular boundary conditions can be directly implemented. Fig. 4.3 shows how the boundary refines as the grid spacing is decreased.

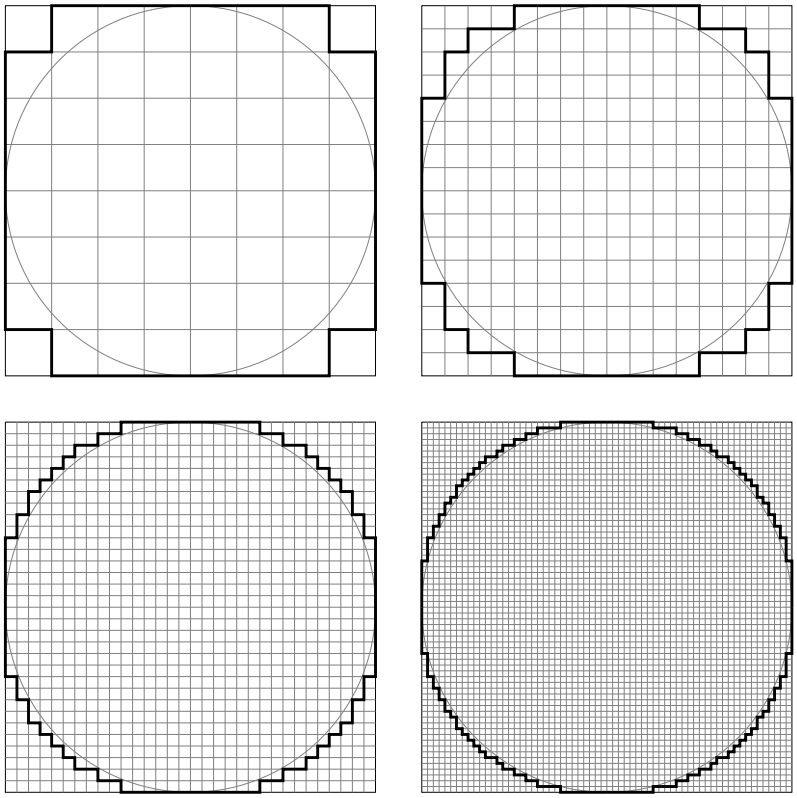

Figure 4.3: Circular boundary conditions for the 8×8, 16×16, 32×32 and 64×64-point membrane models discretized in Cartesian coordinate-system. The displacement of the points outside the area bounded by the solid black line and on the line itself is identically zero for all time steps.

Excitation Before implementing the model, the initial conditions, that is, the excitation of the membrane has to be specified. Since the membrane model is to be used as a component of a drum model, the excitation should be chosen according to this purpose. The realistic modeling of the drumstick and the interaction between the drum and the drumstick yield a much more complicated coupled initial-boundary value problem whose analysis is out of the scope of this thesis. However, the impact of the drumstick may be approximately modeled by setting the initial displacement of the membrane to zero and specifying non-zero initial velocity for a small section of the membrane.

$$u_0(x, y) = 0 \tag{4.22}$$

$$u_{t,0}(x, y) = g(x, y) \tag{4.23}$$

The initial velocity will be specified as a period of a two-dimensional raised cosine function (2D Hann window), as follows:

$$g(x, y) = \begin{cases} 0.5 \cos(\pi D / R_e) + 0.5 & \text{if } D \leq R_e \\ 0 & \text{if } D > R_e \end{cases} \tag{4.24}$$

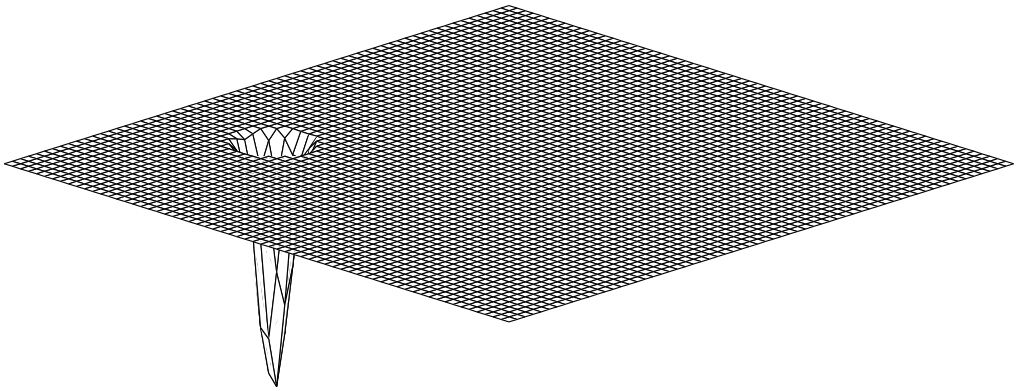

Figure 4.4: Calculated displacement of the 64×64 point membrane model at time step 2.

where R_e denotes the radius of the excitation and D is the distance from the point where the membrane is 'hit'. The expression for $g(x, y)$ has yet to be discretized, too. The following notation will be used:

x coordinate of the center of excitation:	$x_e = m_e h$
y coordinate of the center of excitation:	$y_e = l_e h$
radius of excitation:	$R_e = r_e h$

The distance from the center, D, can be expressed as

$$\begin{aligned} D &= \sqrt{(x - x_e)^2 + (y - y_e)^2} = \\ &= \sqrt{(mh - m_e h)^2 + (lh - l_e h)^2} = \\ &= h\sqrt{(m - m_e)^2 + (l - l_e)^2} \end{aligned}$$

Substituting this into the expression for $g(x, y)$ yields the discretized form of the initial velocity:

$$g(mh, lh) = \begin{cases} 0.5 \cos\left(\frac{\pi}{r_e}\sqrt{(m - m_e)^2 + (l - l_e)^2}\right) + 0.5 & \text{if } (m - m_e)^2 + (l - l_e)^2 \leq r_e^2 \\ 0 & \text{otherwise} \end{cases}$$

Note that contrary to the indices m and l the parameters of the excitation, m_e, l_e and r_e, need not to be integers.

The displacement of the implemented circular membrane model is shown in Fig. 4.4, 4.5 and 4.6. It can be seen that, similarly to the string model, the parameters of the finite difference membrane model has to be chosen properly to maintain stability. The next section is devoted to the stability analysis of two-dimensional models. Fig. 4.7 shows the effect of numerical dispersion to the mode frequencies of the membrane model. It can be seen that, contrarily to the case of the string, numerical dispersion is present even at the parameter values that correspond to the empirical stability margin. This phenomenon will be investigated in detail in Section 4.1.2.

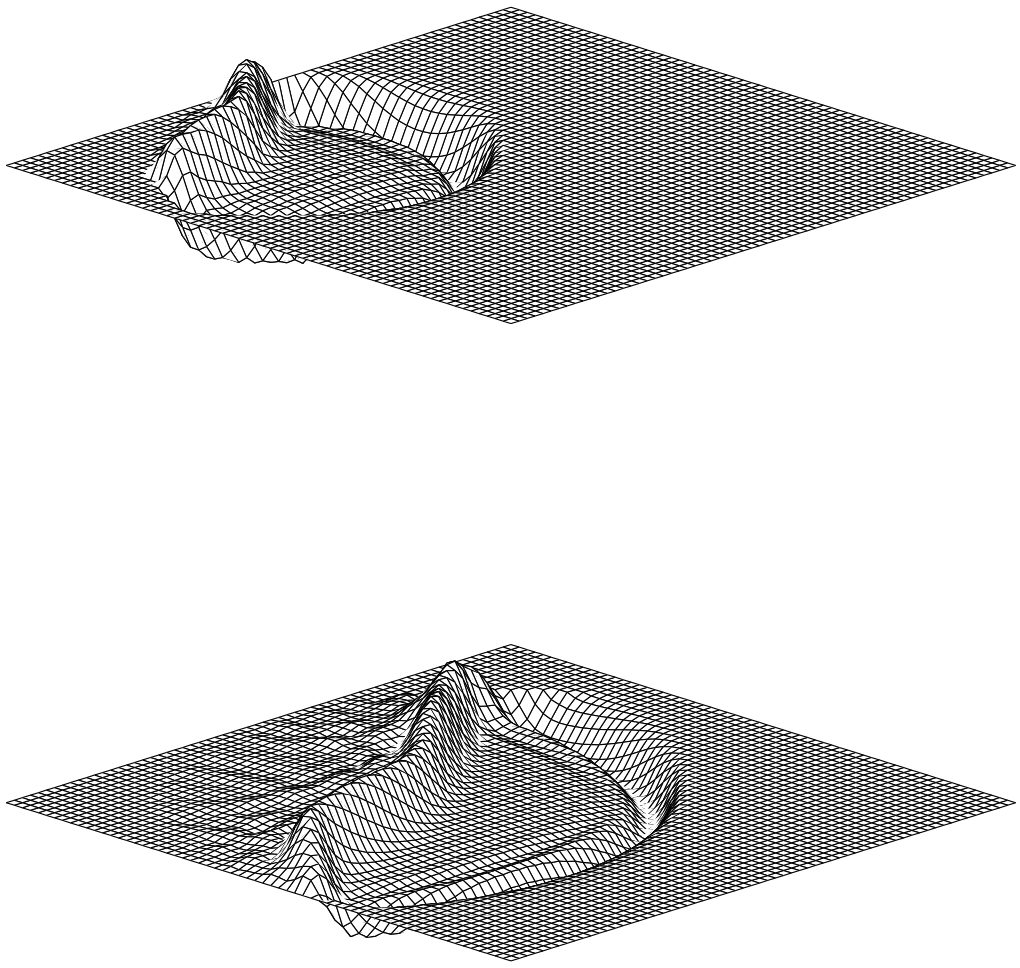

Figure 4.5: Calculated displacement of the stable 64×64 point circular membrane model at time steps 25 and 48.

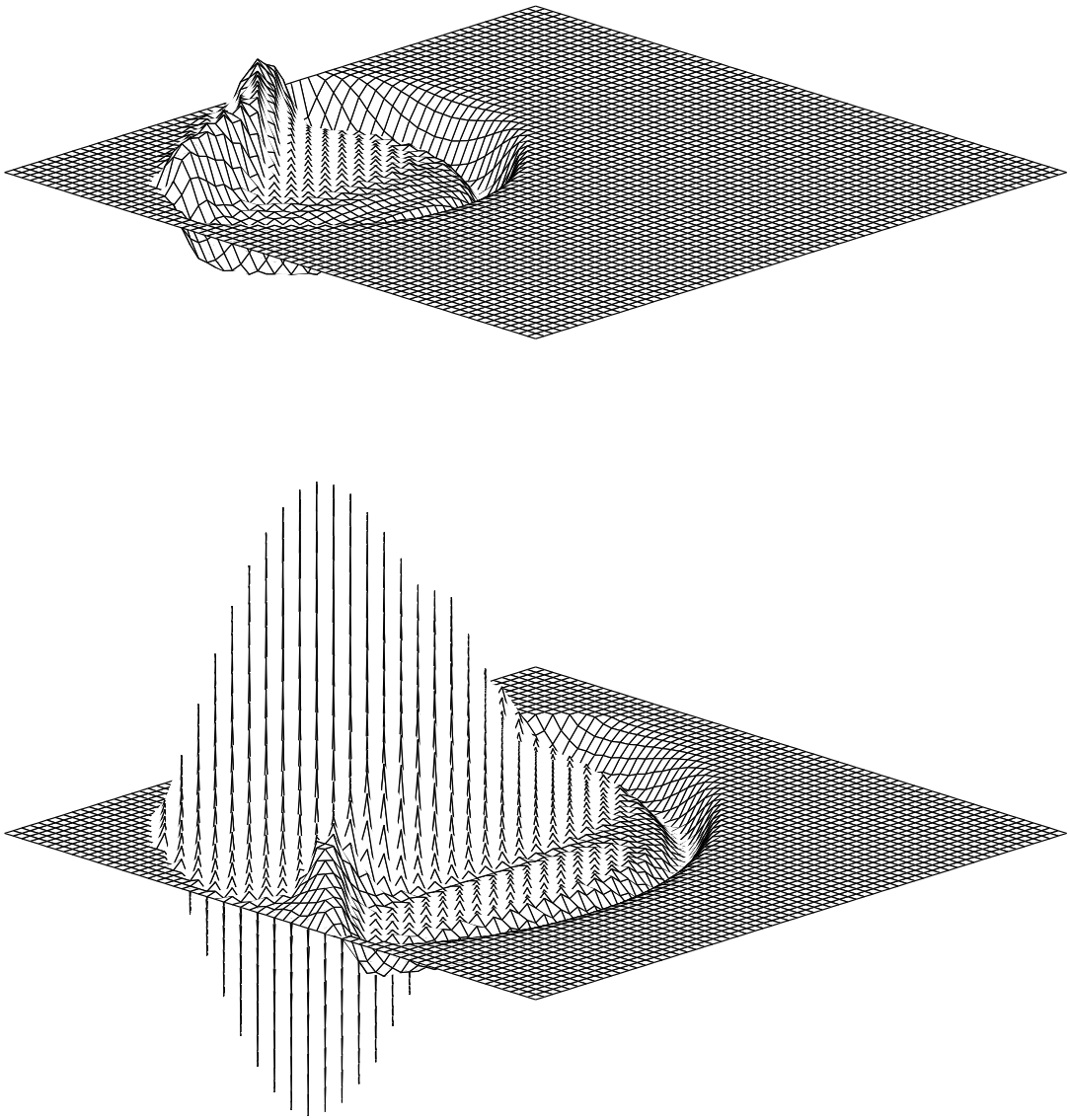

Figure 4.6: Calculated displacement of the unstable 64×64 point circular membrane model at time steps 25 and 48.

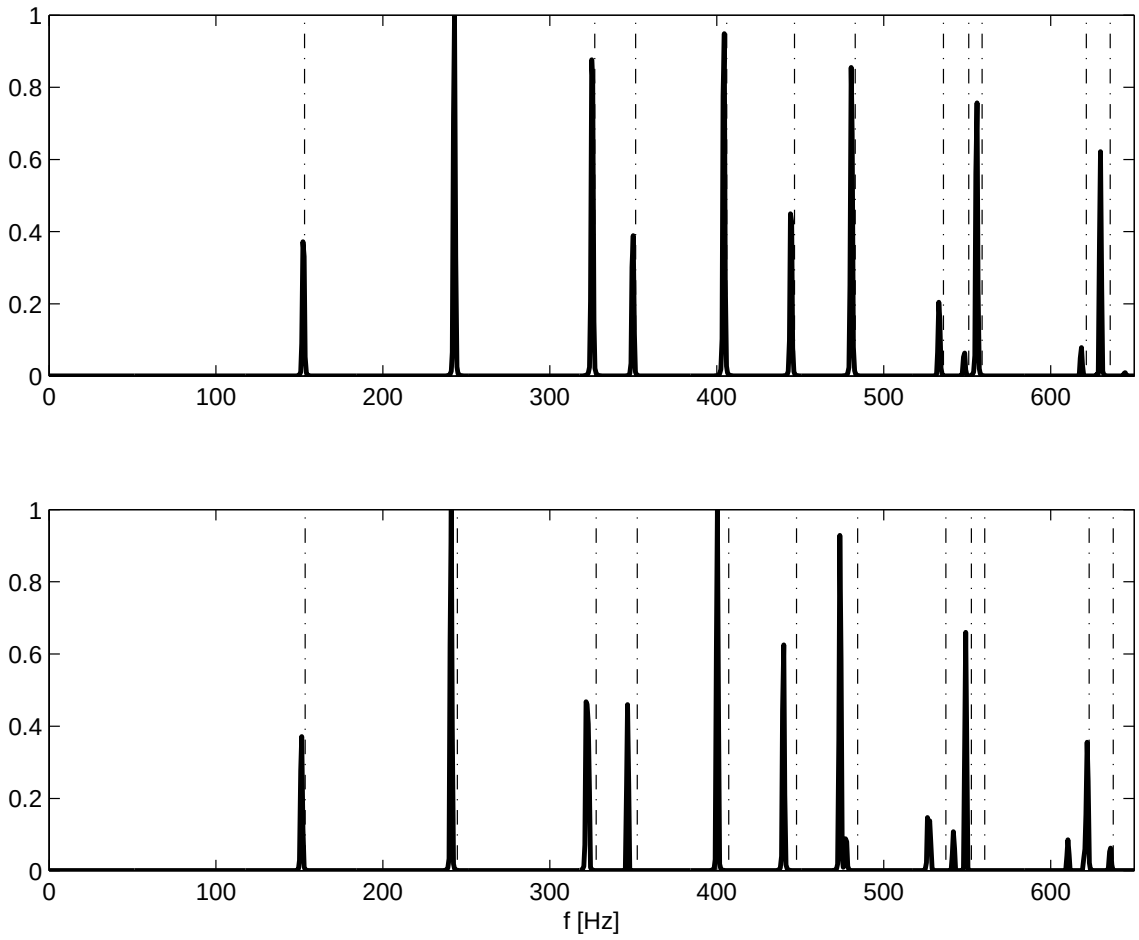

Figure 4.7: The FFT spectra of the displacement-time functions of the membrane with parameter values $h = ck\sqrt{2}$ (stability margin) and $h = 5ck$, respectively. The dashed lines show the mode frequencies obtained by analytical solution of wave equation.

4.1.1 Von Neumann Stability Analysis

The procedure that was presented in Section 3.2.3 can be easily applied to two-dimensional problems, however, the spatial Fourier-transform has now to be performed along both coordinate axes. This is equivalent to applying the two-dimensional Fourier-transform defined as follows:

Definition 4.1: (Spatial Fourier-transform in two dimensions)

$$\mathscr{F}\{u(x,y)\} = U(\beta_x,\beta_y) = \frac{1}{2\pi}\int_{-\infty}^{\infty}\int_{-\infty}^{\infty} u(x,y)e^{-j\beta_x x}e^{-j\beta_y y}dxdy \tag{4.25}$$

$$\mathscr{F}^{-1}\{U(\beta_x,\beta_y)\} = u(x,y) = \frac{1}{2\pi}\int_{-\infty}^{\infty}\int_{-\infty}^{\infty} U(\beta_x,\beta_y)e^{j\beta_x x}e^{j\beta_y y}d\beta_x d\beta_y \tag{4.26}$$

$$\mathscr{F}\{v_{m,l}\} = V(\beta_x,\beta_y) = \frac{1}{2\pi}\,h^2\sum_{l=-\infty}^{\infty}\sum_{m=-\infty}^{\infty} v_{m,l}e^{-jmh\beta_x}e^{-jlh\beta_y} \tag{4.27}$$

$$\mathscr{F}^{-1}\{V(\beta_x,\beta_y)\} = v_{m,l} = \frac{1}{2\pi}\int_{-\frac{\pi}{h}}^{\frac{\pi}{h}}\int_{-\frac{\pi}{h}}^{\frac{\pi}{h}} V(\beta_x,\beta_y)e^{jmh\beta_x}e^{jlh\beta_y}d\beta_x d\beta_y \tag{4.28}$$

Note that the above definition of the discrete-space Fourier-transform is not entirely precise as the spatial frequency variables are not always β_x and β_y. These variables are determined by the interpretation of the indices of the grid function. As an example, let us consider the two-dimensional sequences $a_{i,j}$ and $b_{i,j}$, which are obtained by spatial sampling of the continuous-space functions $a(x,y)$ and $b(x,w)$, respectively. The former is given in the Cartesian, the latter in the triangular coordinate system. If the grid functions a and b are defined as

$$a_{i,j} = a(ih,jh) \tag{4.29}$$

$$b_{i,j} = b(ih,jh) \tag{4.30}$$

then the statement $a_{i,j} = b_{i,j}$ implies that also their Fourier-transforms according to Eq. (4.27) have to be equal. Although the spectra are indeed identical in a formal sense, no sensible conclusions can be deduced from this equality as the expressions on the two sides are defined in different coordinate systems. This is a source of some inconvenience when the spectra of grid functions defined in different coordinate systems are to be compared, however, it can be easily resolved as it will be shown in Section 4.4 and in Appendix B.

The shift theorem presented in Section 3.2.3 can also be easily extended for the two-dimensional case:

Theorem 4.1: (Shift Theorem of the 2-D Discrete-space Fourier-transform)

$$\mathscr{F}\{v_{m+K,l}\} = e^{jKh\beta_x}\mathscr{F}\{v_{m,l}\} \tag{4.31}$$

$$\mathscr{F}\{v_{m,l+K}\} = e^{jKh\beta_y}\mathscr{F}\{v_{m,l}\} \tag{4.32}$$

for any integer K.

By performing the two-dimensional Fourier-transform on the difference equation

$$v_{m,l}^{n+1} = \left[c^2\lambda^2\left(M + M^{-1} + L + L^{-1}\right) + 2\left(1 - c^2\lambda^2\right)I - Z^{-1}\right]\{v_{m,l}^n\} \quad (4.33)$$

we obtain

$$\begin{aligned} V^{n+1}(\beta_x, \beta_y) &= \Big[c^2\lambda^2\left(e^{jh\beta_x} + e^{-jh\beta_x} + e^{jh\beta_y} + e^{-jh\beta_y} - 4\right) + \\ &\qquad +2\Big]V^n(\beta_x, \beta_y) - V^{n-1}(\beta_x, \beta_y) = \quad (4.34) \\ &= 2\left[c^2\lambda^2\left(\cos h\beta_x + \cos h\beta_y - 2\right) + 1\right]V^n(\beta_x, \beta_y) - V^{n-1}(\beta_x, \beta_y) \end{aligned}$$

which is equivalent to

$$V^{n+1}(\beta_x, \beta_y) = 2DV^n(\beta_x, \beta_y) - V^{n-1}(\beta_x, \beta_y) \quad (4.35)$$

where

$$D = c^2\lambda^2\left(\cos h\beta_x + \cos h\beta_y - 2\right) + 1. \quad (4.36)$$

The amplification polynomial thus can be written in the form

$$\Phi(g) = g^2 - 2Dg + 1 = 0 \quad (4.37)$$

which is the same as what was derived in Section 3.2.3 for the ideal string (see Eq. (3.60)), only D is different. It can be seen that D cannot be greater than one, so, according to Theorem 3.6, the scheme is stable if $D \geq -1$, that is,

$$c^2\lambda^2\left(\cos h\beta_x + \cos h\beta_y - 2\right) \geq -2 \quad (4.38)$$

$$c^2\lambda^2 \leq 0.5 \quad (4.39)$$

$$c \leq \frac{1}{\lambda\sqrt{2}} \quad (4.40)$$

which, as expected, corresponds to the empirical stability margin of the membrane model.

4.1.2 Numerical Dispersion in Two Dimensions

Numerical dispersion has been shown to cause the phase velocity of the string model depend on the wave number β. In the two-dimensional case, however, the phase velocity depends on the wave numbers along both x and y axes, which is responsible for a phenomenon that is specific to multidimensional schemes, namely, *direction-dependent* numerical dispersion.

First, let us define the phase velocity in two dimensions in accordance with the one-dimensional case. Applying the Fourier-transform to the two-dimensional wave equation defined as

$$\frac{\partial^2 u}{\partial t^2}(x, y, t) = c^2\left(\frac{\partial^2 u}{\partial x^2}(x, y, t) + \frac{\partial^2 u}{\partial y^2}(x, y, t)\right) \quad (4.41)$$

the following equation is obtained:

$$\begin{aligned}\frac{\partial^2 U}{\partial t^2}(\beta_x,\beta_y,t) &= c^2\left((j\beta_x)^2+(j\beta_y)^2\right)U(\beta_x,\beta_y,t) = \\ &= -c^2\left(\beta_x^2+\beta_y^2\right)U(\beta_x,\beta_y,t) \end{aligned} \tag{4.42}$$

As in Section 3.2.5, this ordinary differential equation can be solved by making the substitution

$$U(\beta_x,\beta_y,t) = A(\beta_x,\beta_y)e^{st} \tag{4.43}$$

which yields

$$s^2 = -c^2\left(\beta_x^2+\beta_y^2\right) \tag{4.44}$$

$$s = \pm jc\sqrt{\beta_x^2+\beta_y^2} \tag{4.45}$$

The solution thus can be written as

$$U(\beta_x,\beta_y,t) = A_+(\beta_x,\beta_y)e^{jc\sqrt{\beta_x^2+\beta_y^2}\,t} + A_-(\beta_x,\beta_y)e^{-jc\sqrt{\beta_x^2+\beta_y^2}\,t} \tag{4.46}$$

where A_+ and A_- are, again, determined by the initial conditions. After sampling this solution, we obtain

$$U(\beta_x,\beta_y,nk) = A_+(\beta_x,\beta_y)\left(e^{jc\sqrt{\beta_x^2+\beta_y^2}\,k}\right)^n + A_-(\beta_x,\beta_y)\left(e^{-jc\sqrt{\beta_x^2+\beta_y^2}\,k}\right)^n \tag{4.47}$$

$$U(\beta_x,\beta_y,nk) = A_+(\beta_x,\beta_y)\left(e^{j\varphi(\beta_x,\beta_y)}\right)^n + A_-(\beta_x,\beta_y)\left(e^{-j\varphi(\beta_x,\beta_y)}\right)^n \tag{4.48}$$

thus the phase velocity of the ideal membrane is defined by

$$c(\beta_x,\beta_y) = \frac{\varphi(\beta_x,\beta_y)}{k\sqrt{\beta_x^2+\beta_y^2}} \tag{4.49}$$

It can be seen that the phase velocity of the ideal membrane depends linearly on the length of the vector $\boldsymbol{\beta} = [\beta_x, \beta_y]$, i.e., the Eucledian distance from the origo of the spatial frequency plane (spatial DC), and it is independent of the direction of $\boldsymbol{\beta}$ defined by the angle

$$\arctan\left(\frac{\beta_y}{\beta_x}\right). \tag{4.50}$$

Linearity and direction-independence of the phase speed causes waves corresponding to any point of the spatial frequency plane propagate with the same speed. The solution of the difference equation Eq. (4.35) can be written as

$$V^n(\beta) = A_+(\beta_x,\beta_y)g_+^n + A_-(\beta_x,\beta_y)g_-^n \tag{4.51}$$

After comparing this equation with Eq. (4.48), the phase velocity of the two-dimensional finite difference scheme can be defined as

$$\gamma(\beta_x,\beta_y) = \frac{arc(g_+)}{k\sqrt{\beta_x^2+\beta_y^2}}. \tag{4.52}$$

Fig. 4.8 shows the phase velocity of the membrane model at the stability margin. It can be seen that in diagonal direction, i.e. if $|\beta_x| = |\beta_y|$, the phase speed corresponds to the analytic solution of the PDE, however, for any other point of the spatial frequency plane, this is not true. In Fig. 4.9, it can be seen that inside the stability margin, dispersion appears also in the diagonal direction, this decreases the direction-dependency of the phase speed to some extent. Direction-dependence in these figures appears as contour lines that are not circular. In the subsequent sections, methods for reduction of direction-dependence will be presented.

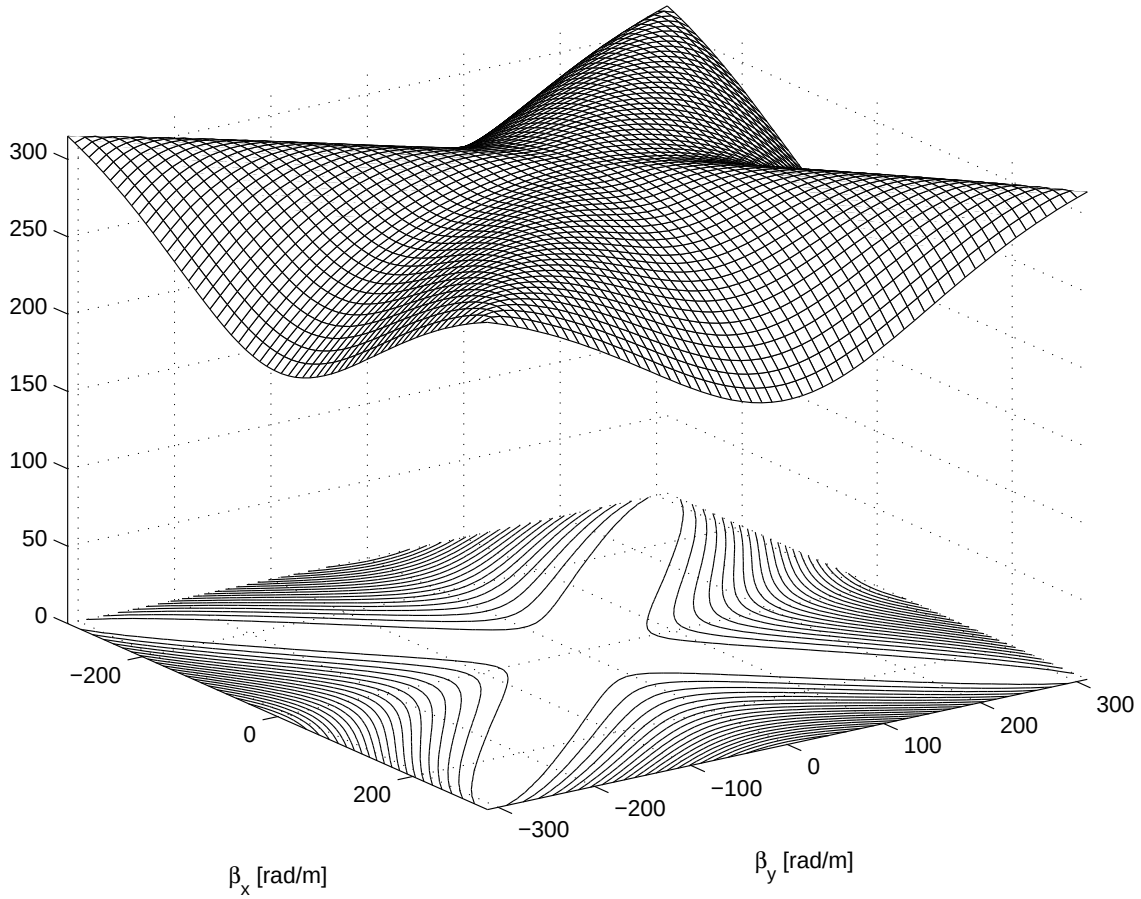

Figure 4.8: Phase speed of the membrane model with parameter values $c = 1/(\sqrt{(}2)\lambda)$ (stability margin) as a function of the spatial frequencies β_x and β_y. The theoretical value of c is 314.98 m/sec.

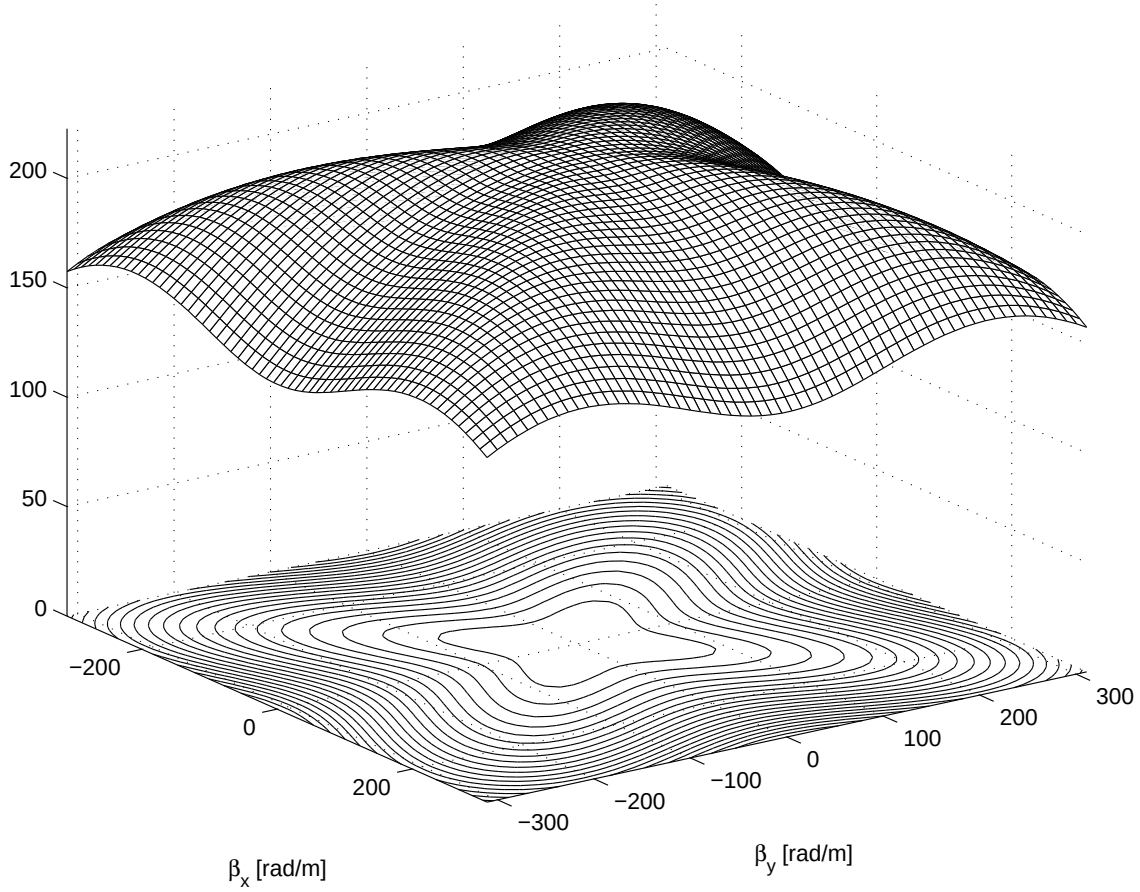

Figure 4.9: Phase speed of the membrane model with parameter values $c = 1/(2\lambda)$ as a function of the spatial frequencies β_x and β_y. The theoretical value of c is 222.73 m/sec.

4.1.3 Higher-Order Accurate Schemes

In this section, we will introduce a scheme for the two-dimensional wave equation that is, contrary to the rest of the schemes under review, fourth-order accurate with respect to space.

Let us consider the Taylor-series expansion of the continuous function $u(x)$ around the grid point x_m. The value of u in the surrounding grid points can be expressed as follows:

$$\begin{aligned} u_{m\pm1} &= u_m \pm h(u_x)_m + \frac{h^2}{2!}(u_{xx})_m \pm \frac{h^3}{3!}(u_{xxx})_m + \\ &\quad + \frac{h^4}{4!}(u_{xxxx})_m \pm \frac{h^5}{5!}(u_{xxxxx})_m + O(h^6) \qquad (4.53) \\ u_{m\pm2} &= u_m \pm 2h(u_x)_m + \frac{4h^2}{2!}(u_{xx})_m \pm \frac{8h^3}{3!}(u_{xxx})_m + \\ &\quad + \frac{16h^4}{4!}(u_{xxxx})_m \pm \frac{32h^5}{5!}(u_{xxxxx})_m + O(h^6). \qquad (4.54) \end{aligned}$$

By taking the sum of u_{m+1} and u_{m-1}, we obtain

$$u_{m+1} + u_{m-1} = 2u_m + h^2(u_{xx})_m + \frac{h^4}{12}(u_{xxxx})_m + O(h^6). \qquad (4.55)$$

Let us also take the sum of u_{m+2} and u_{m-2}:

$$u_{m+2} + u_{m-2} = 2u_m + 4h^2(u_{xx})_m + \frac{4h^4}{3}(u_{xxxx})_m + O(h^6). \qquad (4.56)$$

It can be seen that the fourth-order derivative in these expressions can be eliminated by subtracting Eq. (4.56) from Eq. (4.56) multiplied by 16, which yields

$$16\,(u_{m+1} + u_{m-1}) - (u_{m+2} + u_{m-2}) = 30u_m + 12h^2(u_{xx})_m + O(h^6). \qquad (4.57)$$

By expressing the second-order derivative on the right-hand side, we obtain the following approximation:

$$\begin{aligned} (u_{xx})_m &= \frac{-u_{m+2} + 16u_{m+1} - 30u_m + 16u_{m-1} - u_{m-2}}{12h^2} + O(h^4) = \qquad (4.58) \\ &= \left(\frac{-M^2 + 16M - 30I + 16M^{-1} - M^{-2}}{12h^2}\right)\{u_m\} + O(h^4). \qquad (4.59) \end{aligned}$$

According to Def. 3.7, this is a fourth-order accurate approximation of the second-order spatial derivative. Accordingly, the second-order spatial derivatives of the continuous function $u(x, y)$ of two spatial dimensions can be approximated by the following expressions:

$$\begin{aligned} (u_{xx})^n_{m,l} &\approx \frac{1}{12h^2}\left(16\left(M + M^{-1}\right) - \left(M^2 + M^{-2}\right) - 30I\right)\{v^n_{m,l}\} \qquad (4.60) \\ (u_{yy})^n_{m,l} &\approx \frac{1}{12h^2}\left(16\left(L + L^{-1}\right) - \left(L^2 + L^{-2}\right) - 30I\right)\{v^n_{m,l}\}. \qquad (4.61) \end{aligned}$$

These expressions can be directly substituted into the two-dimensional wave equation. For the time derivative, we keep the second-order accurate approximation that was used so far

$$(u_{tt})^n_{m,l} \approx \frac{1}{k^2}\left(Z + Z^{-1} - 2I\right)\{v^n_{m,l}\} \qquad (4.62)$$

so the resulting scheme, which can be written as

$$\begin{aligned} v_{m,l}^{n+1} &= \Big[\frac{c^2\lambda^2}{12}\Big(16\left(M+M^{-1}+L+L^{-1}\right)- \\ &\quad -\left(M^2+M^{-2}+L^2+L^{-2}\right)-60I\Big)+2I-Z^{-1}\Big]\{v_{m,l}^n\} \end{aligned} \tag{4.63}$$

is (2,4) accurate. By comparing this difference equation with Eq. (4.10), it can be seen that the calculation of the (2,4)-accurate scheme requires four additional additions per every grid point.

Stability Let us examine the stability of this scheme. By performing spatial Fourier-transform on Eq. (4.63), we obtain

$$\begin{aligned} V^{n+1}(\beta_x,\beta_y) &= \Big[\frac{c^2\lambda^2}{6}\Big(16\left(\cos h\beta_x+\cos h\beta_y\right)-\left(\cos 2h\beta_x+\cos 2h\beta_y\right)- \\ &\quad -30\Big)+2\Big]V^n(\beta_x,\beta_y)-V^{n-1}(\beta_x,\beta_y) \end{aligned} \tag{4.64}$$

which is equivalent to

$$V^{n+1}(\beta_x,\beta_y)-2DV^n(\beta_x,\beta_y)+V^{n-1}(\beta_x,\beta_y) = 0 \tag{4.65}$$

where

$$D = \frac{c^2\lambda^2}{12}\left(16\left(\cos h\beta_x+\cos h\beta_y\right)-\left(\cos 2h\beta_x+\cos 2h\beta_y\right)-30\right)+1. \tag{4.66}$$

It can be easily shown that the maximum of D is one, in which case the stability condition was shown to be $D>-1$ (see Theorem 3.6). This stability criterion is satisfied if

$$c^2\lambda^2\left(16\left(\cos h\beta_x+\cos h\beta_y\right)-\left(\cos 2h\beta_x+\cos 2h\beta_y\right)-30\right) \geq -24. \tag{4.67}$$

This can be satisfied for all values of β_x and β_y if

$$c^2\lambda^2\left(16\left(-2\right)-\left(2\right)-30\right) \geq -24 \tag{4.68}$$

$$c^2\lambda^2 \leq \frac{3}{8}. \tag{4.69}$$

Hence the stability criterion is

$$c \leq \sqrt{\frac{3}{8}}\frac{1}{\lambda} \tag{4.70}$$

which is a stricter condition than the one for the simpler, (2,2)-accurate scheme.

Numerical Dispersion As in the previous section, the phase velocity of the scheme can be numerically calculated. Fig. 4.10 and 4.11 shows the phase speed with respect to the wave numbers β_x and β_y for parameter values that are at and inside the stability margin, respectively. It can be seen that the increased order of accuracy has no direct beneficial effect on the dispersion properties of the scheme, that is, numerical dispersion is still present and the direction-dependence has not been decreased. According to [Bilbao 2001], the (2,4)-accurate scheme combined with the interpolation technique that will be presented in the next section can be effectively used to minimize direction-dependence of numerical dispersion, however, this will not be discussed in this thesis.

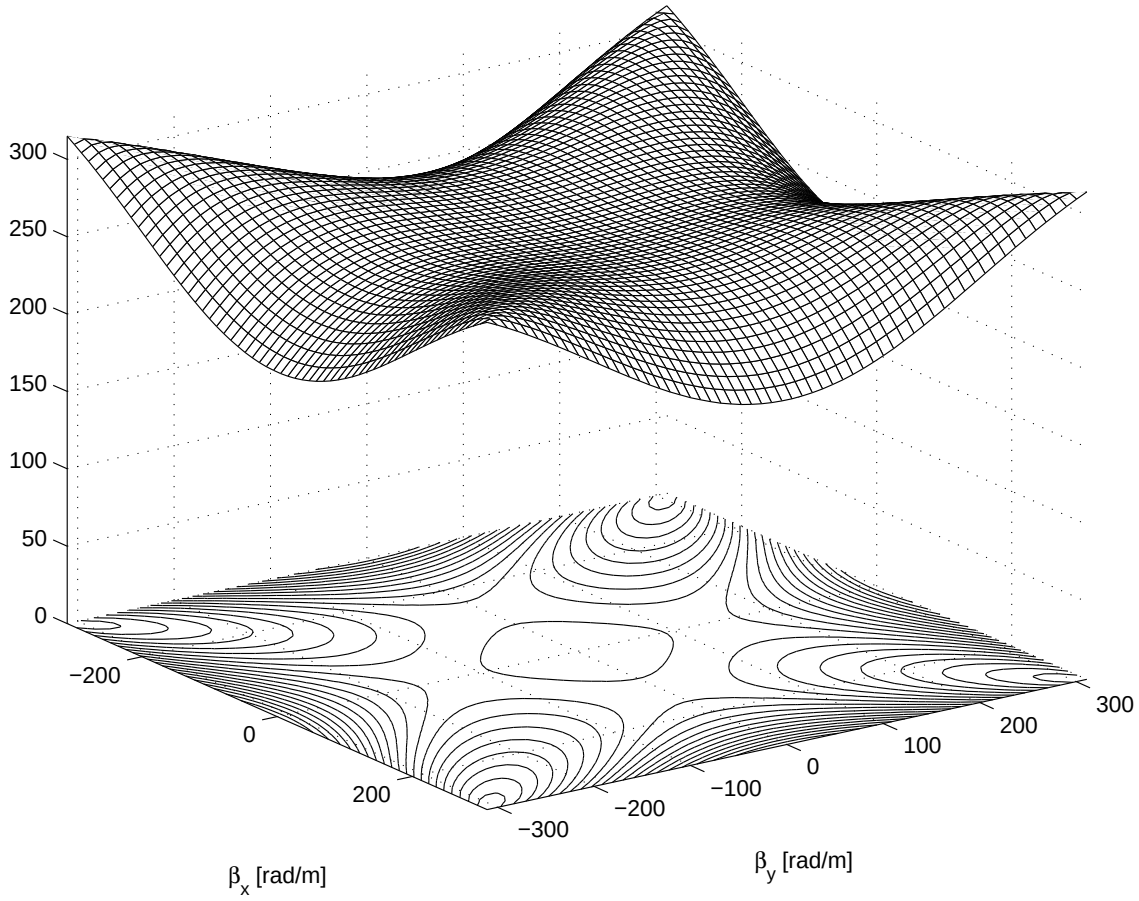

Figure 4.10: Phase speed of the (2,4) accurate membrane model with parameter values $c = \sqrt{(3/8)}/\lambda$ (stability margin) as a function of the spatial frequencies β_x and β_y. The theoretical value of c is 272.78 m/sec.

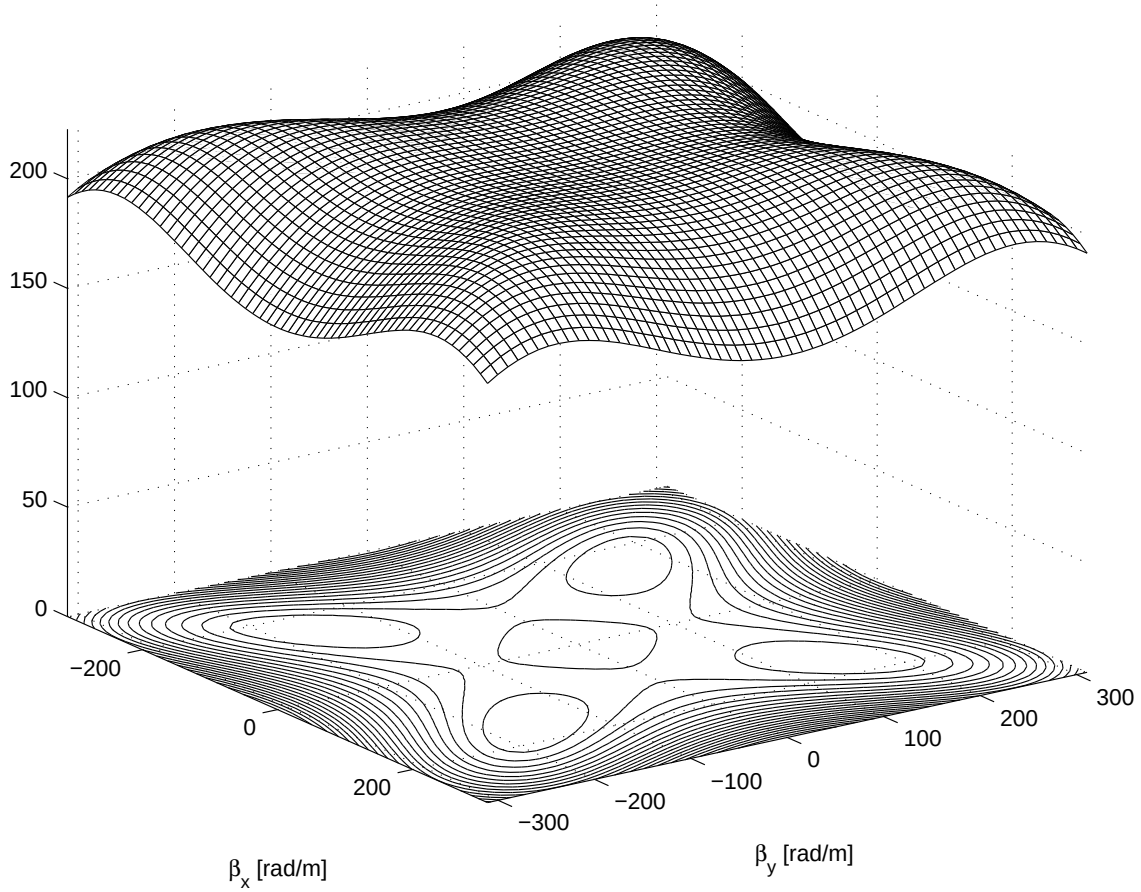

Figure 4.11: Phase speed of the (2,4) accurate membrane model with parameter values $c = 1/(2\lambda)$ as a function of the spatial frequencies β_x and β_y. The theoretical value of c is 222.73 m/sec.

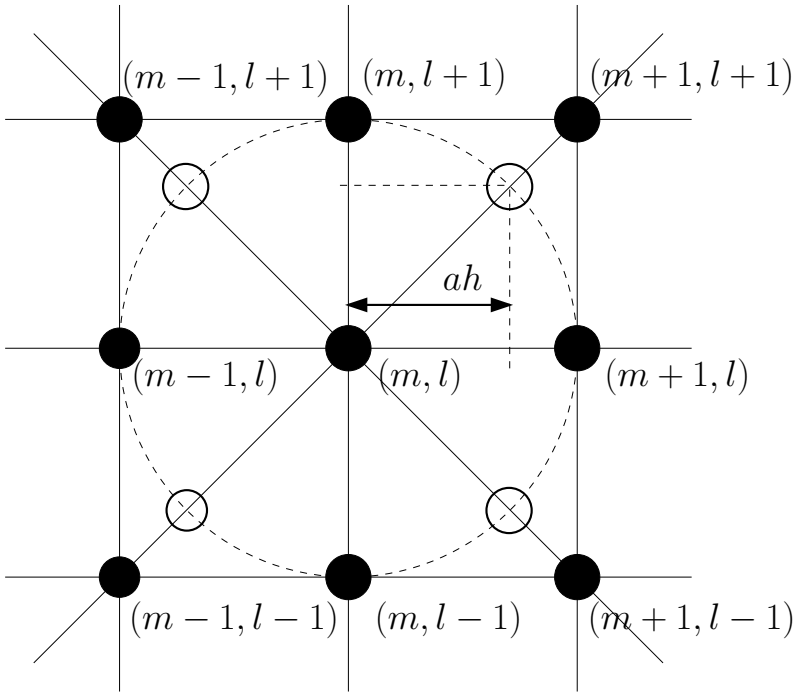

Figure 4.12: Bilinear interpolation of the membrane model discretized in Cartesian coordinate-system. As the grid function is undefined in the points denoted by empty circles, the displacement of the membrane has to be interpolated using the surrounding points (filled circles).

4.2 Interpolated Schemes

The direction-dependence of numerical dispersion in two-dimension can be reduced by using interpolated schemes. The method discussed here was proposed for correcting dispersion error of the digital waveguide mesh ([Savioja and Välimäki 1997], [Savioja and Välimäki 2000]) but it can also be applied to finite difference schemes ([Aird 2002]).

The idea behind this method is to use eight neighboring points in the finite difference approximation of the spatial derivatives instead of four. According to Fig. 4.12, the points denoted with empty circles are also used in the approximation. However, the grid function v is undefined in these points, so interpolation has to be used to obtain the approximate value of displacement. Due to its relative simplicity, we will use bilinear interpolation defined as follows:

$$v^n_{+,+} = \left[a^2 ML + a(1-a)\left(M + L\right) + (1-a)^2 I\right]\{v^n_{m,l}\} \quad (4.71)$$

$$v^n_{-,-} = \left[a^2 M^{-1}L^{-1} + a(1-a)\left(M^{-1} + L^{-1}\right) + (1-a)^2 I\right]\{v^n_{m,l}\} \quad (4.72)$$

$$v^n_{+,-} = \left[a^2 ML^{-1} + a(1-a)\left(M + L^{-1}\right) + (1-a)^2 I\right]\{v^n_{m,l}\} \quad (4.73)$$

$$v^n_{-,+} = \left[a^2 M^{-1}L + a(1-a)\left(M^{-1} + L\right) + (1-a)^2 I\right]\{v^n_{m,l}\} \quad (4.74)$$

where $a = 1/\sqrt{2}$ and $v^n_{+,+}$, $v^n_{-,-}$, $v^n_{+,-}$ and $v^n_{-,+}$ denote the displacement in the four interpolated points on the circle. That is, the displacement in each of the four additional

points (empty circles in Fig. 4.12) is approximated as a linear combination of the displacement in the four surrounding grid points. The spatial derivatives can be approximated by using only the four interpolated points in a way analogous to the before-mentioned approximations:

$$\frac{\partial^2 u}{\partial x^2} + \frac{\partial^2 u}{\partial y^2} \approx \frac{K}{h^2}\left(v^n_{+,+} + v^n_{-,-} + v^n_{+,-} + v^n_{-,+} - 4v^n_m\right) = \delta^2_\star\{v^n_{m,l}\}. \tag{4.75}$$

The consistency of this approximation can be analyzed by Taylor-series expansion. It can be shown that $\delta^2_\star$ is a consistent, second-order accurate approximation of the spatial derivatives if $K = 1/(2a)$. It is easy to see that the linear combination of consistent operators is also consistent if the sum of their coefficients is one, so we obtain our final expression for the spatial approximation:

$$\frac{\partial^2}{\partial x^2} + \frac{\partial^2}{\partial y^2} \approx \frac{1}{2}\left(\delta^2_+ + \delta^2_\star\right). \tag{4.76}$$

Substituting this expression into the two-dimensional wave equation yields

$$\begin{aligned} v^{n+1}_{m,l} = {} & \big[a_1\left(ML + M^{-1}L^{-1} + M^{-1}L + ML^{-1}\right) + \\ & + a_2\left(M + M^{-1} + L + L^{-1}\right) + a_3 I - Z^{-1}\big]\{v^n_{m,l}\} \end{aligned} \tag{4.77}$$

which is equivalent to

$$\begin{aligned} v^{n+1}_{m,l} = {} & a_1\left(v^n_{m+1,l+1} + v^n_{m-1,l-1} + v^n_{m+1,l-1} + v^n_{m-1,l+1}\right) + \\ & + a_2\left(v^n_{m+1,l} + v^n_{m-1,l} + v^n_{m,l+1} + v^n_{m,l-1}\right) + a_3 v^n_{m,l} - v^{n-1}_{m,l} \end{aligned} \tag{4.78}$$

where the constans are

$$a_1 = c^2\lambda^2 a/4 \tag{4.79}$$

$$a_2 = c^2\lambda^2(2-a)/2 \tag{4.80}$$

$$a_3 = c^2\lambda^2(a-4) + 2. \tag{4.81}$$

By applying Von Neumann analysis in the usual way, we obtain the stability condition

$$c \leq \frac{1}{\lambda}\sqrt{\frac{1}{2-a}}. \tag{4.82}$$

The phase speed with respect to spatial frequencies is shown in Fig. 4.13 and 4.14. In can be seen that the direction-dependence of the phase speed is greatly reduced.

Another approach for correcting direction-dependent dispersion is presented in [Bilbao and Smith 2003]. Let us furst define the operator $\delta^2_\times$, which is also a second-order accurate approximation of $\partial^2/\partial x^2 + \partial^2/\partial y^2$ (see Fig. 4.15):

$$\delta^2_\times = \frac{1}{2h^2}\left(ML + M^{-1}L^{-1} + M^{-1}L + ML^{-1} - 4I\right). \tag{4.83}$$

The spatial derivatives may be approximated by the linear combination of two consistent

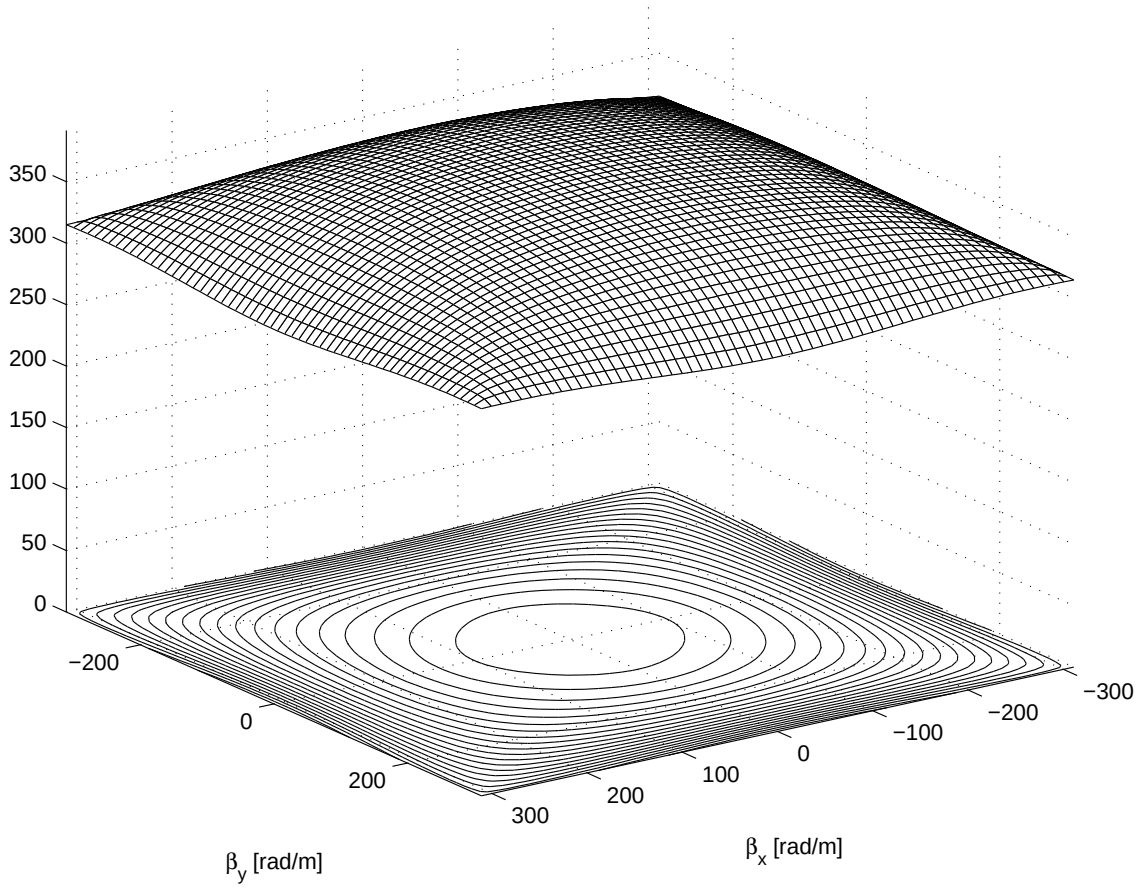

Figure 4.13: Phase speed of the interpolated scheme at the stability margin as a function of the spatial frequencies β_x and β_y. The theoretical value of c is 391.76 m/sec.

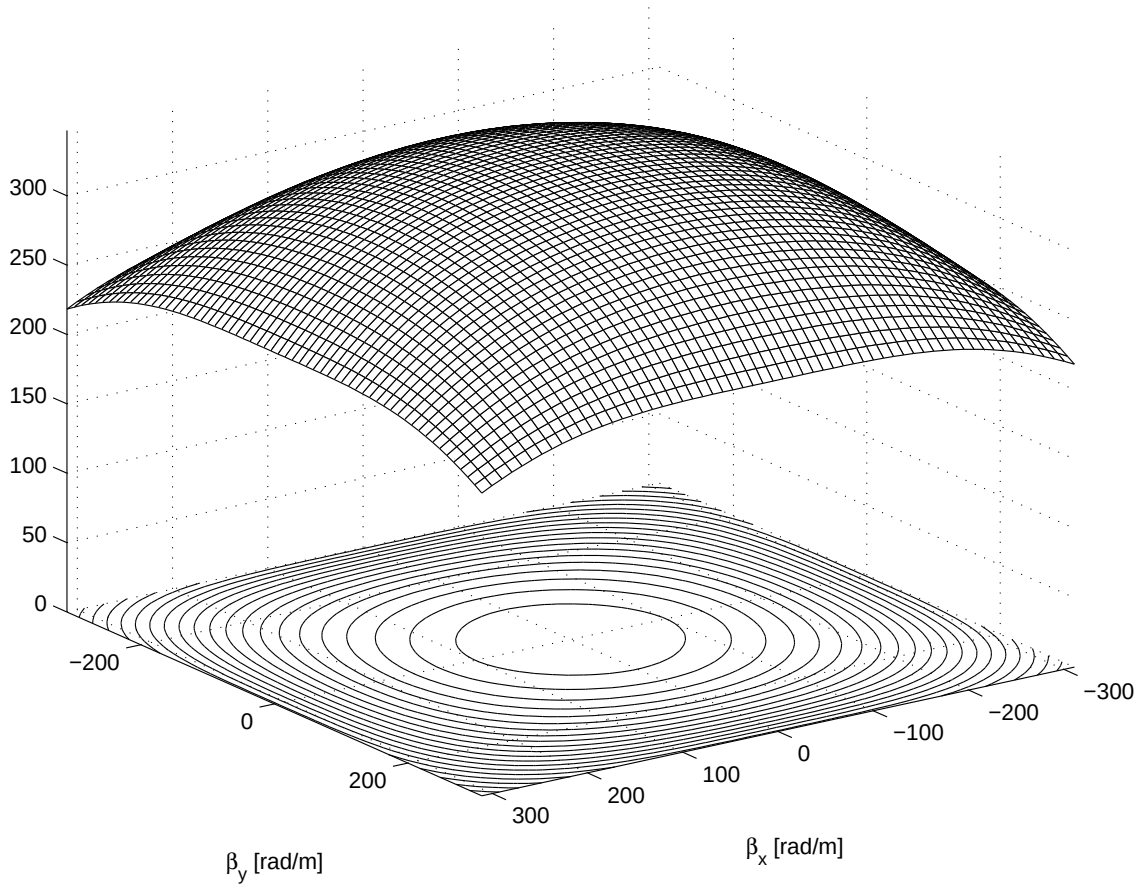

Figure 4.14: Phase speed of the interpolated scheme at the inside the stability margin as a function of the spatial frequencies β_x and β_y. The theoretical value of c is 347.16 m/sec.

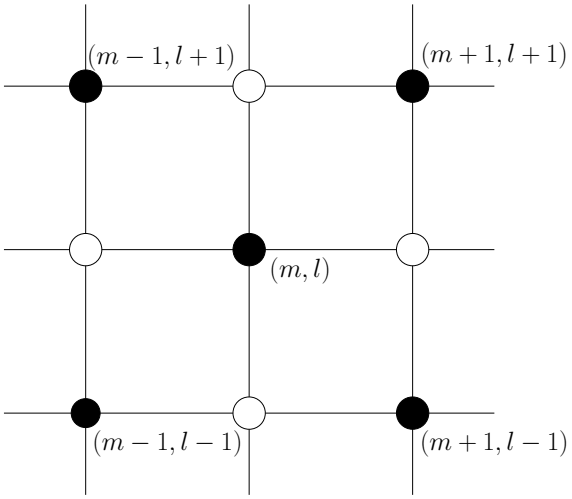

Figure 4.15: Illustration of the $\delta_{\times}^2$ operator. The points involved in the approximation of the spatial derivatives are filled with black.

finite difference operators:

$$\frac{\partial^2}{\partial x^2} + \frac{\partial^2}{\partial y^2} \approx \left(p\delta_+^2 + (1-p)\delta_{\times}^2\right). \tag{4.84}$$

It can be shown that if $p = 1 - a/2 = 0.6464$ then Eq. (4.84) is equivalent to Eq. (4.76). According to [Bilbao and Smith 2003], the minimally direction-dependent numerical dispersion allowed by this scheme belongs to the parameter value $p = 2/3$. Besides, in [Bilbao 2001, p. 332], the combination of the techniques introduced in this and the previous section is presented, that is, a (2,4)-accurate interpolated scheme. It is shown that by using this method, higher degree of direction-independence can be achieved.

4.3 Finite Difference Schemes for the Damped Membrane

4.3.1 Frequency-independent Damping

According to Chapter 2, damping can be represented by subtracting the term $d_1 u_t$ from the two-dimensional wave equation, that is,

$$\frac{\partial^2 u}{\partial t^2} = c^2 \left(\frac{\partial^2 u}{\partial x^2} + \frac{\partial^2 u}{\partial y^2} \right) - d_1 \frac{\partial u}{\partial t}. \tag{4.85}$$

The additional term $d_1 u_t$ can be approximated in several ways. By applying the forward, backward and central time operators (see Eq. (3.4), (3.5) and (3.6)), we obtain the following finite difference schemes:

$$\delta_t^2\{v_m^n\} = \left[c^2\left(\delta_x^2 + \delta_y^2\right) - d_1\delta_{t+}\right]\{v_m^n\} \tag{4.86}$$

$$\delta_t^2\{v_m^n\} = \left[c^2\left(\delta_x^2 + \delta_y^2\right) - d_1\delta_{t-}\right]\{v_m^n\} \tag{4.87}$$

$$\delta_t^2\{v_m^n\} = \left[c^2\left(\delta_x^2 + \delta_y^2\right) - d_1\delta_{t0}\right]\{v_m^n\}. \tag{4.88}$$

All of these schemes can be rearranged to the form of

$$v_{m,l}^{n+1} = \left[a_1\left(M + M^{-1} + L + L^{-1}\right) + a_2 I + a_3 Z^{-1}\right]\{v_{m,l}^n\}. \tag{4.89}$$

The constants a_1, a_2 and a_3 are determined by the operator used for approximating u_t in the PDE, and are listed in Table 4.1. The complexity of the scheme is not affected

	a_1	a_2	a_3
FW	$c^2\lambda^2/(d_1k+1)$	$(2(1-2c^2\lambda^2)+d_1k)/(d_1k+1)$	$-1/(d_1k+1)$
BW	$c^2\lambda^2$	$2(1-2c^2\lambda^2)-d_1k$	d_1k-1
CNT	$2c^2\lambda^2/(d_1k+2)$	$4(1-2c^2\lambda^2)/(d_1k+2)$	$(d_1k-2)/(d_1k+2)$

Table 4.1: Values of the constants a_1, a_2 and a_3 in Eq. (4.89) with regard to the way the term u_t in Eq. (4.85) is approximated. FW, BW and CNT denote the forward, backward and central time approximation of u_t, respectively.

by the choice of the operator. However, the stability of the scheme is influenced to some extent. By applying the usual steps of von Neumann analysis to Eq. (4.89), we obtain the amplification polynomial

$$\Phi(g) = g^2 - 2Dg - a_3 \tag{4.90}$$

where

$$D = a_1\left(\cos h\beta_x + \cos h\beta_y\right) + \frac{a_2}{2}. \tag{4.91}$$

The scheme is stable if the roots of Φ are less than or equal to one for all values of β_x and β_y, that is,

$$|g_\pm| = \left| D \pm \sqrt{D^2 + a_3} \right| \leq 1. \tag{4.92}$$

	FW	BW	CNT
$c \leq$	$\frac{\sqrt{2+d_1 k}}{2\lambda}$	$\frac{\sqrt{2-d_1 k}}{2\lambda}$	$\frac{1}{\lambda\sqrt{2}}$

Table 4.2: Maximal values of c that yield a stable scheme for Eq. (4.85) with the term u_t approximated by the forward (FW), backward (BW) and central (CNT) time operator, respectively.

The stability limits for c obtained by solving this inequality are listed in Table 4.2. It can be seen that the stability conditions are compatible with our previous results, that is, if d_1 is zero then the stability conditions in Table 4.2 become simplified to the stability condition of the undamped membrane (see Eq. (4.40)). Hereafter, the central approximation will be used as the stability of the scheme obtained this way is independent of the value of d_1. Furthermore, this choice, contrarily to the other two methods, does not detract from the overall accuracy of the scheme[2].

Fig. 4.16 shows the effect of damping in the displacement-time functions generated by the finite difference scheme according to Eq. (4.88) for several values of the parameter d_1. It can be seen that, as expected, the damping effect is more significant for larger values of d_1.

4.3.2 Frequency-dependent Damping

According to Chapter 2, the frequency-dependence of the damping can be taken into account by the following form of the wave equation:

$$\frac{\partial^2 u}{\partial t^2} = c^2 \left(\frac{\partial^2 u}{\partial x^2} + \frac{\partial^2 u}{\partial y^2} \right) - d_1 \frac{\partial u}{\partial t} + d_2 \frac{\partial}{\partial t} \left(\frac{\partial^2 u}{\partial x^2} + \frac{\partial^2 u}{\partial y^2} \right). \tag{4.93}$$

The derivatives with respect to space in the rightmost term will be approximated in the usual way using the operators δ_x^2 and δ_y^2. For the first-order time derivative in the same term, however, applying the central difference operator δ_{t0}, as in the previous section, yields an implicit scheme. Implementation and analysis of implicit schemes is out of the scope of this thesis. Therefore, in order to obtain an explicit scheme for Eq. (4.93), the backward difference operator δ_{t-} will be used, that is,

$$\delta_t^2 \{v_{m,l}^n\} = \left[c^2 \left(\delta_x^2 + \delta_y^2 \right) - d_1 \delta_{t0} + d_2 \delta_{t-} \left(\delta_x^2 + \delta_y^2 \right) \right] \{v_{m,l}^n\}. \tag{4.94}$$

After expressing the value of v on time level $n+1$, we obtain

$$\begin{aligned} v_{m,l}^{n+1} = {} & \left[a_1 \left(M + M^{-1} + L + L^{-1} \right) + a_2 I \right] \{v_{m,l}^n\} + \\ & + \left[a_3 \left(M + M^{-1} + L + L^{-1} \right) + a_4 I \right] \{v_{m,l}^{n-1}\} \end{aligned} \tag{4.95}$$

[2]The accuracy of δ_{t0} is two while δ_{t+} and δ_{t-} are first-order accurate approximations (see Table 3.1 in Section 3.2.4).

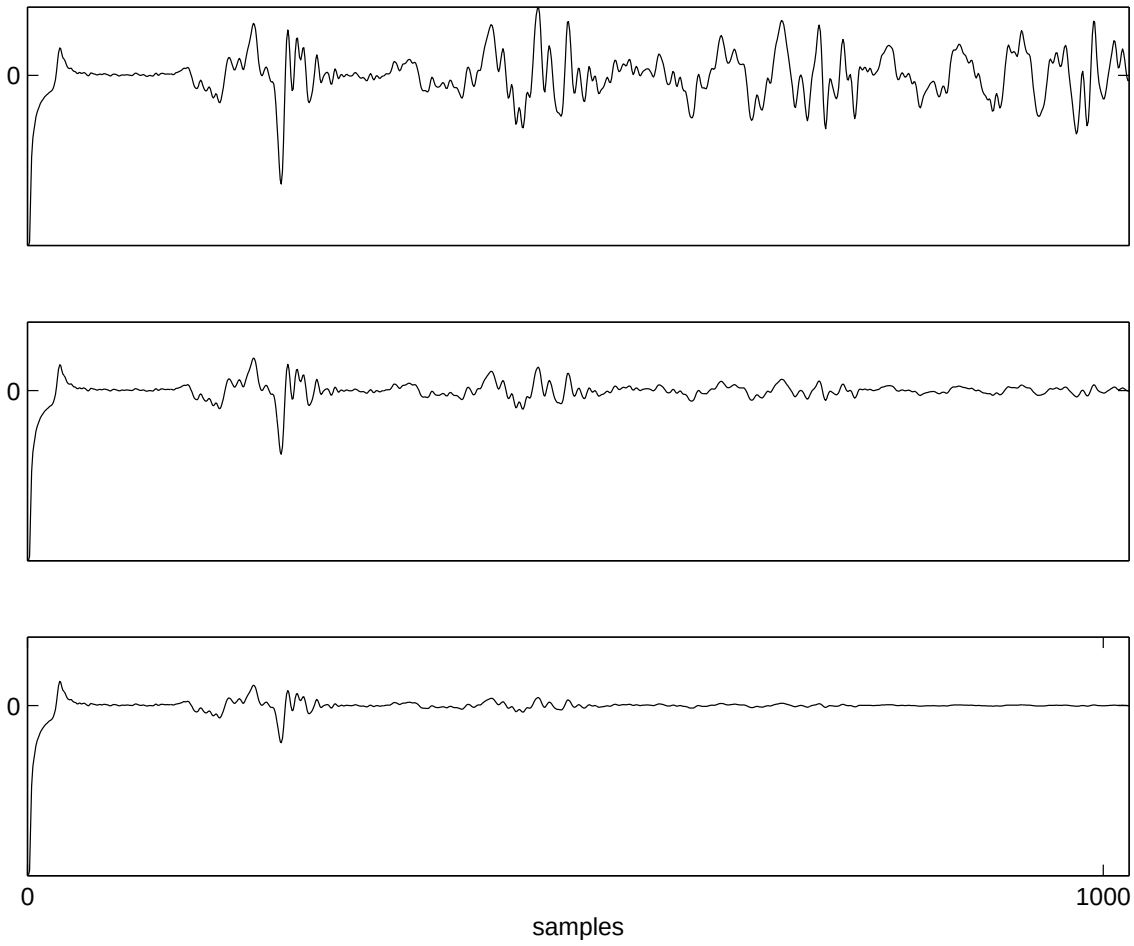

Figure 4.16: Displacement of a point of the the membrane model including frequency-independent damping as a function of time. The top, center and bottom figures were generated by setting the value of d_1 to zero, 200 and 400, respectively.

where the constants are defined as

$$\begin{aligned} a_1 &= 2\nu\left(c^2\lambda^2 + d_2\mu\right) && (4.96)\\ a_2 &= 4\nu\left(1 - 2c^2\lambda^2 - 2d_2\mu\right) && (4.97)\\ a_3 &= -2\nu d_2\mu && (4.98)\\ a_4 &= \nu\left(d_1 k + 8d_2\mu - 2\right) && (4.99)\\ \mu &= k/h^2 && (4.100)\\ \nu &= 1/(2 + d_1 k). && (4.101) \end{aligned}$$

Neumann-analysis leads to the following stability condition:

$$c \leq \frac{\sqrt{2h^2 - 8d_2 k}}{2k}. \tag{4.102}$$

The expression on the right-hand side has to be real which yields an additional restriction for the value of d_2:

$$d_2 \leq \frac{h^2}{4k}. \tag{4.103}$$

By definition, the amplification factors g_+ and g_- describe how the spatial frequency spectrum is changed while proceeding form time step n to $n+1$. More precisely, the spectrum is multiplied by the amplification factors in each time step. Accordingly, if the magnitude of the amplification factors is one, it means that there is no damping in the model, that is, the waves will not decay. If the magnitude is constant with respect to the spatial frequencies, and it is less than one, then frequency-independent damping is present, and each spatial frequency component of the waves decay at the same rate. If $|g_\pm|$ is not constant with respect to β_x and β_y, then the damping is frequency-dependent, which is illustrated in Fig. 4.17. The values of the parameter d_2 were chosen with regard to visualization purposes. For modeling the sound of a drum, usually d_2 has to be chosen to be less then 0.1. It can be seen in Fig. 4.17 that frequency-dependent damping can be regarded as a low-pass filter in the spatial frequency domain.

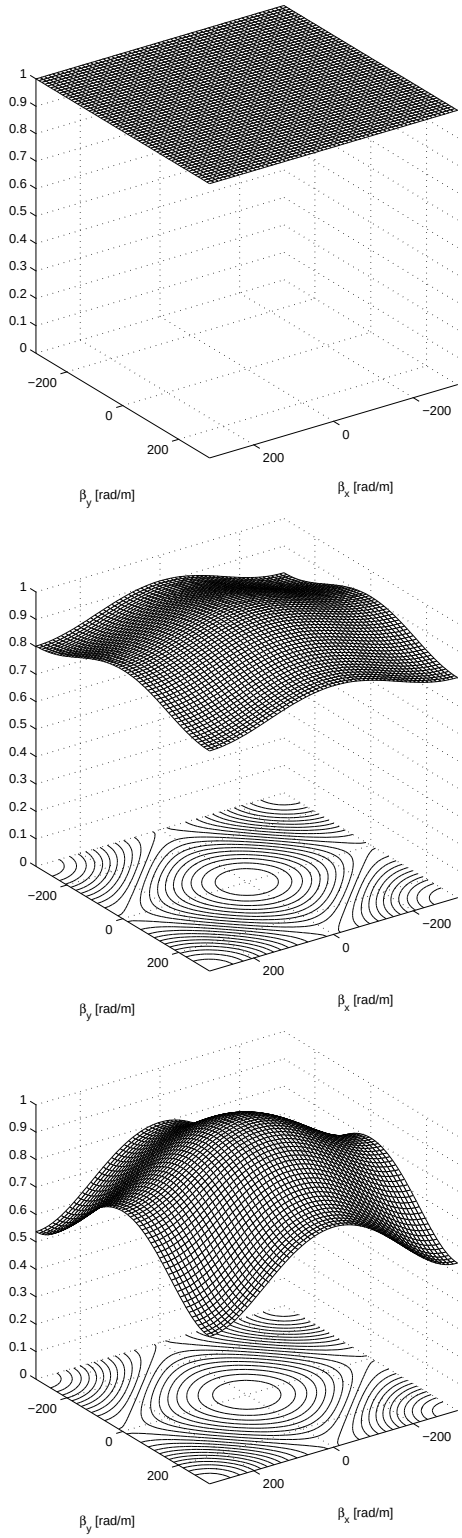

Figure 4.17: Magnitude of the amplification factors with respect to the wave numbers β_x and β_y for the membrane model with frequency-dependent damping for the parameter values d_2 equals 0, 0.2 and 0.4, respectively.

4.4 Discretization in Triangular Coordinate System

In this section, we will discuss the triangular discretization of a membrane in great detail. Some of the results presented here can be found in [Aird 2002] and in [Bilbao 2001].

Discretization of the PDE Let us consider the triangular form of the two-dimensional wave equation, which was introduced in Chapter 2:

$$\frac{\partial^2 u}{\partial t^2} = c^2 \frac{2}{3} \left(\frac{\partial^2 u}{\partial x^2} + \frac{\partial^2 u}{\partial w^2} + \frac{\partial^2 u}{\partial z^2} \right). \tag{4.104}$$

This form of the PDE suggests that the displacement u is a function of four variables, however, the unit vectors along the three spatial coordinate axes x, w and z are linearly dependent, hence the spatial variable z can be expressed as a linear combination of the other two spatial variables. Consequently, u only depends on t, x and w. As before, the continuous function u will be approximated only in a discrete set of points, however, these points are now defined in the triangular coordinate system as follows:

$$u(x_m, w_q, t_n) \approx v^n_{m,q} \tag{4.105}$$

where

$$x_m = mh \tag{4.106}$$
$$w_q = qh \tag{4.107}$$
$$t_n = nk. \tag{4.108}$$

The index variables m, q and n are integers. The spatial indices in the triangular coordinate system can be interpreted according to Fig. 4.18. The spatial shift operators can be defined

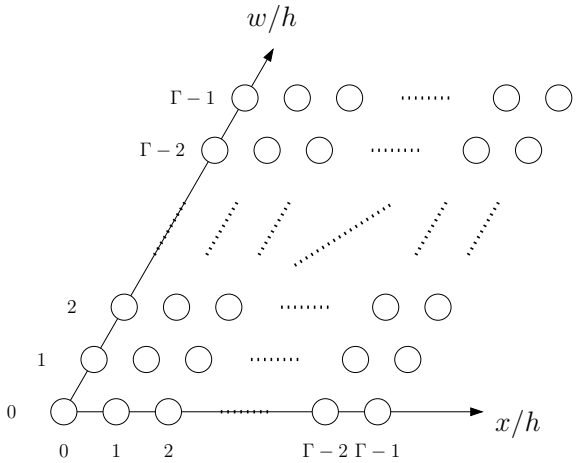

Figure 4.18: Illustration of the indices of a grid function in triangular coordinate system. The $\Gamma \times \Gamma$ point triangular mesh corresponds to a diamond-shaped domain of space with length along side L, where $L = (\Gamma - 1)h$ and $m, q \in [0, \Gamma - 1]$.

as follows:

$$\begin{aligned} M\{v^n_{m,q}\} &= v^n_{m+1,q} & \qquad M^{-1}\{v^n_{m,q}\} &= v^n_{m-1,q} \\ Q\{v^n_{m,q}\} &= v^n_{m,q+1} & \qquad Q^{-1}\{v^n_{m,q}\} &= v^n_{m,q-1}. \end{aligned}$$

The formal definition of the shift operators is identical with what was presented in Section 4.1 for the Cartesian coordinate system. However, as the coordinate axes are different, the indices should be interpreted differently. The meaning of the identity operator is the same.

$$I\{v^n_{m,q}\} = v^n_{m,q}. \tag{4.109}$$

For the reasons presented above, the unit shift operators along the z axis can be expressed by the other operators as follows:

$$MQ^{-1}\{v^n_{m,q}\} = v^n_{m+1,q-1} \qquad \text{(positive unit shift along the } z \text{ axis)} \tag{4.110}$$

$$M^{-1}Q\,\{v^n_{m,q}\} = v^n_{m-1,q+1} \qquad \text{(negative unit shift along the } z \text{ axis)}. \tag{4.111}$$

Let us also define the difference operators using the above definitions:

$$\delta_x^2 = \frac{1}{h^2}\left(M - 2I + M^{-1}\right) \tag{4.112}$$

$$\delta_w^2 = \frac{1}{h^2}\left(Q - 2I + Q^{-1}\right) \tag{4.113}$$

$$\delta_z^2 = \frac{1}{h^2}\left(MQ^{-1} - 2I + M^{-1}Q\right). \tag{4.114}$$

It can be easily seen that δ_x^2, δ_w^2 and δ_z^2 are second-order accurate approximations of the differential perators $\partial^2/\partial x^2$, $\partial^2/\partial w^2$ and $\partial^2/\partial z^2$, respectively. By replacing the corresponding derivatives in Eq. (4.104), we obtain

$$\delta_t^2\{v^n_{m,q}\} = c^2\frac{2}{3}\left(\delta_x^2 + \delta_w^2 + \delta_z^2\right)\{v^n_{m,q}\} \tag{4.115}$$

which can be rearranged to the usual explicit form:

$$\begin{aligned} v^{n+1}_{m,q} = \Bigg[& c^2\lambda^2\frac{2}{3}\big(M + M^{-1} + Q + Q^{-1} + \\ & + MQ^{-1} + M^{-1}Q - 6I\big) + 2I\Bigg]\{v^n_{m,q}\} - v^{n-1}_{m,q}. \end{aligned} \tag{4.116}$$

The points that are needed by the approximation of the spatial derivatives are shown in Fig. 4.19.

Implementation of Circular Boundary Conditions According to the results of Chapter 2, the boundary conditions corresponding to a circular membrane in triangular coordinate system can be formulated as follows:

$$u(x,w,t) = 0 \qquad \text{if} \qquad \left(x + \frac{w}{2} - x_0 - \frac{w_0}{2}\right)^2 + \left(\frac{\sqrt{3}}{2}w - \frac{\sqrt{3}}{2}w_0\right)^2 \geq R^2 \tag{4.117}$$

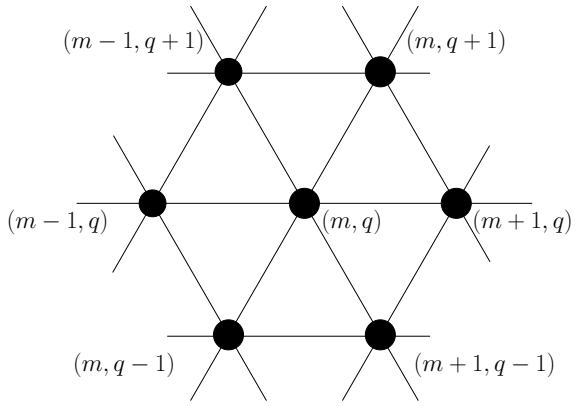

Figure 4.19: The points involved in approximation of the spatial derivatives in triangular coordinate system.

where R is the radius of the membrane. In order to maximally utilize the avalaible area, the center of the circle has to coincide with the center of the diamond-shaped domain shown in Fig. 4.18. This point corresponds to the triangular coordinates $x_0 = w_0 = L/2$. However, contrary to the Cartesian discretization, the radius of the circle cannot equal to $L/2$ because in this case the circle does not fit the available space (see Fig. 4.20 a)). The maximum value of the radius that yields a circle of appropriate size is $R = L\sqrt{3}/4$ (see Fig. 4.20 b)). In order to construct a scheme that is comparable with the one that was obtained by Cartesian discretization, however, the radius of the circle has to be equal to $L/2$. While keeping the maximal utilization of the available area in view, this can be accomplished in two ways:

- Increasing the values of L and h to $L' = L\frac{2}{\sqrt{3}}$ and $h' = h\frac{2}{\sqrt{3}}$ (see Fig. 4.20 c)).

- Increasing the value of L to $L' = L\frac{2}{\sqrt{3}}$ while keeping the value of h unchanged.

The first method has several advantages over the second one:

- The number of grid points is unchanged, thus the computational load is not increased.

- Contrary to the second case, the radius of the membrane can be modeled exactly. In the second case, if Γ is integer then $\Gamma' = (L'/h + 1)$ is not an integer, that is, L' and the radius has to be approximated.

Accordingly, the first method will be used, which is illustrated in Fig. 4.20 c). For clarity, we will not use the L' and h' notations, however, L and h will denote the modified values of these parameters in the rest of this section.

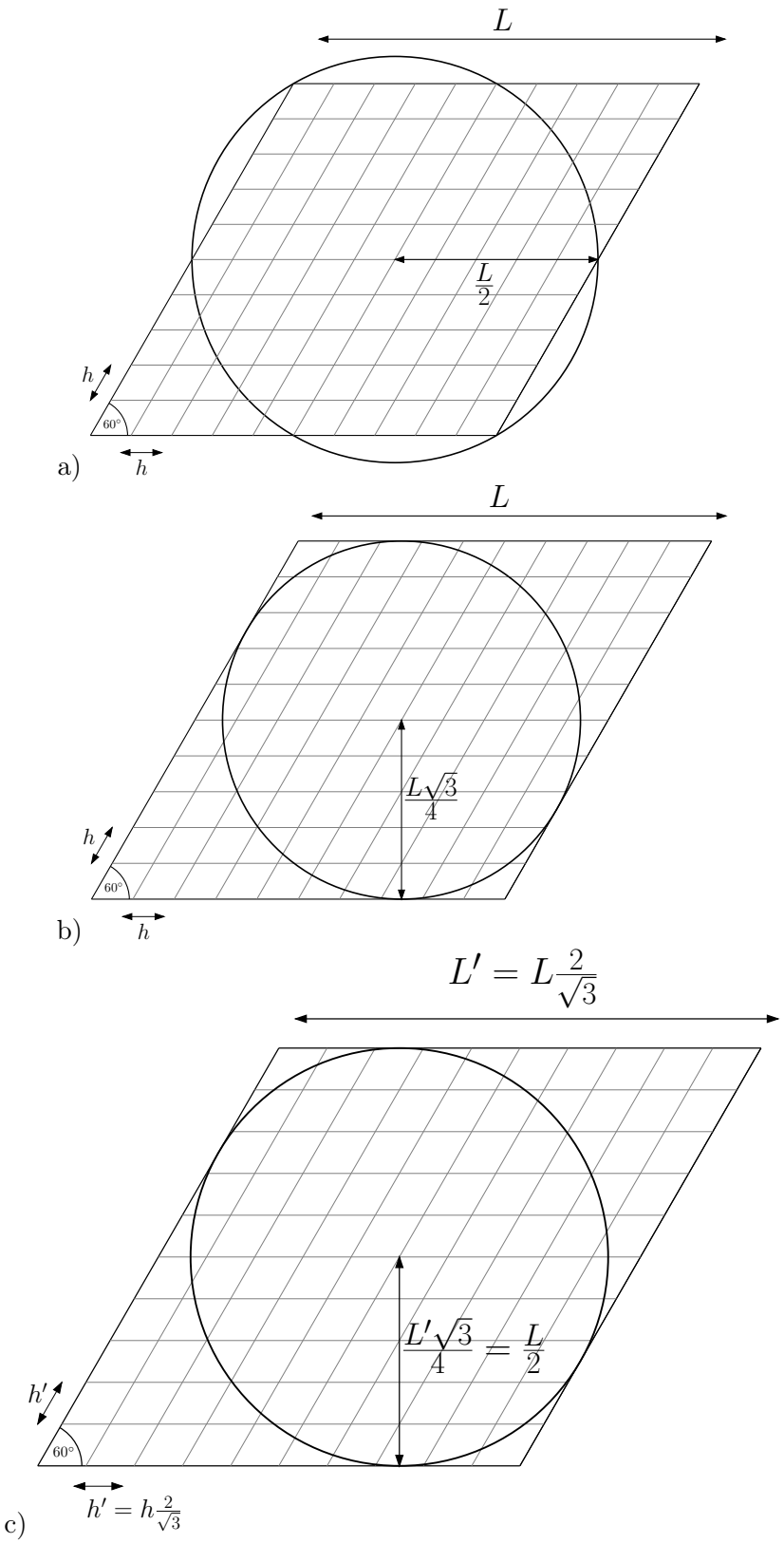

Figure 4.20: Implementation of circular boundary conditions.

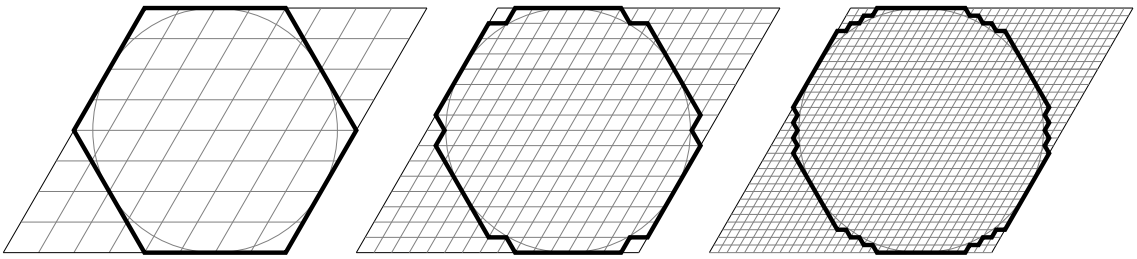

Figure 4.21: Circular boundary conditions for the 8×8, 16×16 and 32×32-point membrane models discretized in triangular coordinate-system. The displacement of the points outside the area bounded by the solid black line and on the line itself is identically zero for all time steps.

Let us discretize the boundary conditions defined by Eq. (4.117) by making the following substitutions:

$$x = mh \tag{4.118}$$

$$w = qh \tag{4.119}$$

$$x_0 = w_0 = \frac{L}{2} = \frac{\Gamma-1}{2}h \tag{4.120}$$

$$R = L\frac{\sqrt{3}}{4} = (\Gamma-1)\frac{\sqrt{3}}{4}h \tag{4.121}$$

We obtain

$$v^n_{m,q} = 0 \qquad \text{if} \qquad \left(m+\frac{q}{2}-\frac{\Gamma-1}{2}\frac{3}{2}\right)^2+\frac{3}{4}\left(q-\frac{\Gamma-1}{2}\right)^2 \geq \left((\Gamma-1)\frac{\sqrt{3}}{4}\right)^2 \tag{4.122}$$

which can be implemented directly. Fig. 4.21 shows how the boundary is refined as the value of h is decreased. By comparing this to the circular boundary conditions discretized in the Cartesian coordinate system shown in Fig. 4.3, it can be seen that the triangular coordinate system yields a smoother boundary.

Excitation For the triangular model, the same excitation will be used that was presented in Section 4.1, that is, the initial displacement is zero and the initial velocity, $g(x,w)$, is a two-dimensional raised cosine function. According to the above, the initial displacement can be easily transformed to the triangular form needed by the triangular model. Without dealing with the details, we only present the results. The initial velocity in triangular coordinates can be expressed as follows:

$$g(mh,qh) = \begin{cases} 0.5\cos\left(\pi\frac{d}{r_e}\right)+0.5 & \text{if } d \leq r_e \\ 0 & \text{if } d > r_e \end{cases}$$

where $r_e h$ is the radius of excitation and dh is the distance from the center of excitation. The variable d is defined as

$$d = \sqrt{\left(m+\frac{q}{2}-m_e-\frac{q_e}{2}\right)^2+\frac{3}{4}(q-q_e)^2} \tag{4.123}$$

The triangular coordinates of the center of excitation are $m_e h$ and $q_e h$.

According to the above results, the initial-boundary value problem representing a circular membrane can be written in the following form:

Scheme:

$$v_{m,q}^{n+1} = a_1\Big(v_{m+1,q}^n + v_{m-1,q}^n + v_{m,q+1}^n + v_{m,q-1}^n + v_{m+1,q-1}^n + v_{m-1,q+1}^n\Big) + a_2 v_{m,q}^n - v_{m,q}^{n-1} \tag{4.124}$$

Initial conditions:

$$v_{m,q}^0 = 0 \tag{4.125}$$

$$v_{m,q}^1 = kg(mh, qh) \tag{4.126}$$

Boundary conditions:

$$v_{m,q}^n = 0 \quad \text{if} \quad \left(m + \frac{q}{2} - \frac{\Gamma-1}{2}\frac{3}{2}\right)^2 + \frac{3}{4}\left(q - \frac{\Gamma-1}{2}\right)^2 \geq \left((\Gamma-1)\frac{\sqrt{3}}{4}\right)^2 \tag{4.127}$$

where $a_1 = c^2\lambda^2\frac{2}{3}$ and $a_2 = 2\,(1-3a_1)$. The displacement calculated according to this model is shown in Fig. 4.22

Stability The two-dimensional spatial Fourier-transform according to Def. 4.1 can be formally applied to any grid function with two spatial dimensions. However, as the spatial variables of a grid function are different in the Cartesian and the triangular coordinate systems, the spatial frequency variables are not expected to be the same either. That is, the spatial frequency spectrum of a triangular grid function is dependent on the wave numbers denoted by β_x and β_w. The shift theorem of the Fourier-transform, however, holds true so Fourier-transformation of Eq. (4.116) yields

$$V^{n+1}(\beta_x, \beta_w) = \left[2c^2\lambda^2\frac{2}{3}\Big(\cos h\beta_x + \cos h\beta_w + \cos h\,(\beta_x - \beta_w) - 3\Big) + 2\right]V^n(\beta_x, \beta_w) - V^{n-1}(\beta_x, \beta_w). \tag{4.128}$$

In order to be comparable with our foregoing results, Eq. (4.128) has to be expressed in the wave numbers of the Cartesian coordinate-system, β_x and β_y. According to the results of Appendix B, this can be accomplished by making the substitution

$$\beta_w = \frac{1}{2}\beta_x + \frac{\sqrt{3}}{2}\beta_y \tag{4.129}$$

and dividing each term of the equation by the determinant of the transform

$$\det \mathbf{S} = \frac{2\sqrt{3}}{3} \tag{4.130}$$

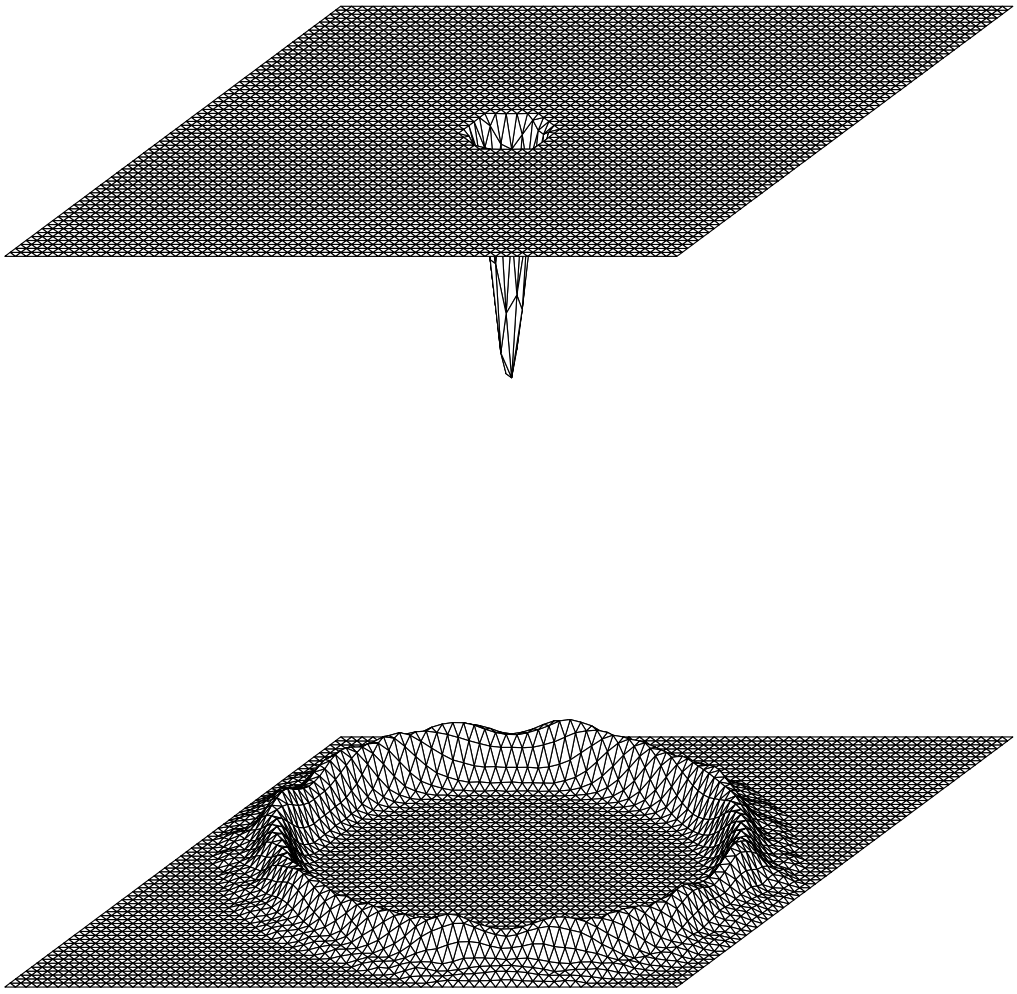

Figure 4.22: Displacement calculated by the 64×64 point triangular membrane model 'hit' at its center at time steps 2 and 42. The parameter c equals $\sqrt{2/3}/\lambda$, which corresponds to the stability margin.

where S was defined in Chapter 2. After some trigonometry we obtain

$$\hat{V}^{n+1} = \left[2 + 2c^2\lambda^2\frac{2}{3}\left(\cos h\beta_x + 2\cos\left(\frac{h}{2}\beta_x\right)\cos\left(\frac{h\sqrt{3}}{2}\beta_y\right) - 3\right)\right]\hat{V}^n - \hat{V}^{n-1} \tag{4.131}$$

where $\hat{V}^n$ is used as a notational shortcut for

$$\frac{3}{2\sqrt{3}}\,V^n\left(\beta_x, \frac{1}{2}\beta_x + \frac{\sqrt{3}}{2}\beta_y\right). \tag{4.132}$$

Eq. (4.131) results in the amplification polynomial of the usual form:

$$\Phi(g) = g^2 - 2Dg + 1 = 0 \tag{4.133}$$

where

$$D = 1 + c^2\lambda^2\frac{2}{3}\left(\cos h\beta_x + 2\cos\left(\frac{h}{2}\beta_x\right)\cos\left(\frac{h\sqrt{3}}{2}\beta_y\right) - 3\right). \tag{4.134}$$

Apparently, D cannot be greater than one, thus the usual stability criterion, i.e., $D \geq -1$ can be used (see Theorem 3.6). It can be shown that the minimum of the expression in parentheses is

$$\min_{\beta_x,\beta_y}\left\{\cos h\beta_x + 2\cos\left(\frac{h}{2}\beta_x\right)\cos\left(\frac{h\sqrt{3}}{2}\beta_y\right)\right\} = -\frac{3}{2} \tag{4.135}$$

which implies the following condition of stability:

$$c^2\lambda^2\frac{2}{3}\left(-\frac{3}{2} - 3\right) \geq -2 \tag{4.136}$$

$$c^2\lambda^2 \leq \frac{2}{3} \tag{4.137}$$

that is,

$$c \leq \frac{1}{\lambda}\sqrt{\frac{2}{3}}. \tag{4.138}$$

By comparing this with the stability criterion of the Cartesian membrane model, which is

$$c \leq \frac{1}{\lambda}\frac{1}{\sqrt{2}} \tag{4.139}$$

it can be seen that the triangular discretization allows using higher values of c (with the other variables unchanged) without resulting in an unstable model.

Let us discuss the case when the number of grid points is chosen to be equal to the number of grid points of the Cartesian model. As shown on page 72, a modified value of h, i.e., $h' = h\frac{2}{\sqrt{3}}$ is used. Since

$$c_{\max} \sim \frac{1}{\lambda} = \frac{h}{k} \tag{4.140}$$

that is, the maximum value of c that yields a stable model is directly proportional to h, the triangular discretization allows using a Λ times higher maximum value of c, where Λ is calculated as

$$\Lambda = \frac{\frac{2}{\sqrt{3}}\sqrt{\frac{2}{3}}}{\frac{1}{\sqrt{2}}} = \frac{4}{3}. \tag{4.141}$$

Accordingly, the stability condition for the triangular scheme with the grid spacing $h' = \frac{2}{\sqrt{3}}\, h$ is

$$c \leq \Lambda \frac{1}{\sqrt{2}}\, \frac{1}{\lambda} = \frac{1}{\lambda}\sqrt{\frac{8}{9}} \tag{4.142}$$

where $\lambda = k/h$.

Numerical Dispersion Numerical calculation of the phase velocity transformed to β_x and β_y in the usual way yields Fig. 4.23 and 4.24. It can be seen that at the stability margin, the surface around spatial DC is flat, that is, for low spatial frequencies, the effect of numerical dispersion is not significant. The same is true for every consistent scheme, however, in the triangular case, the flat area is wider than for the rest of the schemes under review, which yields a wider set of wave numbers that are not affected by numerical dispersion.

Fig. 4.24 was calculated with the value of c that corresponds to the stability margin of the Cartesian membrane model. The flatness of the surface is not present in this case, however, the direction-dependence of the phase velocity is not significant.

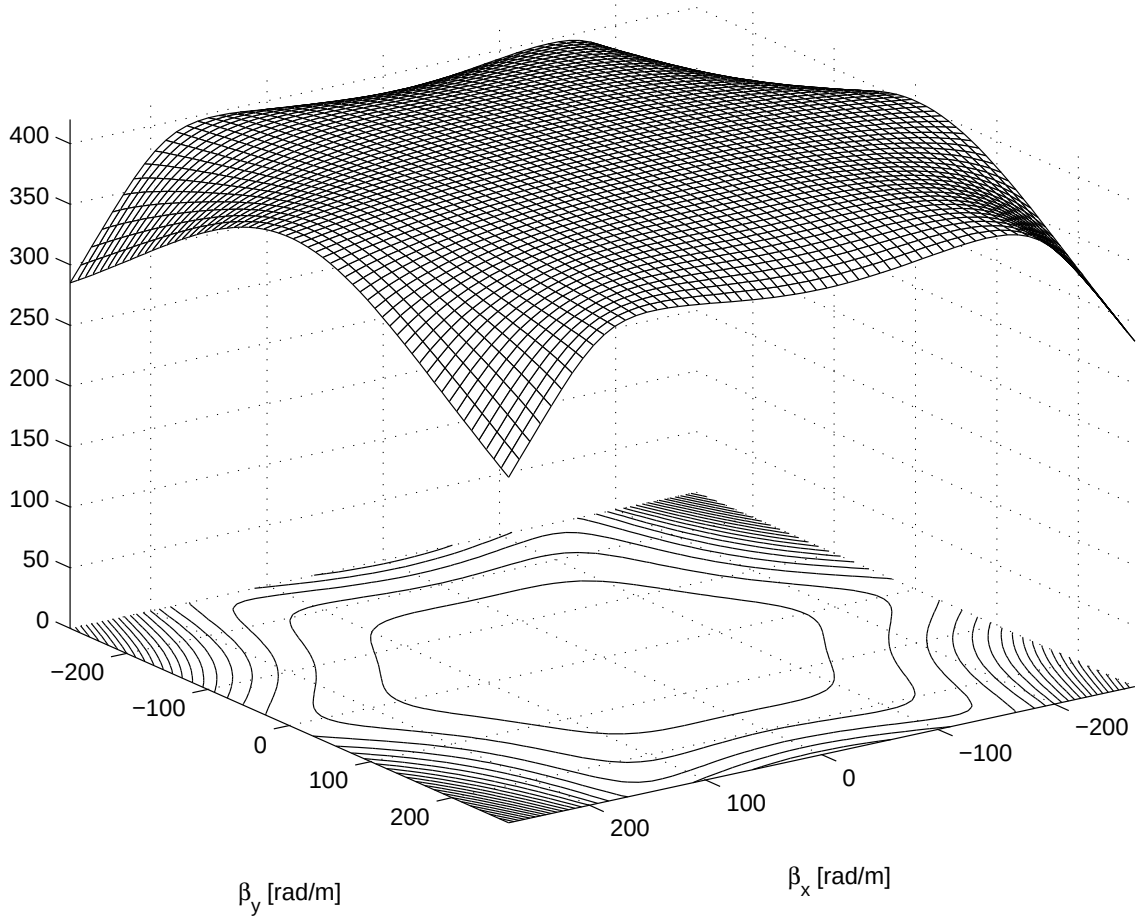

Figure 4.23: Phase speed of the membrane model in triangular coordinate system at the stability margin as a function of the spatial frequencies β_x and β_y. The theoretical value of c is 419.98 m/sec.

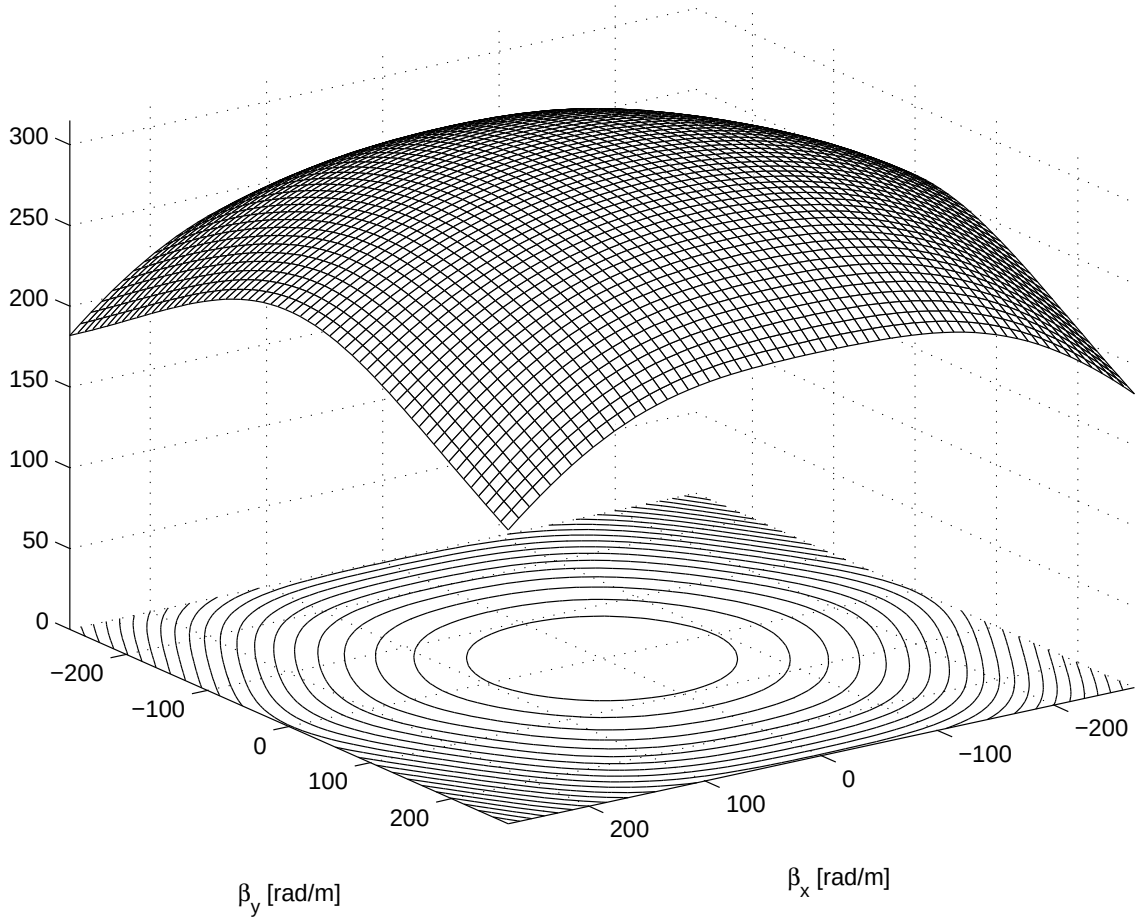

Figure 4.24: Phase speed of the membrane model in triangular coordinate system at the stability margin of the Cartesian model as a function of the spatial frequencies β_x and β_y. The theoretical value of c is 314.98 m/sec.

	Cartesian	4th-order Cartesian	Interpolated Cartesian	Triangular
$c_{\max}$	$\frac{1}{\lambda}\sqrt{\frac{1}{2}}$	$\frac{1}{\lambda}\sqrt{\frac{3}{8}}$	$\frac{1}{\lambda}\sqrt{\frac{1}{1-a}}$	$\frac{1}{\lambda}\sqrt{\frac{8}{9}}$

Table 4.3: Stability margins of the schemes under discussion for the parameter c. The constant a equals $1/\sqrt{2}$.

4.5 Comparison of the Discretization Methods

In this section, we will compare four types of discretization techniques discussed so far, namely, the simple Cartesian, the fourth-order, the interpolated and the triangular discretization from the following points of view: stability, numerical dispersion and computational complexity.

Stability The stability margins of the reviewed schemes for the undamped membrane are summarized in Table 4.3. It can be seen that from this point of view, the triangular discretization has the most advantageous properties as it allows using values of the parameter c almost twice as large as the simple Cartesian model and almost three times as large as in the case of the fourth-order accurate scheme. The second best solution with respect to stability is the interpolated Cartesian scheme.

On the other hand, according to the discussion in Section 3.2.3, if a membrane with a given value of c is to be modeled then the triangular scheme needs a lower value of the spatial grid spacing in order to be close to the stability margin. Operating near the stability margin is advantageous with respect to numerical dispersion. Using more grid points definitely improves the quality of the generated sound, however, it also increases computational load.

Numerical Dispersion To compare the different types of finite difference schemes, we may consider the maximal and minimal relative errors of the phase velocity. The definition of these characteristics for the Cartesian scheme is illustrated in Fig. 4.25. The minimal and maximal phase speed error curves for the discussed schemes for the undamped membrane are shown in Fig. 4.26. These characteristics can be interpreted in the following way. If both curves are relatively close to zero percent then the dispersion error is not significant. It can be seen that the error of the phase velocity of the Cartesian scheme in diagonal direction is zero, however, in other directions and for different parameter values, this is not the case. In general, the overall dispersion error is smaller if the system is relatively close to its stability margin. It can be seen that at the stability margin, the minimum and maximum curves of the triangular scheme are close to zero, however, inside the stability domain of parameters, the overall dispersion error of the fourth-order scheme can be less significant.

Low level of direction-dependence of a scheme appears in the error plot as relatively close minimum and maximum curves. It can be seen that the Cartesian and the fourth-

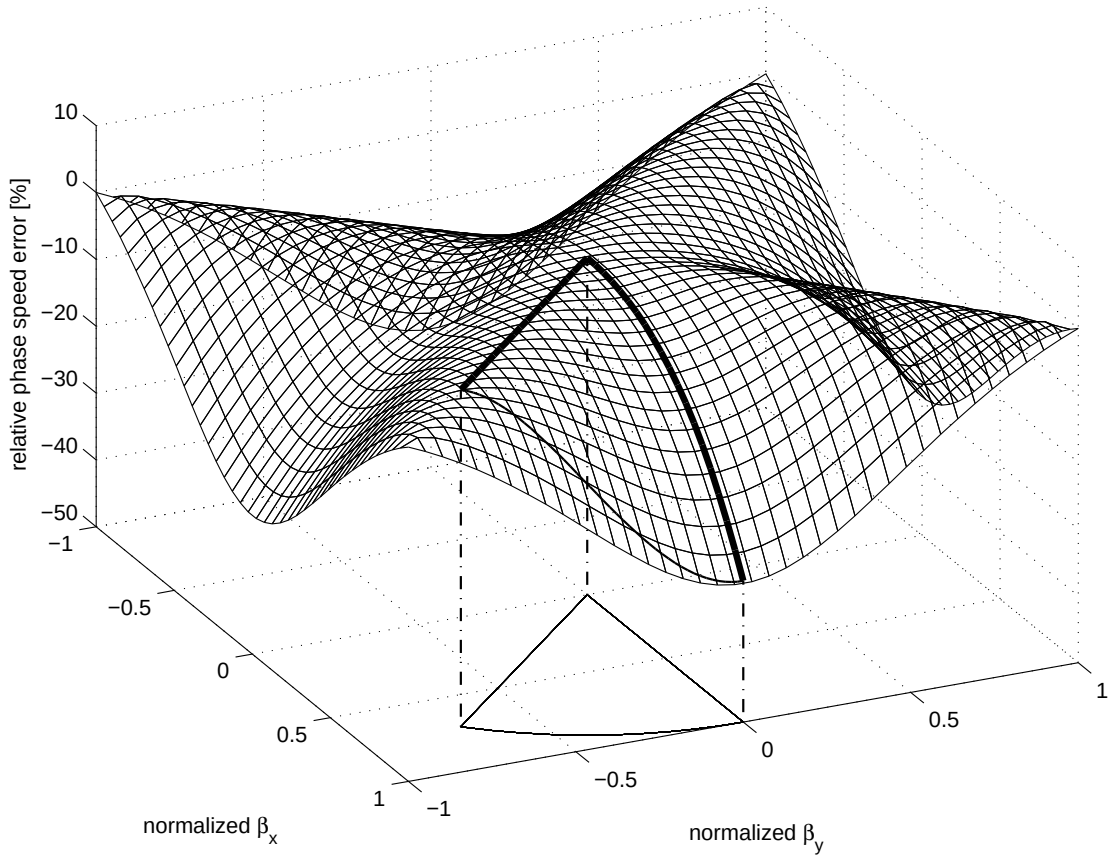

Figure 4.25: Relative error of the phase velocity of the Cartesian scheme defined as $\frac{\gamma(\beta_x,\beta_y)-c}{c}$ at the stability margin with respect to the normalized spatial frequencies $\beta_x/(\pi/h)$ and $\beta_y/(\pi/h)$, respectively. The error along the direction of its highest and lowest values is emphasized by thick lines.

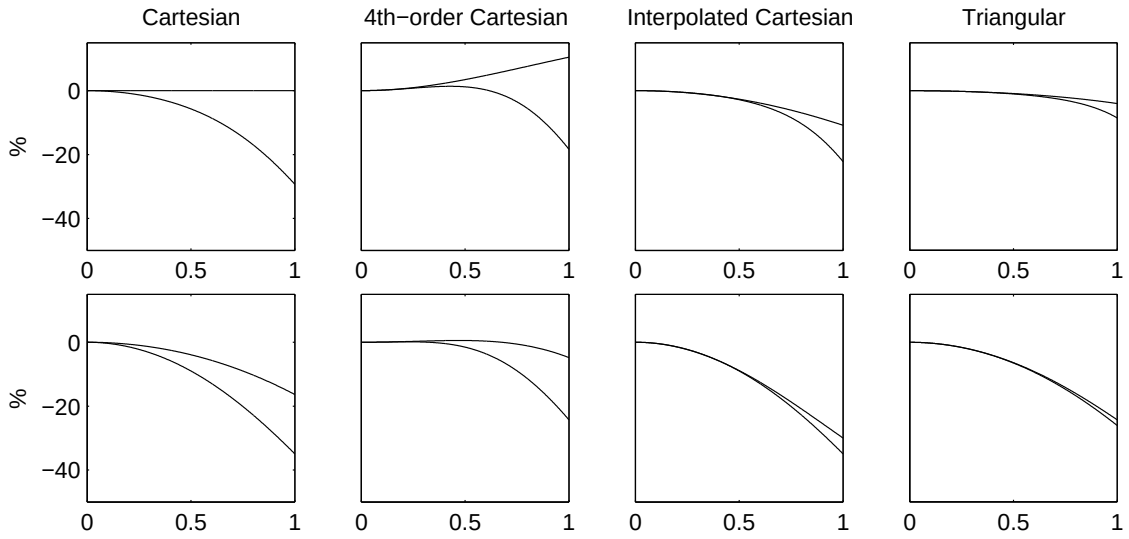

Figure 4.26: Minimal and maximal relative phase speed error curves for different types of two-dimensional schemes with respect to the normalized spatial frequency (see Fig. 4.25). The figures were generated by calculating the relative phase speed error defined as $\frac{\gamma(\beta_x,\beta_y)-c}{c}$ for spatial frequencies that correspond to the directions of the highest and lowest values of the error, respectively. The characteristics in the top row were generated using parameter values corresponding to the stability margins of each scheme. The pictures in the bottom row correspond to schemes with $c = \frac{1}{\lambda}\sqrt{\frac{1}{8}}$, which yields a stable scheme for each discretization method under review.

order schemes are quite poor from this point of view, and the triangular scheme has even better properties than the one obtained by the interpolated Cartesian discretization.

In the field of instrument modeling, we are generally interested in the modal frequencies of the discretized model. Although numerical dispersion causes the modes of the model to differ from the theoretical modal frequency values, we will not attempt to precisely describe this effect. However, some qualitative remarks can be made with respect to the relation between the dispersion characteristics in Fig. 4.26 and the frequency spectra of the displacement-time functions generated by the membrane models.

Fig. 4.27 shows the FFT spectra generated using the same values of c, k and h for each scheme. The parameter values correspond to the second row of pictures in Fig. 4.26. The lack of frequency components above 6-9 kHz is is due to spatial sampling, which restricts the wave numbers to be less than π/h in all spatial directions. According to Eq. (2.22), the temporal frequency that corresponds to the limit of the spatial frequencies is

$$f_{\max} = \beta_{\max} \frac{c}{2\pi} = \frac{\pi}{h} \frac{c}{2\pi} \quad = \quad \frac{c}{2h} \tag{4.143}$$

which in the case under discussion equals to 7.8 kHz, except for the triangular scheme. According to Section 4.4, in order to model a circular membrane with the same number of points as the Cartesian models, in the triangular scheme higher value of h, i.e. $h' = 2h/\sqrt{3}$ has to be used. This implies a lower maximum frequency, 6.75 kHz, for the triangular scheme. These are only theoretical values that correspond to the ideal case where the phase speed equals c for all wave numbers. In the discretized models, the frequency limits are slightly different due to numerical dispersion.

The phase velocity error of the fourth-order scheme, contrary to the others, can be positive, which causes frequency components to be present above the 7.8 kHz limit. The frequency components in the rest of the schemes are below the limits calculated above. The most significant effect of numerical dispersion can be observed in the case of the interpolated scheme, whose maximum frequency components are far below $f_{\max}$ compared to the other schemes. From this, we may deduce that the significance of direction-dependence of the numerical dispersion is secondary[3], and the point is to keep the overall dispersion error close to zero. This can be accomplished by using parameter values close to the stability margin. The FFT spectra of the membrane models in this case are shown in Fig. 4.28.

Computational Complexity Besides stability and numerical dispersion, another important characteristic of the different types of schemes is computational complexity. Table 4.4 summarizes the number of additions, multiplications and memory access instructions per grid point per time step required by the schemes under discussion. It can be seen that the simple Cartesian scheme is the best and the triangular scheme is the second best solution from this point of view. In the case of triangular discretization, the ratio of the areas of the circle and the diamond-shaped domain (see Fig. 4.20), i.e., the 'effective' area

[3]This statement is not necessarily true for applications where real-time implementation is not a requirement. As proposed in [Savioja and Välimäki 2000], if no significant direction-dependence of the dispersion is inherent in the model, the overall numerical dispersion can be almost perfectly removed by off-line processing using frequency-warping techniques.

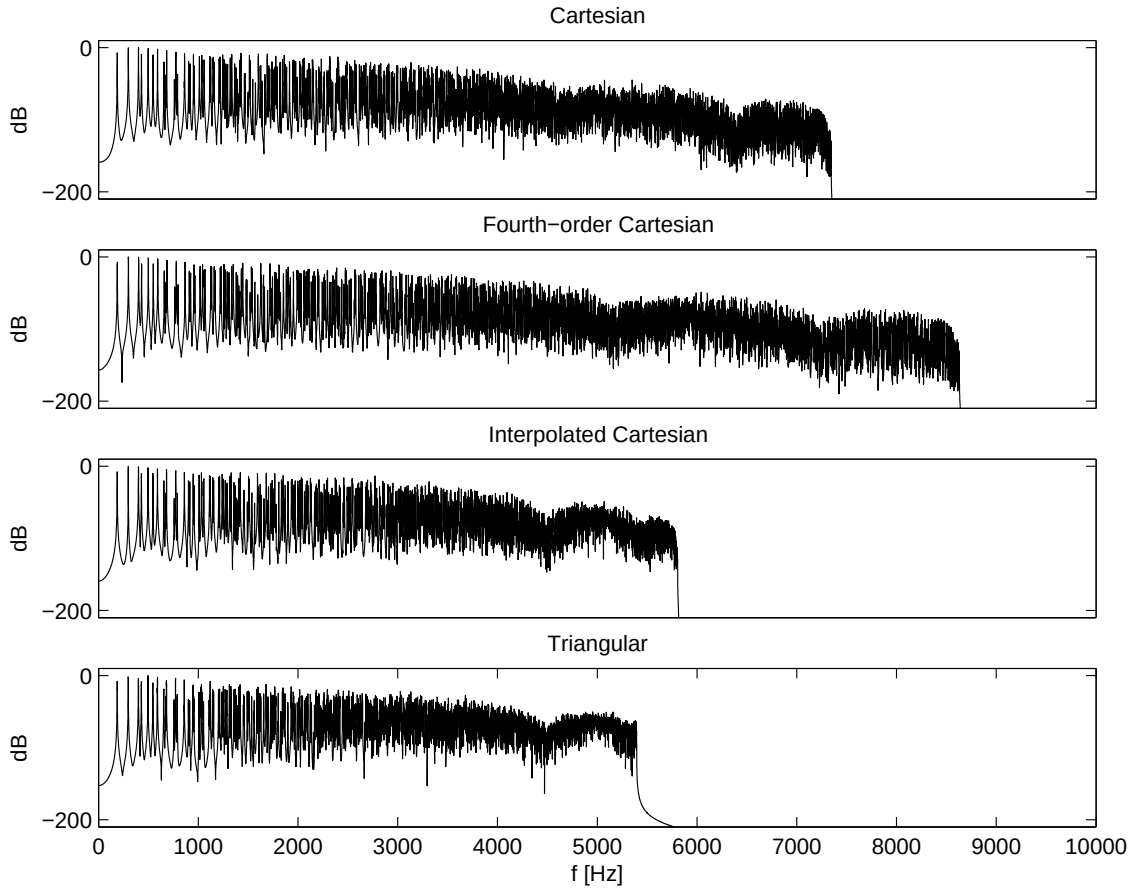

Figure 4.27: FFT spectra of the displacement-time functions generated by finite difference schemes using various discretization methods. The parameter values are identical for each scheme: $f_s = 44.1$ kHz, $\Gamma = 64$, $c = 247.49$ m/s.

	Cartesian	4th-order Cartesian	Interpolated Cartesian	Triangular
ADD	5	9	9	7
MPY	2	2	3	2
LOAD	6	10	10	8

Table 4.4: Computational complexity of the different types of schemes under review. The 'ADD', 'MPY' and 'LOAD' rows of the table contain the number of addition, multiplication and load from memory instructions required to calculate the new value of the displacement in one grid point in a time step, respectively.

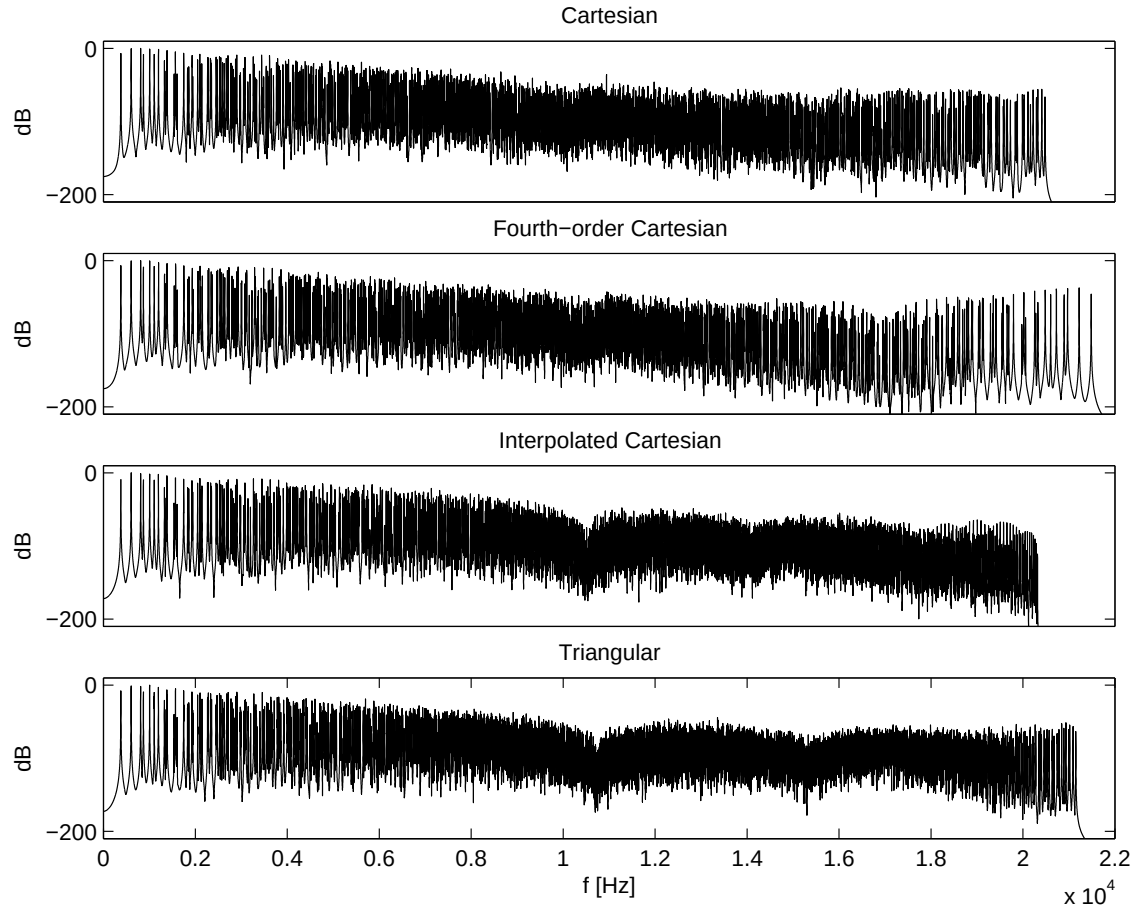

Figure 4.28: FFT spectra of the displacement-time functions generated by finite difference schemes using various discretization methods. While using the fixed parameter values $c = 500$ m/s and $f_s = 44.1$ kHz, the number of grid points, i.e., Γ and therefore the grid spacing h was adjusted according to the stability margin of each scheme.

compared to the entire area of the mesh is smaller than in the case of the other types of discretization. This means that the displacement has to be computed in lower number of grid points, which moderates the overall computational complexity of the triangular scheme.

Let us summarize the results of this section. The effect of numerical dispersion is less significant if the parameter values are close to the stability margin. If the theoretical phase speed c and the temporal sampling period k is already determined by the environment and the physical system that is to be modeled, then the value of the grid spacing h has to be chosen to be as low as possible with respect to the stability condition and the available computational resources. The discretization technique that can be implemented with the lowest value of h, i.e., with the highest number of grid points, according to the above considerations may be the best choice. The effect of numerical dispersion to the generated sound from a perceptual point of view can be an object of future analysis, e.g., by performing listening tests. However, using more grid points is advantageous even if numerical dispersion is not considered because the increased number of grid points also increases the number of normal modes taken into account, which results in a richer spectrum and higher quality of the generated sound.

4.6 Implementing Nonlinear Behaviour

The model examined in this section differs from the finite difference schemes discussed so far in that the previously presented methods, e.g., the von Neumann analysis, cannot be applied to this case. The reason we have still included this section is that the effect of nonlinearity is essential in many types of drums. In spite of this fact, the technique presented here has not been an object of research in the field of membrane modeling until recently.

In the following, we will discretize the nonlinear membrane model including frequency-dependent damping that was presented in Section 2.3.5. Let us consider the nonlinear equation for the damped membrane according to Eq. (2.44):

$$\frac{\partial^2 u}{\partial t^2} = c(t)^2 \left(\frac{\partial^2 u}{\partial x^2} + \frac{\partial^2 u}{\partial y^2} \right) - d_1 \frac{\partial u}{\partial t} + d_2 \frac{\partial}{\partial t} \left(\frac{\partial^2 u}{\partial x^2} + \frac{\partial^2 u}{\partial y^2} \right) \tag{4.144}$$

where

$$c^2 \;=\; \frac{\mathscr{T}}{\rho_S} = \frac{\mathscr{T}_0 + a_S \mathscr{T}_1(t)}{\rho_S}. \tag{4.145}$$

The nonlinear tension, $\mathscr{T}_1(t)$, can be calculated in the following way (see Eq. (2.40)):

$$\mathscr{T}_1(t) \;=\; \frac{1}{4} \frac{E}{1-p} \frac{1}{L^2} \int_0^L \int_0^L \left(u_x^2 + u_y^2 + \frac{1}{2} u_x^2 u_y^2 \right) dxdy. \tag{4.146}$$

This expression can be easily discretized by the finite difference method. Let us approximate the derivatives u_x and u_y by the center difference operators δ_{x0} and δ_{y0}, that is,

$$(u_x)^n_{m,l} \;\approx\; \delta_{x0}\{v^n_{m,l}\} = \frac{1}{2h} \left(v^n_{m+1,l} - v^n_{m-1,l} \right) \tag{4.147}$$

$$(u_y)^n_{m,l} \;\approx\; \delta_{y0}\{v^n_{m,l}\} = \frac{1}{2h} \left(v^n_{m,l+1} - v^n_{m,l-1} \right). \tag{4.148}$$

In this section, we will use the notations $D_x = \delta_{x0}\{v^n_{m,l}\}$ and $D_y = \delta_{y0}\{v^n_{m,l}\}$. The integrals in Eq. (4.146) can be approximated by summation, which yields

$$\mathscr{T}_1(nk) = (\mathscr{T}_1)^n \;=\; \frac{1}{4} \frac{E}{1-p} \frac{1}{L^2} \, h^2 \sum_{m=0}^{\Gamma-1} \sum_{l=0}^{\Gamma-1} \left(D_x^2 + D_y^2 + \frac{1}{2} D_x^2 D_y^2 \right). \tag{4.149}$$

Note that n in $(\mathscr{T}_1)^n$ indicates the time step and not raising to a power.

The discretized model for Eq. (4.144) with $c(t) = c$ was already derived in Section 4.3.2:

$$\begin{aligned} v^{n+1}_{m,l} \;=\; & \left[a_1 \left(M + M^{-1} + L + L^{-1} \right) + a_2 I \right] \{v^n_{m,l}\} + \\ & + \left[a_3 \left(M + M^{-1} + L + L^{-1} \right) + a_4 I \right] \{v^{n-1}_{m,l}\} \end{aligned} \tag{4.150}$$

In the nonlinear model, the parameters of the above equation that depend on c (i.e., a_1 and a_2) will not be constants as c is changed at every time-step. Accordingly, the nonlinear model can be implemented by calculating the values of a_1 and a_2 for time step n and then

evaluating Eq. (4.150). The expressions for $(a_1)^n$ and $(a_2)^n$ can be obtained by making the substitution

$$c^2 = \frac{\mathscr{T}_0 + a_S \left(\mathscr{T}_1\right)^n}{\rho_S} \tag{4.151}$$

into the formulae of a_1 and a_2 according to Eq. (4.96) and (4.97), which yields

$$(a_1)^n = A_1 + \mathscr{T}^n B_1 \tag{4.152}$$
$$(a_2)^n = A_2 + \mathscr{T}^n B_2 \tag{4.153}$$

where

$$A_1 = 2d_2\mu\nu \tag{4.154}$$
$$B_1 = 2\nu\lambda^2/\rho_S \tag{4.155}$$
$$A_2 = 4\nu\left(1 - 2d_2\mu\right) \tag{4.156}$$
$$B_2 = -8\nu\lambda^2/\rho_S \tag{4.157}$$

and

$$\mathscr{T}^n = \mathscr{T}_0 + a_S \left(\mathscr{T}_1\right)^n. \tag{4.158}$$

Let us summarize the calculations that has to be performed in each time-step to implement the nonlinear membrane model:

1. Calculate $\mathscr{T}^n$ according to Eq. (4.158) and Eq. (4.149).
2. Calculate $(a_1)^n$ and $(a_2)^n$ according to Eq. (4.152) and Eq. (4.153).
3. Calculate the displacement at time step $n + 1$ according to Eq. (4.150).

Fig. 4.29 shows spectrograms generated by the membrane model with zero (left) and nonzero (right) values of the parameter a_S. If $a_S = 0$ then the model is actually simplified to the linear model shown in the previous sections. It can be seen in the figure on the right-hand side that the modal frequencies of the nonlinear model are decreasing over time. Fig. 4.30 shows the spectrograms of a recorded tom-tom sound sample and the nonlinear membrane model. It can be seen that tension modulation can be used effectively to model the time-varying pitch of real drums.

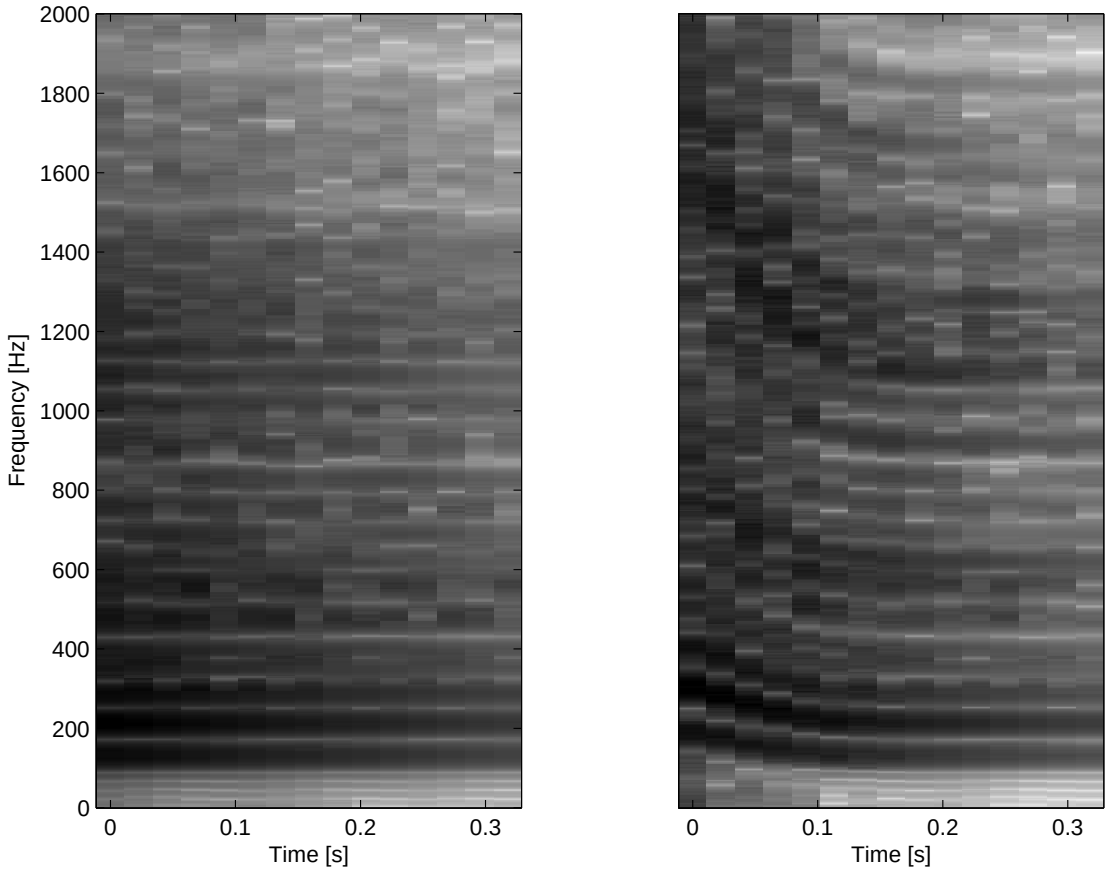

Figure 4.29: Spectrograms calculated from the displacement of a point of the linear (left) and nonlinear (right) membrane models, respectively. The modal frequencies of the nonlinear model are decreased over time.

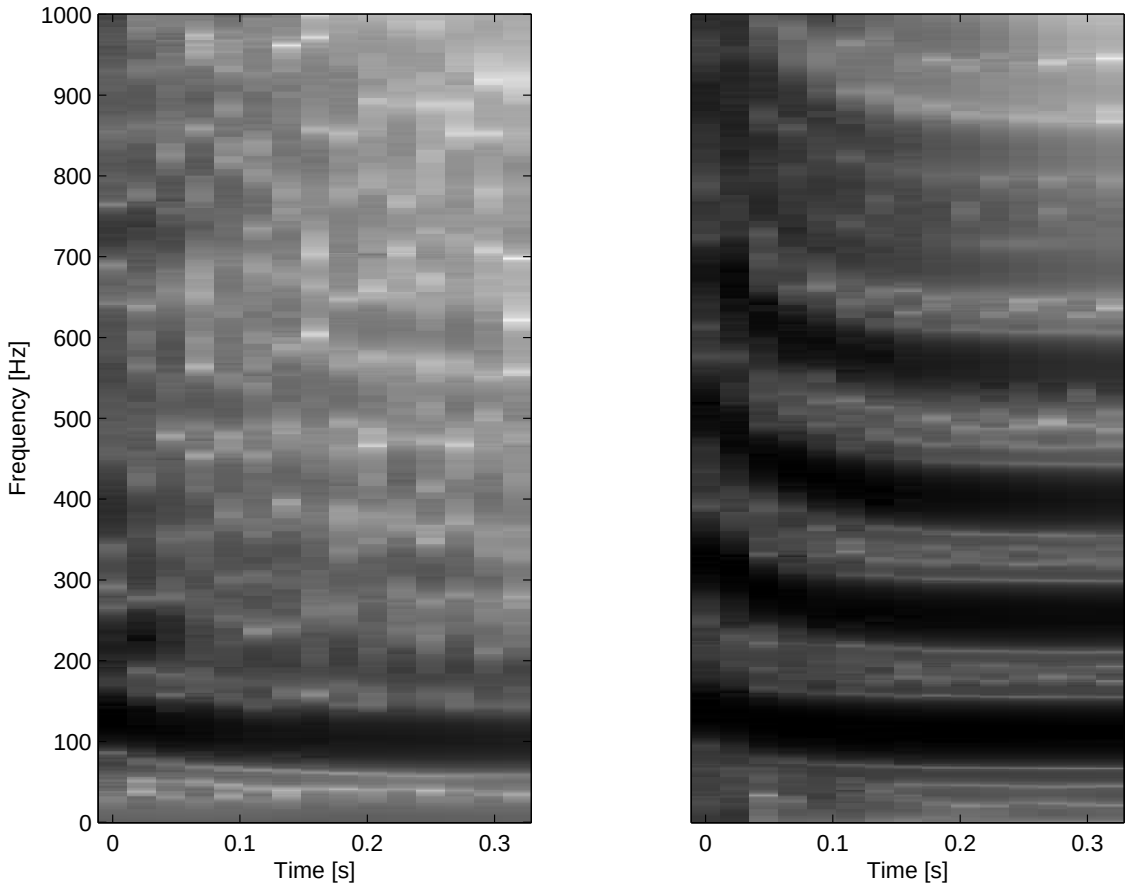

Figure 4.30: Spectrograms calculated from a recorded sound sample of a tom-tom drum (left) and the displacement of a point of the nonlinear membrane model.

4.7 Summary

In this chapter, we have discussed several types of finite difference schemes for the acoustic membrane. The basic idea has remained the same as it was in the previous chapter, i.e., approximating the derivatives of the differential equation by finite differences. The difficulties in discussing problems with two spatial dimensions are mainly due to the complicated expressions that can be derived by the finite difference method. However, there are no theoretical complications compared to the one-dimensional case.

The technique of von Neumann analysis, by using the two-dimensional Fourier-transform, was shown to be applicable to the finite difference schemes derived in this chapter, except for the nonlinear model. Stability analysis of each discussed scheme was shown to be equivalent to solving a transcendental inequality. We have laid special emphasis on the discussion of numerical dispersion in two dimensions. Direction-dependence of the phase velocity due to dispersion has been examined for each scheme under review. It was shown that, contrary to the case of the string discussed in the previous chapter, schemes with two spatial dimensions inhere numerical dispersion even at the stability limit.

Four different types of discretization were compared in Section 4.5. According to the results, it can be concluded that several factors have to be considered to find the most suitable scheme for a given problem. It was shown that there is no easy way to make this decision, however, performing listening tests using different types of drum models, which can be one of the research directions of the future, may prove to be useful from this point of view.

In Section 4.3.1, 4.3.2 and 4.6, damping and nonlinear behaviour have been added to the membrane model discretized in the Cartesian coordinate system. Modeling these effects is essential in creating a drum model with realistic sound. However, in the case of the other discretization techniques, especially the triangular one, these effects have not yet been implemented by the author, thus this can be one of the objects of future research.

Chapter 5

Conclusions and Future Directions

In this thesis we have discussed several aspects of physics-based membrane modeling and summarized the fundamentals of the finite difference method. In Chapter 2, some essential remarks on partial differential equations with respect to instrument modeling were presented. Most of the concepts introduced in this chapter have long history in scientific research and are well understood. However, summarizing them in one place, as done in this chapter, is uncommon in the literature.

In Chapter 3, the basics of the finite difference method were presented. The main result of this chapter is that it has provided a uniform framework of well-established concepts for the rest of the thesis. The fundamental notions of this field were explained in detail with special respect to the technicalities of instrument modeling. It is believed by the author that this chapter, together with the next one, can be a useful resource for anyone interested in instrument modeling as the fundamentals of this method are reviewed here in a more easily interpretable way than in most available textbooks.

In Chapter 4, several physical models for the membrane have been derived and reviewed. For most of these models, stability conditions and figures illustrating the dispersion error were provided. In Section 4.5, the discretization methods that had been discussed in the previous sections were compared with respect to their stability- and dispersion properties and computational complexity. Analyzing these properties, although it has resulted in some useful remarks, has proven to be insufficient for comparing the physical models from the viewpoint of sound quality. In the future, this difficulty could be resolved by performing listening tests for the perceptual evaluation of the various models.

The author intends to continue the research on physics-based membrane modeling in the future. Two main directions of future research can be foreseen, one of them focusing on the theoretical and the other on the practical aspects of instrument modeling. However, no definite borderline between the two category can be drawn as they are closely related. The first direction includes further investigation of the theoretical aspects of finite difference modeling and its connection to other methods with regard to the digital waveguide, and the time domain finite element methods. Some of the relations between the different modeling techniques are well documented. Nevertheless, the discussion of the time domain finite element method in the context of sound synthesis, for instance, is uncommon in the

literature. In the opinion of the author, constructing more accurate instrument models is a direct consequence of better understanding of several related methods. At a more fundamental level, having a more thorough knowledge of the mathematics of partial differential equations and their analytical solutions is also necessary for the future research. Consequently, going further into this topic is also among future plans.

The practical direction of the future research include implementation and analysis of finite difference models that has not yet been examined by the author. The questions of real-time realization are planned to be answered by implementing the membrane models on digital signal processors. Besides, the implementation of these models on PC in C or C++ would accelerate experimentation with altering the model parameters compared to the Matlab programs developed so far.

Both practical and theoretical perspectives are seen in improving the mathematical models of the membranes and drums by making measurements on real instruments including the effect of excitation on the overall sound. The ultimate goal from a practical viewpoint is to construct models for the entire instrument and implement them in real-time. The models have to be verified, from the viewpont of musical applicability, by performing listening tests.

It can be seen that the list of possible future directions of research are quite lengthy. However, the most urgent objective, according to the author's opinion, is to form a firm foundation for the future research by closer inspection of the mathematical principles physical modeling is based upon.

Bibliography

Aird, M.-L. 2002. *Musical Instrument Modelling Using Digital Waveguides*, PhD thesis, University of Bath, p. 171.

Bensa, J., Bilbao, S., Kronland-Martinet, R. and Smith, J. O. 2003. The Simulation of Piano String Vibration: From Physical Models to Finite Difference Schemes and Digital Waveguides, *J. Acoust. Soc. Am.* **114**(2): 1095–1107.

Bilbao, S. 2001. *Wave and Scattering Methods for the Numerical Integration of Partial Differential Equations*, PhD thesis, Stanford University, California, USA, p. 376.

Bilbao, S. and Smith, J. O. 2003. Finite Difference Schemes and Digital Waveguide Networks for the Wave Equation: Stability, Passivity, and Numerical Dispersion, *IEEE Trans. Speech Audio Proc.* **11**(3): 255–266.

Dahl, S. 1997. *Spectral changes in the tom-tom related to striking force*, Master's thesis, KTH College of Engineering, Haninge.

Dudgeon, D. E. and Mersereau, R. M. 1995. *Multidimensional Digital Signal Processing*, Prentice-Hall, Upper Sadle River, NJ, USA.

Fletcher, N. H. and Rossing, T. D. 1998. *The Physics of Musical Instruments*, Springer-Verlag, New York, USA, p. 756. 2nd ed. (1st ed. 1991).

Hiller, L. and Ruiz, P. 1971a. Synthesizing Musical Sounds by Solving the Wave Equation for Vibrating Objects: Part 1, *J. Audio Eng. Soc.* **19**(6): 462–470.

Hiller, L. and Ruiz, P. 1971b. Synthesizing Musical Sounds by Solving the Wave Equation for Vibrating Objects: Part 2, *J. Audio Eng. Soc.* **19**(7): 542–550.

Kinsler, L. E., Frey, A. R., Coppens, A. B. and Sanders, J. V. 1999. *Fundamentals of Acoustics*, John Wiley and Sons, Inc., Hoboken, NJ, USA, p. 548. 4th ed.

Petrausch, S. and Rabenstein, R. 2005. Tension Modulated Nonlinear 2D Models for Digital Sound Synthesis with the Functional Transformation Method, University of Erlangen-Nuremberg.

Savioja, L. and Välimäki, V. 1997. Improved discrete-time modeling of multi-dimensional wave propagation using the interpolated digital waveguide mesh, *Proc. IEEE Int. Conf. Acoust., Speech, and Sign. Proc.*, Vol. 1, Munich, Germany, pp. 459–462.

Savioja, L. and Välimäki, V. 2000. Reducing the Dispersion Error in the Digital Waveguide Mesh Using Interpolation and Frequency-Warping Techniques, *IEEE Trans. Speech Audio Proc.* **8**(2): 184–194.

Smith, J. O. 1991. Viewpoints on the History of Digital Synthesis, *Proc. Int. Computer Music Conf.*, Montreal, Canada, pp. 1–10.

Strikwerda, J. C. 1989. *Finite Difference Schemes and Partial Differential Equations*, Wadsworth and Brooks, Pacific Grove, CA, USA.

Tolonen, T., Välimäki, V. and Karjalainen, M. 1998. Evaluation of Modern Sound Synthesis Methods, *Technical Report 48*, Helsinki University of Technology, Laboratory of Acoustics and Audio Signal Processing, Espoo, Finland, p. 114. URL: `http://www.acoustics.hut.fi/~ttolonen/sound_synth_report.html`.

Trefethen, L. N. 1996. *Finite Differences and Spectral Methods for Ordinary and Partial Differential Equations*, unpublished text, p. 325. Draft available at URL: `http://www.comlab.ox.ac.uk/people/nick.trefethen/pdetext.html`.

Välimäki, V. 2004. Physics-Based Modeling of Musical Instruments, *Acta Acust. – Acust.* **90**: 611–617.

Välimäki, V., Pakarinen, J., Erkut, C. and Karjalainen, M. 2006. Discrete-time Modelling of Musical Instruments, *Reports on Progress in Physics* **69**(1): 1–78.

Zwillinger, D. 1997. *Handbook of Differential Equations*, Academic Press, p. 856. 3rd ed.

Appendix A

Derivation of the Wave Equation in Triangular Coordinate System

In this appendix, the derivation of the two-dimensional wave equation in triangular coordinates will be presented. Let us proceed from the Cartesian form of the wave equation:

$$\frac{\partial^2 u}{\partial t^2} = c^2 \left(\frac{\partial^2 u}{\partial x^2} + \frac{\partial^2 u}{\partial y^2} \right). \tag{A.1}$$

According to the definition of the triangular coordinate system, the directional derivatives of the function u in the directions of the coordinate axes w and z can be expressed as follows:

$$\frac{\partial u}{\partial w} = \frac{1}{2}\frac{\partial u}{\partial x} + \frac{\sqrt{3}}{2}\frac{\partial u}{\partial y} \tag{A.2}$$

$$\frac{\partial u}{\partial z} = \frac{1}{2}\frac{\partial u}{\partial x} - \frac{\sqrt{3}}{2}\frac{\partial u}{\partial y} \tag{A.3}$$

By making the sum and the difference of Eq. (A.2) and Eq. (A.3), we obtain the following expressions for u_x and u_y:

$$\frac{\partial u}{\partial x} = \frac{\partial u}{\partial w} + \frac{\partial u}{\partial z} \tag{A.4}$$

$$\frac{\partial u}{\partial y} = \frac{\sqrt{3}}{2} \left(\frac{\partial u}{\partial w} - \frac{\partial u}{\partial z} \right). \tag{A.5}$$

By repeatedly applying the formula of Eq. (A.4), the following expression can be obtained for the second order derivative of u with respect to x:

$$\frac{\partial^2 u}{\partial x^2} = \frac{\partial}{\partial x}\left(\frac{\partial u}{\partial w} \right) + \frac{\partial}{\partial x}\left(\frac{\partial u}{\partial z} \right) = \tag{A.6}$$

$$= \left(\frac{\partial^2 u}{\partial w^2} + \frac{\partial^2 u}{\partial w \partial z} \right) + \left(\frac{\partial^2 u}{\partial w \partial z} + \frac{\partial^2 u}{\partial z^2} \right) = \tag{A.7}$$

$$= \frac{\partial^2 u}{\partial w^2} + 2\frac{\partial^2 u}{\partial w \partial z} + \frac{\partial^2 u}{\partial z^2}. \tag{A.8}$$

The expression for u_{yy} can be derived in a similar fashion by using Eq. (A.5):

$$\frac{\partial^2 u}{\partial y^2} = \frac{1}{3}\left(\frac{\partial^2 u}{\partial w^2} - 2\frac{\partial^2 u}{\partial w \partial z} + \frac{\partial^2 u}{\partial z^2}\right). \tag{A.9}$$

By substituting these expressions into Eq. (A.1), we obtain the triangular form of the wave equation:

$$\frac{\partial^2 u}{\partial t^2} = c^2 \frac{4}{3}\left(\frac{\partial^2 u}{\partial w^2} + \frac{\partial^2 u}{\partial w \partial z} + \frac{\partial^2 u}{\partial z^2}\right). \tag{A.10}$$

This formula can be simplified by observing that

$$\frac{2}{3}\frac{\partial^2 u}{\partial w^2} + \frac{4}{3}\frac{\partial^2 u}{\partial w \partial z} + \frac{2}{3}\frac{\partial^2 u}{\partial z^2} = \frac{\partial^2 u}{\partial x^2} \tag{A.11}$$

which yields the final form of the wave equation in triangular coordinates:

$$\frac{\partial^2 u}{\partial t^2} = c^2 \frac{2}{3}\left(\frac{\partial^2 u}{\partial w^2} + \frac{\partial^2 u}{\partial z^2} + \frac{\partial^2 u}{\partial x^2}\right). \tag{A.12}$$

Appendix B

Coordinate Transform in the Spatial Frequency Domain

In Section 4.4, we stated that the spatial spectrum of a grid function defined in the triangular coordinate system, $V(\beta_x, \beta_w)$, can be expressed as a function of the spatial frequencies of the Cartesian coordinate system, β_x and β_y, in the following way:

$$V(\beta_x, \beta_y) = \frac{1}{\det \mathbf{S}} V\left(\beta_x,\ \beta_w = \frac{1}{2}\,\beta_x + \frac{\sqrt{3}}{2}\,\beta_y\right) \tag{B.1}$$

where, according to Section 2.3.3,

$$\mathbf{S} = \begin{bmatrix} 1 & -\sqrt{3}/3 \\ 0 & 2\sqrt{3}/3 \end{bmatrix} \tag{B.2}$$

thus

$$\det \mathbf{S} = \frac{2\sqrt{3}}{3}. \tag{B.3}$$

Without this transformation, the spectra of the two grid functions defined in different coordinate systems could not be compared. In this appendix, the derivation of Eq. (B.1) will be presented.

First, let us define the two-dimensional spatial Fourier-transform using vector notation.

Definition B.1: (Spatial Fourier-transform in two dimensions (vector notation))

$$U(\boldsymbol{\beta}) = \frac{1}{2\pi} \int_{\mathbb{R}^2} u(\mathbf{x}) e^{-j\boldsymbol{\beta}^{\mathrm{T}}\mathbf{x}} d\mathbf{x} \tag{B.4}$$

$$u(\mathbf{x}) = \frac{1}{2\pi} \int_{\mathbb{R}^2} U(\boldsymbol{\beta}) e^{j\boldsymbol{\beta}^{\mathrm{T}}\mathbf{x}} d\boldsymbol{\beta} \tag{B.5}$$

$$V(\boldsymbol{\beta}) = \frac{1}{2\pi} h^2 \sum_{m \in \mathbb{Z}^2} v(\mathbf{m}) e^{-jh\boldsymbol{\beta}^{\mathrm{T}}\mathbf{m}} \tag{B.6}$$

$$v(\mathbf{m}) = \frac{1}{2\pi} \int_{\left[-\frac{\pi}{h}, \frac{\pi}{h}\right]^2} V(\boldsymbol{\beta}) e^{jh\boldsymbol{\beta}^{\mathrm{T}}\mathbf{m}} d\boldsymbol{\beta} \tag{B.7}$$

where

$$\mathbf{x} = \begin{bmatrix} x_1 \\ x_2 \end{bmatrix}, \boldsymbol{\beta} = \begin{bmatrix} \beta_1 \\ \beta_2 \end{bmatrix}, \mathbf{m} = \begin{bmatrix} m_1 \\ m_2 \end{bmatrix} \tag{B.8}$$

$$x_1, x_2, \beta_1, \beta_2 \in \mathbb{R} \tag{B.9}$$

$$m_1, m_2 \in \mathbb{Z}. \tag{B.10}$$

The interpretation of the variables depends on the coordinate system, e.g., in the Cartesian coordinate system x_1 and x_2 correspond to x and y, respectively.

Let us start with deriving the relationship between the spectra of a two-dimensional continuous-space signal $u(\mathbf{x})$ and the discrete-space signal (i.e., grid function) $v(\mathbf{m})$ which is obtained by periodic sampling of the continuous signal. In two and more dimensions, contrarily to the one-dimensional case, periodic sampling can be performed in many ways. However, for our purpose, the review of the simplest case, the *square sampling*, is sufficient. In this case, the discrete signal is obtained by

$$v(\mathbf{m}) = u(h\mathbf{m}) \tag{B.11}$$

that is, the sampling is performed along the x and y axes, and the sampling period is equal (h) along both axes[1]. According to Eq. (B.5),

$$v(\mathbf{m}) = u(h\mathbf{m}) = \frac{1}{2\pi} \int_{\mathbb{R}^2} U(\boldsymbol{\beta}) e^{jh\boldsymbol{\beta}^{\mathrm{T}}\mathbf{m}} d\boldsymbol{\beta}. \tag{B.12}$$

The integral over an infinite domain can be expressed as an infinite sum of integrals over finite domains as follows:

$$\int_{\mathbb{R}^2} U(\boldsymbol{\beta}) e^{jh\boldsymbol{\beta}^{\mathrm{T}}\mathbf{m}} d\boldsymbol{\beta} = \sum_{\mathbf{p}\in\mathbb{Z}^2} \int_{D(\mathbf{p})} U(\boldsymbol{\beta}) e^{jh\boldsymbol{\beta}^{\mathrm{T}}\mathbf{m}} d\boldsymbol{\beta} \tag{B.13}$$

where $\mathbf{p} = \begin{bmatrix} p_1 & p_2 \end{bmatrix}^{\mathrm{T}}$ and the domain $D(\mathbf{p})$ is defined as

$$\begin{aligned} D(\mathbf{p}) = \Big\{ & \beta_x : \frac{1}{h}(-\pi - 2\pi p_1) \le \beta_x < \frac{1}{h}(\pi - 2\pi p_1), \\ & \beta_y : \frac{1}{h}(-\pi - 2\pi p_2) \le \beta_y < \frac{1}{h}(\pi - 2\pi p_2) \Big\}. \end{aligned} \tag{B.14}$$

That is, the spatial frequency-domain is divided into squares whose length along sides equals to $2\pi/h$. By making the formal substitution

$$\boldsymbol{\beta} = \boldsymbol{\xi} - \frac{2\pi}{h}\mathbf{p} \tag{B.15}$$

Eq. (B.14) can be written as

$$\begin{aligned} D(\mathbf{p}) = D = \Big\{ & \xi_x : \frac{-\pi}{h} \le \xi_x < \frac{\pi}{h}, \\ & \xi_y : \frac{-\pi}{h} \le \xi_y < \frac{\pi}{h} \Big\} \end{aligned} \tag{B.16}$$

[1]The general form of Eq. (B.11) which applies to all types of two-dimensional sampling is $v(\mathbf{m}) = u(\mathbf{S}\mathbf{m})$ where S is the sampling matrix (see [Dudgeon and Mersereau 1995, Chapter 1]).

thus, Eq. (B.13) takes the form of[2]

$$\begin{aligned}\int_{\mathbb{R}^2} U(\boldsymbol{\beta}) e^{jh\boldsymbol{\beta}^T\mathbf{m}} d\boldsymbol{\beta} &= \int_{\left[-\frac{\pi}{h},\frac{\pi}{h}\right]^2} \sum_{\mathbf{p}\in\mathbb{Z}^2} U\left(\boldsymbol{\xi} - \frac{2\pi}{h}\mathbf{p}\right) e^{jh\left(\boldsymbol{\xi}-\frac{2\pi}{h}\mathbf{p}\right)^{\mathrm{T}}\mathbf{m}} d\boldsymbol{\xi} = \\ &= \int_{\left[-\frac{\pi}{h},\frac{\pi}{h}\right]^2} \sum_{\mathbf{p}\in\mathbb{Z}^2} U\left(\boldsymbol{\xi} - \frac{2\pi}{h}\mathbf{p}\right) e^{jh\boldsymbol{\xi}^{\mathrm{T}}\mathbf{m}}\, e^{-j2\pi\mathbf{p}^{\mathrm{T}}\mathbf{m}} d\boldsymbol{\xi}. \quad \text{(B.17)}\end{aligned}$$

The second exponential on the right-hand side of Eq. (B.17) is one for all values of the integer vectors $\mathbf{m}$ and $\mathbf{p}$, so, after eliminating the dummy variable $\boldsymbol{\xi}$, we obtain the final form of the expression:

$$\int_{\mathbb{R}^2} U(\boldsymbol{\beta}) e^{jh\boldsymbol{\beta}^T\mathbf{m}} d\boldsymbol{\beta} = \int_{\left[-\frac{\pi}{h},\frac{\pi}{h}\right]^2} \left[\sum_{\mathbf{p}\in\mathbb{Z}^2} U\left(\boldsymbol{\beta} - \frac{2\pi}{h}\mathbf{p}\right)\right] e^{jh\boldsymbol{\beta}^{\mathrm{T}}\mathbf{m}}\, d\boldsymbol{\beta}. \quad \text{(B.18)}$$

After substituting this into Eq. (B.12) and comparing with the inverse formula of the discrete-space Fourier-transform (Eq. (B.7)), it is apparent that the expression between square brackets in Eq. (B.18) is the spectrum of the sampled signal, that is,

$$V(\boldsymbol{\beta}) = \sum_{\mathbf{p}\in\mathbb{Z}^2} U\left(\boldsymbol{\beta} - \frac{2\pi}{h}\mathbf{p}\right). \quad \text{(B.19)}$$

This relation is the two dimensional expression of the well known effect of periodic sampling, namely, that the spectrum of the sampled signal is the periodic extension of the analog signal.

Another relation is yet to be derived, namely, the one that connects the spectra of a continuous-space signal in Cartesian and triangular coordinate systems. The relationship between the space-domain signals and their spectra is known:

$$u_1(\mathbf{x}) \iff U_1(\boldsymbol{\beta}) \quad \text{(B.20)}$$

$$u_2(\mathbf{x}') \iff U_2(\boldsymbol{\beta}'). \quad \text{(B.21)}$$

The vectors $\mathbf{x}$ and $\mathbf{x}'$ contain the spatial variables of the Cartesian and the triangular coordinate systems, respectively. Similarly, $\boldsymbol{\beta}$ and $\boldsymbol{\beta}'$ contain the spatial frequency variables corresponding to the two coordinate systems. What we are looking for is the relationship between $U_1(\boldsymbol{\beta})$ and $U_2(\boldsymbol{\beta}')$ if we know that, according to Section 2.3.3, the triangular form of the function $u_1(\mathbf{x})$ is defined as

$$u_2(\mathbf{x}') = u_1(\mathbf{S}^{-\mathbf{1}}\mathbf{x}') \quad \text{(B.22)}$$

where the matrix of the linear transform $\mathbf{S}$ is defined by Eq. (2.30). According to Eq. (B.4), the Fourier-transform of $u_1(\mathbf{x})$ is

$$U_1(\boldsymbol{\beta}) = \frac{1}{2\pi}\int_{\mathbb{R}^2} u_1(\mathbf{x}) e^{-j\boldsymbol{\beta}^{\mathrm{T}}\mathbf{x}} d\mathbf{x}. \quad \text{(B.23)}$$

[2]The mathematically precise definition of the domain of integration is $\left[-\frac{\pi}{h},\frac{\pi}{h}\right)^2$, however, if the integrand does not contain Dirac delta components, which we assume, then using $\left[-\frac{\pi}{h},\frac{\pi}{h}\right]^2$ makes no difference.

Similarly, the Fourier-transform of $u_2(\mathbf{x}')$ is defined as

$$U_2(\boldsymbol{\beta}') = \frac{1}{2\pi}\int_{\mathbb{R}^2} u_2(\mathbf{x}')e^{-j(\boldsymbol{\beta}')^{\mathrm{T}}\mathbf{x}'}d\mathbf{x}' = \tag{B.24}$$

$$= \frac{1}{2\pi}\int_{\mathbb{R}^2} u_1(\mathbf{S^{-1}x}')e^{-j(\boldsymbol{\beta}')^{\mathrm{T}}\mathbf{x}'}d\mathbf{x}' \tag{B.25}$$

By making the substitution $\mathbf{x}' = \mathbf{Sx}$, we obtain

$$U_2(\boldsymbol{\beta}') = \frac{1}{2\pi}\int_{\mathbb{R}^2} u_1(\mathbf{S^{-1}Sx})e^{-j(\boldsymbol{\beta}')^{\mathrm{T}}\mathbf{Sx}}d\left(\mathbf{Sx}\right) = \tag{B.26}$$

$$= \frac{1}{2\pi}\int_{\mathbb{R}^2} \det\mathbf{S}\; u_1(\mathbf{x})e^{-j(\boldsymbol{\beta}')^{\mathrm{T}}\mathbf{Sx}}d\mathbf{x} = \tag{B.27}$$

$$= \det\mathbf{S}\,\frac{1}{2\pi}\int_{\mathbb{R}^2} u_1(\mathbf{x})e^{-j\left(\mathbf{S}^{\mathrm{T}}\boldsymbol{\beta}'\right)^{\mathrm{T}}\mathbf{x}}d\mathbf{x}. \tag{B.28}$$

By comparing Eq. (B.28) with Eq. (B.4), it can be seen that

$$U_2(\boldsymbol{\beta}') = \det\mathbf{S}\; U_1\left(\mathbf{S}^{\mathrm{T}}\boldsymbol{\beta}'\right). \tag{B.29}$$

The grid function $u_2(\mathbf{m})$ can be obtained by periodic sampling of $u_2(\mathbf{x}')$, defined by Eq. (B.22), according to Eq. (B.11). By applying the above results (Eq. (B.19) and Eq. (B.29)), the following relationship can be derived:

$$V_2(\boldsymbol{\beta}') = \sum_{\mathbf{p}\in\mathbb{Z}^2} U_2\left(\boldsymbol{\beta}' - \frac{2\pi}{h}\mathbf{p}\right) = \tag{B.30}$$

$$= \det\mathbf{S}\sum_{\mathbf{p}\in\mathbb{Z}^2} U_1\left(\mathbf{S}^{\mathrm{T}}\boldsymbol{\beta}' - \frac{2\pi}{h}\mathbf{p}\right) = \tag{B.31}$$

$$= \det\mathbf{S}\; V_1\left(\mathbf{S}^{\mathrm{T}}\boldsymbol{\beta}'\right) \tag{B.32}$$

that is,

$$V_2(\boldsymbol{\beta}') = \det\mathbf{S}\; V_1\left(\mathbf{S}^{\mathrm{T}}\boldsymbol{\beta}'\right). \tag{B.33}$$

The inverse relation can be obtained by making the substitution $\boldsymbol{\beta}' = \left(\mathbf{S}^{\mathrm{T}}\right)^{-1}\boldsymbol{\beta}$

$$V_1\left(\boldsymbol{\beta}\right) = \frac{1}{\det\mathbf{S}}\; V_2\left(\left(\mathbf{S}^{\mathrm{T}}\right)^{-1}\boldsymbol{\beta}\right). \tag{B.34}$$

As $\beta = [\beta_x, \beta_y]^{\mathrm{T}}$, and

$$\left(\mathbf{S}^{\mathrm{T}}\right)^{-1} = \begin{bmatrix} 1 & 0 \\ 1/2 & \sqrt{3}/2 \end{bmatrix} \tag{B.35}$$

we obtain

$$V_1\left(\begin{bmatrix} \beta_x \\ \beta_y \end{bmatrix}\right) = \frac{3}{2\sqrt{3}}\; V_2\left(\begin{bmatrix} \beta_x \\ \frac{1}{2}\,\beta_x + \frac{\sqrt{3}}{2}\,\beta_y \end{bmatrix}\right) \tag{B.36}$$

This equation can be rewritten in the scalar form

$$V_1\left(\beta_x, \beta_y\right) = \frac{3}{2\sqrt{3}}\; V_2\left(\beta_x,\; \frac{1}{2}\beta_x + \frac{\sqrt{3}}{2}\beta_y\right) \tag{B.37}$$

that is, we have proven Eq. (B.1).